Inaugural Dissertation

for

obtaining the doctoral degree

of the

Combined Faculties of Mathematics, Engineering and Natural Sciences

of the

Ruprecht - Karls - University

Heidelberg

Presented by

M.Sc. Laura Theile (nee Werner)

Born in Torgau, Germany

Oral examination: 30.04.2024

Cell type-dependent functions of centrosome linker components and their role in centrosome clustering and mitotic spindle formation

Referees: Prof. Dr. Elmar Schiebel

Prof. Dr. Sylvia Erhardt

Table of content

Summary

The centrosome is the main microtubule organizing center (MTOC) of animal cells. It consists of mother and daughter centrioles that are surrounded by the so called pericentriolar matrix (PCM), a cloud of proteins. During interphase, cells contain only one main MTOC consisting of two centrosomes kept together via centrosome cohesion. The current understanding of centrosome cohesion involves two distinct pathways: the centrosome linker and microtubule (MT)-based cohesion. The best described and most studied centrosome linker proteins are C-Nap1 and Rootletin and its interactor CEP68. C-Nap1 forms a ring-like structure at the proximal end of both centrioles and organizes the Rootletin/CEP68 filaments. In late G2/prophase the Never in mitosis A-related kinase 2 (Nek2) efficiently phosphorylates C-Nap1 and Rootletin to dissolve the centrosome linker, which then leads to centrosome separation in G2/prophase. Afterwards the two centrosomes are move apart to form the opposite poles of the mitotic spindle. Over the time, many different proteins have been proposed as potential centrosome linker components, but the exact function and the structure of the centrosome linker is still unclear.

During this study, I identified Ninein as a centrosome linker component downstream of C-Nap1 that links the two centrosomes together in RPE1 cells. In contrast, in HCT116, U2OS and Caco-2 cells Rootletin and Ninein establish centrosome cohesion together. Overamplified centrosomes, which occur either naturally in Caco-2 cancer cells or after *PLK4*-induced centrosome amplification use the linker for centrosome clustering in interphase. Under these conditions, Rootletin showed centrosome linker function in RPE1 cells. Surprisingly, despite linker disassembly in G2/prophase, the absence of C-Nap1 extends the duration of metaphase in cells with centrosome amplification. This is evidenced through the continued activation of the spindle assembly checkpoint (SAC), as suggested by the signal accumulation of MAD1 and BUB1 at kinetochores. The reduced MT nucleation activity of centrosomes lacking C-Nap1 and the prolonged nuclear envelope breakdown in linker-deficient prophase cells are likely to be a reason for the observed mitotic defects. Consequently, C-Nap1 deficient cells with centrosome amplification show an increase in multipolar spindle formation and chromosome mis-segregation. These defects become more pronounced with partial inhibition of the kinesin HSET, a protein that typically clusters supernumerary centrosomes during mitosis.

In conclusion, this study sheds light on the cell type-dependent differences of the centrosome linker and the function in clustering overamplified centrosomes during interphase. Moreover, the results in C-Nap1 deficient cells with multiple centrosomes indicate an unknown impact of the centrosome linker on pseudo-bipolar spindle formation and chromosome segregation in mitosis.

Zusammenfassung

Das Zentrosom ist das wichtigste Mikrotubuli-Organisationszentrum (MTOC) in tierischen Zellen. Es besteht aus Mutter- und Tochterzentriolen und ist von der sogenannten perizentriolaren Matrix (PCM) umgeben. Während der Interphase haben Zellen nur ein MTOC, welches aus zwei Zentrosomen besteht, die durch die Zentrosomenkohäsion zusammengehalten werden. Das derzeitige Verständnis der Zentrosomenkohäsion umfasst zwei verschiedene Wege: den Zentrosomen-Linker und die auf Mikrotubuli (MT)-basierende Kohäsion. Die am besten beschriebenen und am meisten untersuchten Zentrosomen-Linkerproteine sind C-Nap1 und Rootletin und sein Bindepartner CEP68. C-Nap1 bildet eine ringförmige Struktur am proximalen Ende der beiden Zentriolen und organisiert die Rootletin/CEP68 Filamente. In der G2/Prophase phosphoryliert Nek2 kinase (Never in mitosis A-related kinase 2) die Linker Proteine C-Nap1 und Rootletin, um den Zentrosomenlinker aufzulösen, was zur Trennung der Zentrosomen führt. Anschließend werden die beiden Zentrosomen auseinander bewegt, um die entgegengesetzten Pole der mitotischen Spindel zu bilden.

Während dieser Studie identifizierte ich Ninein als ein Zentrosomen-Linker-Protein stromabwärts von C-Nap1, das die beiden Zentrosomen in RPE1-Zellen miteinander verbindet. Im Gegensatz dazu stellen Rootletin und Ninein in HCT116-, U2OS- und Caco-2-Zellen gemeinsam den Zusammenhalt der Zentrosomen sicher. Überamplifizierte Zentrosomen, die entweder natürlicherweise in Caco-2-Krebszellen oder nach PLK4-induzierter Zentrosomen-Amplifikation vorkommen, nutzen den Linker zur Bildung von Zentrosomen-Clustern in der Interphase. Unter diesen Bedingungen zeigte Rootletin eine Zentrosomen-Linker-Funktion in RPE1-Zellen. Trotz der Auflösung des Linkers in der G2/Prophase verlängerte das Fehlen von C-Nap1 überraschenderweise die Dauer der Metaphase in Zellen mit Zentrosomen-Amplifikation. Dies wird durch die anhaltenden Aktivierung des Spindle assembly checkpoints (SAC) deutlich, was durch die Akkumulation von MAD1- und BUB1-Signalen an den Kinetochoren beobachtet wurde. Die verringerte MT-Nukleationsaktivität von Zentrosomen ohne C-Nap1 und die verlängerte Auflösung der Kernhülle in Zellen ohne Linker sind wahrscheinlich ein Grund für die beobachteten mitotischen Defekte. Folglich zeigen C-Nap1-defiziente Zellen mit Zentrosomen-Amplifikation eine Zunahme von Zellen mit multipolaren Spindeln und

Fehlern in der Chromosomensegregation. Diese Defekte verstärken sich durch die teilweise Hemmung des Kinesins HSET, einem Protein, das normalerweise überzählige Zentrosomen während der Mitose bündelt.

Zusammenfassend zeigt diese Studie die zelltypabhängigen Unterschiede des Zentrosomen-Linkers und die Funktion bei der Clusterbildung von überamplifizierten Zentrosomen während der Interphase. Darüber hinaus deuten die Ergebnisse in C-Nap1-defizienten Zellen mit mehr als zwei Zentrosomen auf einen unbekannten Einfluss des Zentrosomen-Linkers auf die pseudo-bipolare Spindelbildung und die Chromosomensegregation während der Mitose hin.

1 Introduction

1.1 The eucaryotic cell cycle

1.1.1 Overview

Cell division is an essential program that ensures continuity and progression of life. All living organisms use cell division to reproduce and develop. The basic principle behind is that a new cell can only duplicate from an already existing cell (Alberts et al. 2022). Cell division can produce a completely new organism, such as in unicellular bacteria and yeast. In contrast, multicellular organism, like mammals, need a sophisticated series of cell division and several rounds of duplication to build up a functional organism (Alberts et al. 2022). In adult mammals, cell division is essential for survival, because it is needed to guarantee the replacement of dead or dying cells. The orderly sequence of duplication and division events are called the cell cycle (Figure 1) (Alberts et al. 2022; Hartwell and Weinert 1989; Vermeulen, Van Bockstaele, and Berneman 2003). The cell cycle varies among different species; however, the underlying objective is universal: transferring the genetic information to the subsequent generation of newly formed cells (Alberts et al. 2022).

The cell cycle is composed of two major stages: interphase and M phase. During interphase the cell takes all necessary precautions for the upcoming mitosis, like cell growth and DNA replication. Interphase is subdivided into G1, S and G2 phase (Figure 1). After mitotic exit in G1 phase (Gap phase 1), the cell focuses on growing via increasing the cellular content and expressing genes needed for DNA replication to prepare for the upcoming synthesis phase (S phase). During S phase the DNA in each chromosome is replicated to ensure two identical copies of the genome. G2 phase (Gap phase 2) is between S phase and mitosis, where the cell size is further increasing to prepare for the cell division during the upcoming M phase (Alberts et al. 2022). In addition, genes are expressed that are needed for mitosis.

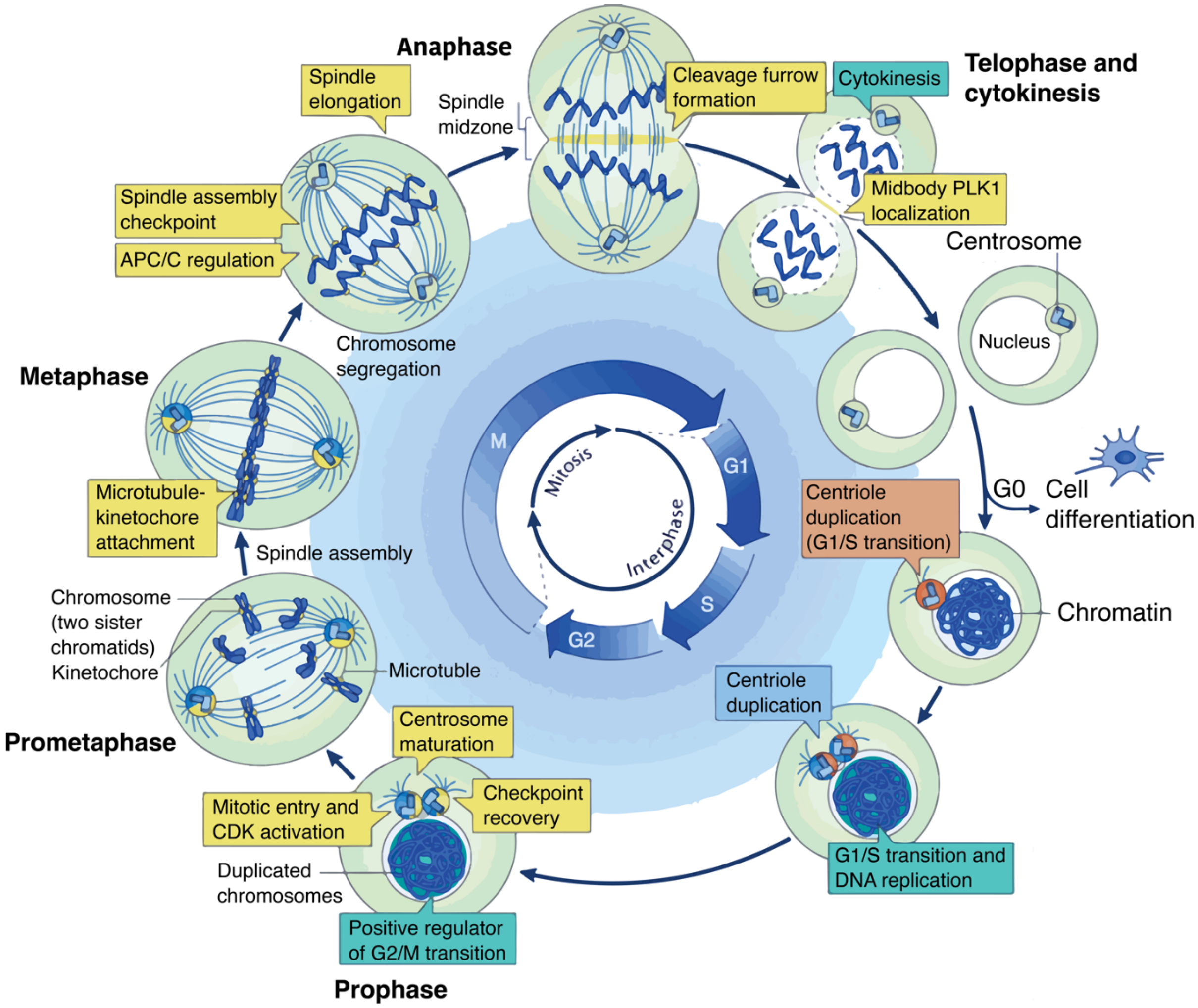

Figure 1 Schematic presentation of the eukaryotic cell cycle phases. The cell cycle is divided into interphase (G1, S, G2 phase) and mitosis (M phase). During interphase the cell duplicates the DNA and centrioles to prepare for chromosome segregation in mitosis. After spindle assembly in metaphase the duplicated chromosomes are segregated and move to the opposite spindle poles in anaphase. Finally, cytokinesis is separating the cytoplasm to create two independent daughter cells. The cell cycle is completed. Figure is adapted and modified from Zitouni et al., 2014.

The M phase consists of prophase, prometaphase, metaphase, anaphase and telophase (Figure 1) (Alberts et al. 2022). During prophase the replicated chromosome, now each consisting of two connected sister chromatids, condensate and the kinetochores can start to assemble onto the centromeric regions (Alberts et al. 2022; Gascoigne and Cheeseman 2011). Outside of the nucleus the two centrosomes start to separate to initiate mitotic spindle formation. Afterwards the nuclear envelope breakdown (NEBD) happens in prometaphase. The spindle MTs connect to the joined together sister chromatids via the attachment to their two opposite kinetochores. The counterbalance of the pulling forces generated by kinetochore MTs originating from the opposite spindle poles are required in metaphase for correct chromosome alignment in the center of the mitotic spindle (metaphase plate) (Alberts et al. 2022). In anaphase the replicated chromosomes synchronously separate and move apart to the spindle poles to start forming the daughter chromosomes. After the daughter chromosomes arrived at the opposite poles of the mitotic spindle during telophase, they start to decondense. A new nuclear envelope (NE) starts to form around each set of chromosomes. The formation of two new nuclei marks the end of mitosis. Cytokinesis ensures the division of the cytoplasm starting from the spindle midzone to separate the cell into two daughter cells each with one nucleus. The cell cycle is now completed (Alberts et al. 2022; Vermeulen et al. 2003).

However, a cell can exit the cell cycle after discontinuing of cell proliferation and division. This quiescence phase, also called G0 phase, is often find in differentiated or stem cells. Under certain conditions, like growth stimuli, some cell types such as liver and stem cells can re-enter the cell cycle (Alberts et al. 2022; Vermeulen et al. 2003). Figure 1 shows a schematic overview of the cell cycle including the different phases with important biological events.

1.1.2 Cell cycle checkpoints

All steps and events during the cell cycle are tightly controlled by a complex network of regulatory proteins. The cell cycle control system consists of biochemical switches (on/off) to initiate specific cell cycle events and to enhance the accuracy and reliability of cell cycle progression (Alberts et al. 2022). Most important is the regulation at three major transition phases during cell cycle progression, starting with the cell cycle entry (START point) in late G1, followed by the G2/M transition (Figure 2). After metaphase-to-anaphase transition the cell can complete mitosis and divide into two daughter cells via cytokinesis (Alberts et al. 2022).

To control and regulate the transition stages four important checkpoints need to be passed and satisfied (Basu et al. 2022; El-Aouar Filho et al. 2017; Lukas, Lukas, and Bartek 2004; Vermeulen et al. 2003). The G1 checkpoint controls, beside cell size and environmental conditions (nutrients, growth factors, etc.), also DNA damage in the cell before entering S phase. During S phase the intra-S checkpoint ensures complete duplicated DNA without damages similar to the following G2/M checkpoint that additionally checks the cell size (Basu et al. 2022). After entering the M phase, the spindle assembly checkpoint (SAC) detects improper alignment of chromosomes to the mitotic spindle by checking MT attachment at the kinetochores (Alberts et al. 2022). Defects in MT attachment cause activation of different SAC components like Mitotic arrest deficient (Mad) and budding uninhibited by benomyl (Bub) proteins (Vermeulen et al. 2003). To satisfy the SAC and proceed to anaphase all chromosomes need to be correctly bi-orientated and aligned.

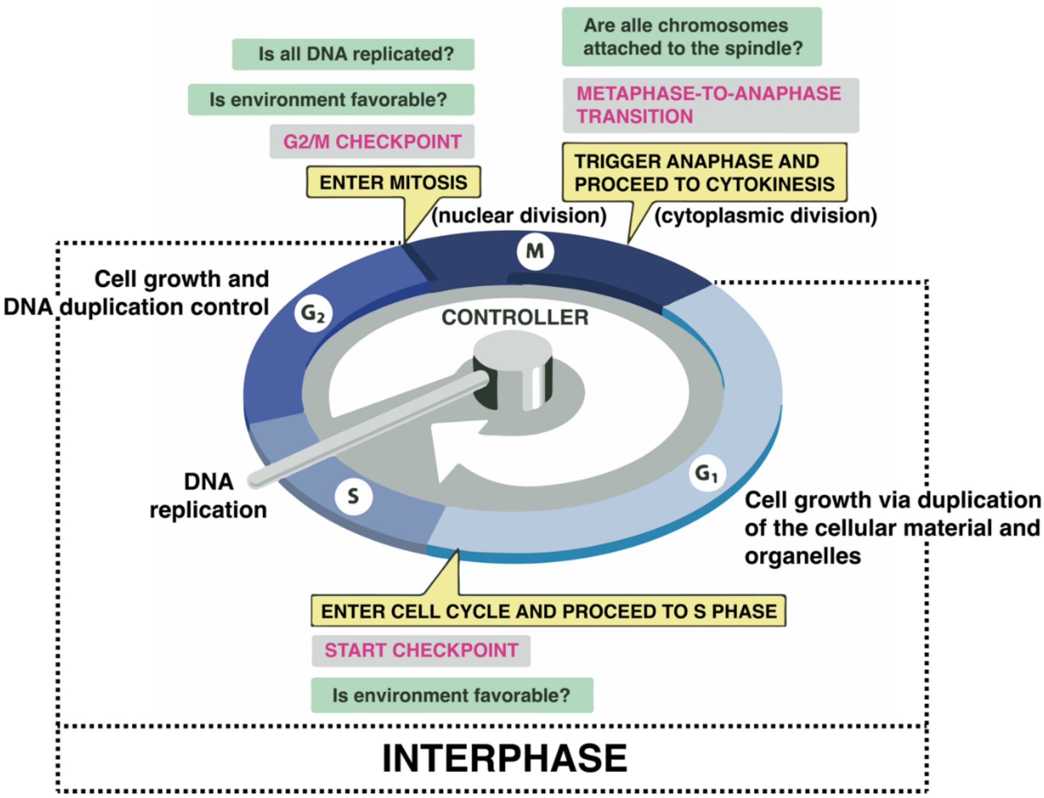

Figure 2 Regulation of the cell cycle. The cell cycle control system is essential to initiate the major events, like DNA replication, mitosis and cytokinesis, during the cell cycle. The signal feedback system ensures that only after correct completion of a cell cycle event the cell can progress further. Otherwise, the control system initiates cell arrest. Different checkpoints during the cell cycle are important for correct and error-free cell division. Figure is adapted and modified from Alberts et al., 2022.

1.1.3 Regulation of the cell cycle

The two key regulator proteins to ensure correct cell division are the cyclin-dependent kinases (CDKs), a family of serine/threonine protein kinases, and the cyclins (Basu et al. 2022; El-Aouar Filho et al. 2017; Martínez-Alonso and Malumbres 2020; Vermeulen et al. 2003). As the name implies already, CDK activity depends on the binding to cyclin. The cyclin-CDK complex activates the protein kinase to trigger specific events during the cell cycle. Compared to the CDK levels, which stay constant over the cell cycle, protein levels of cyclins oscillate during the cell cycle progression to provide time specific activity of the resulting protein complex (Martínez-Alonso and Malumbres 2020). Additionally, CDKs get activated, inhibited or degraded via CDK-activating kinases (CAKs), CDK-inhibitor kinase (CIKs; e.g. Wee1) and ubiquitin-ligase protein complexes (e.g. ubiquitin ligase Skp, Cullin, F-box complex (SCF)) (Alberts et al. 2022; Glotzer, Murray, and Kirschner 1991; Lim and Kaldis 2013; Matthews, Bertoli, and de Bruin 2022; Nakayama and Nakayama 2006).

Cyclins are divided into different classes, defined by the cell cycle stages where they form a complex with the CDK subunit to activate its function (Alberts et al. 2022; Martínez-Alonso and Malumbres 2020). G1- and G1/S-cyclins are important to enter the cell cycle whereas S-cyclins are important to trigger DNA duplication. M-cyclins stimulate the transition from G2 to mitosis (Alberts et al. 2022). In mammalian cells usually cyclin D is important for the G0-to-G1 transition to initiate the cell cycle entry and for the G1 progression (Martínez-Alonso and Malumbres 2020). Cyclin E controls DNA replication during S phase. In G2/M cyclin A regulate chromosome segregation and start of mitosis followed by the control through early mitosis by cyclin B, also called the mitotic cyclin. An overview of the important cyclins and their CDK partners including biological processes during cell cycle is shown in Figure 3.

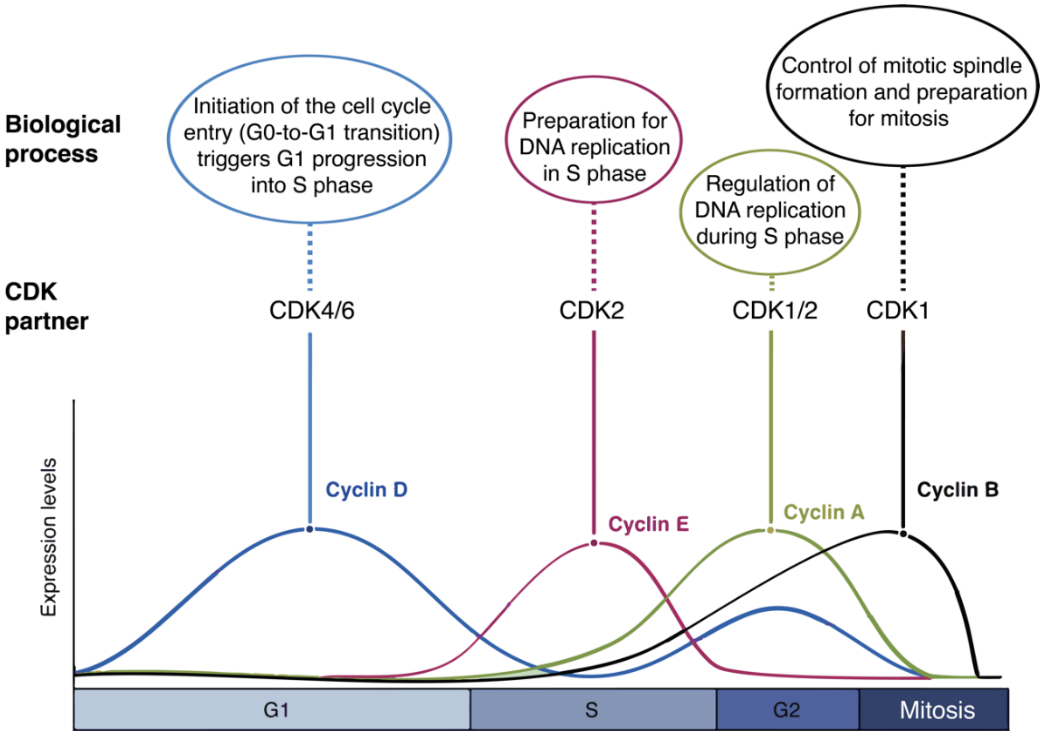

Figure 3 The Cyclin-CDK dependent cell cycle regulation. Linear representation of the cell cycle phases including the Cyclins, their CDK partners and substrates linked to significant cellular processes. Figure is adapted and modified from Martínez-Alonso & Malumbres, 2020.

Various protein kinases, e.g. ataxia-telangiectasia-mutated (ATM) and ataxia and rad3 related (ATR), act as sensors for DNA damage and stabilize p53 after activation. Activated p53 causes expression of p21 and other DNA damage response proteins (Basu et al. 2022; Lukas et al. 2004; Vermeulen et al. 2003). To arrest the cell p21 inhibits CDK activity via binding directly to the CDK-Cyclin complexes. DNA repair proteins try to fix the damage but if the DNA damage is irreparable p53 will start to initiate apoptosis to eliminate the defective cell (Basu et al. 2022; Malumbres and Barbacid 2009; Vermeulen et al. 2003).

1.2 The centrosome

1.2.1 Structure and function of the centrosome

The centrosome, a membraneless organelle, was first discovered and described by the revolutionary work from Boveri, van Benenden, and others in the late 19^{th} century. It consists of two cylindrical MT-based core structures, called centrioles, and is surrounded by a protein dense matrix, the pericentriolar material (PCM) (Figure 4). In average a human centriole is 500 nm long (from proximal to distal end) with a diameter of 250 nm (Bowler et al. 2019; Gönczy and Hatzopoulos 2019; Winey and O'Toole 2014). The hollow barrel structure shows an impressive nine-fold radial symmetry of MTs (Gönczy and Hatzopoulos 2019). The centriole core is based on a cartwheel-like scaffold at the proximal end of the centriole that controls assembly of MT triplets (Figure 4A) (Gönczy and Hatzopoulos 2019). SAS-6 is the key component for the formation of the central hub with the nine spokes to initiate the symmetrical nine-fold architecture (Gönczy and Hatzopoulos 2019; Guichard et al. 2013; Winey and O'Toole 2014). On top of the spokes is the pinhead structure, mainly composed of CEP135. The pinhead connects the cartwheel with the centriolar MT triplets (Fujita, Yoshino, and Chiba 2016; Kim et al. 2008). Each MT triplet contains A-, B- and C-tubules. The connection between the A-tubule of one triplet to the C-tubule of the adjacent triplet is called A-C linker and is another important structural component that probably helps to stabilize the centriole structure (Figure 4A) (Fujita et al. 2016; Guichard et al. 2013). After centriole elongation with the help of CPAP, SPICE and CEP120, CP110 and CEP97 limit the centriole length by acting as 'cap' for the MTs on the distal end of the centriole (Figure 4B) (Gönczy and Hatzopoulos 2019; Winey and O'Toole 2014).

EM-images of the PCM usually showed an electron dense cloud around the centrioles. Interestingly, high resolution microscopy revealed that it is a hierarchically organized structure based on different proteins layers made of CEP192, CEP152, Cdk5Rap2, NEDD1 and γ-tubulin (Figure 4C) (Fry et al. 2017). The γ-tubulin ring complex (γTuRC) is the main MT nucleation complex of the PCM (Rale, Kadzik, and Petry 2018). To increase the necessary MT nucleation ability for spindle assembly in mitosis the PCM needs to expand (Figure 4C). For this reason, the mitotic PCM is less organized compared to the PCM during interphase (Fry et al. 2017; Rale et al. 2018).

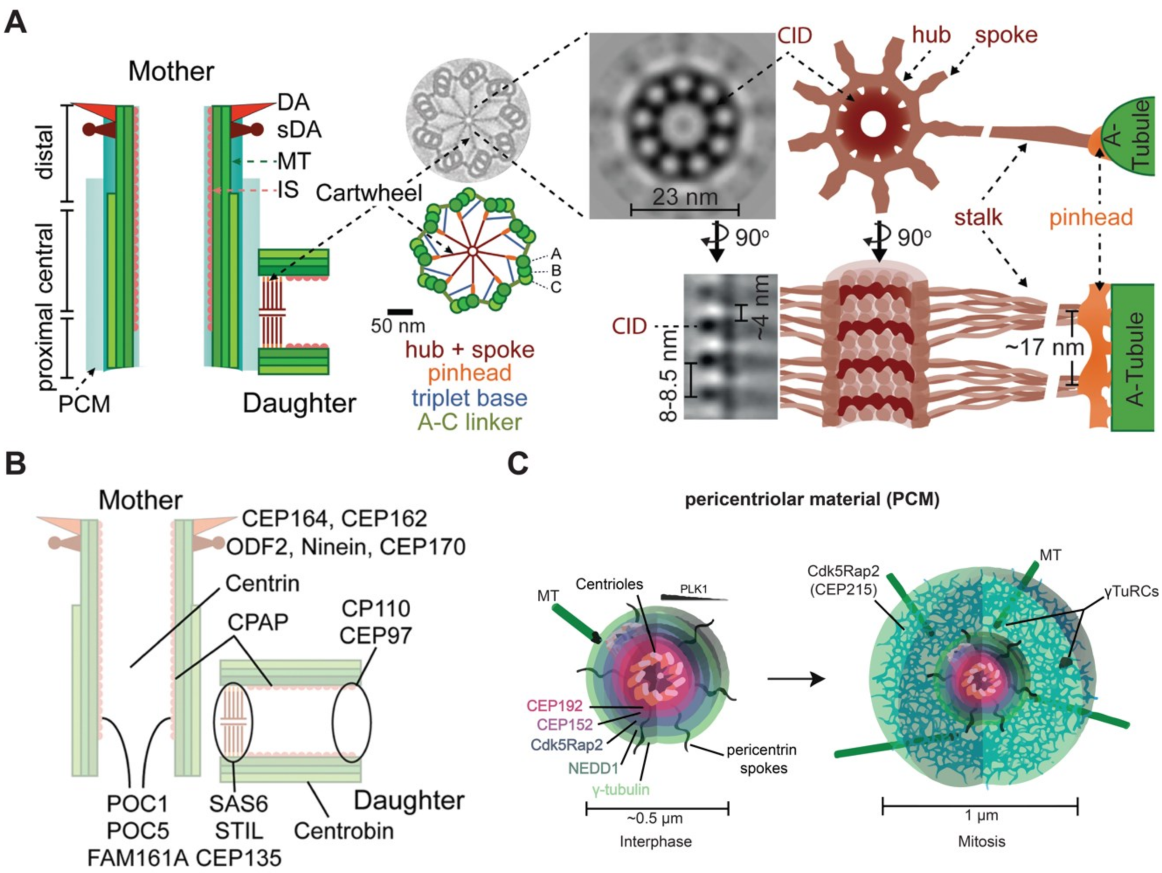

Figure 4 Structure of the centrosome. A Schematic overview of the nine-fold symmetric centriole structure including the cartwheel, the central hub with the nine spokes and triplet bases with the A-C linker. **B** Important protein localizations at the mother centriole (DAs and SDAs) and at the daughter centriole. **C** Hierarchical organisation of the PCM in interphase and mitosis. **A, B** are taken and adapted from Jana, 2021. **C** is taken and modified from Rale et al., 2018

The two interphase centrioles of a centrosome are distinct in age and structure. The older centriole, termed as mother, contains sub-distal (SDAs) and distal appendages (DAs) functioning in MT anchoring and ciliogenesis (Figure 4B) (Mazo et al. 2016). The younger centriole, called daughter centriole, will acquire this structure one and half cell cycles later in the upcoming mitosis. The DAs proteins, like CEP164, are essential for the mother centriole to convert into a basal body after docking to the plasma membrane in mammalian cells (Figure 4B) (Mazo et al. 2016; Yang et al. 2018). In contrast, SDAs proteins, mostly ODF2, Ninein and CEP170, play a crucial role for MT anchoring and nucleation at the centrosome to spatial organize MT (Figure 4B) (Bowler et al. 2019; Mazo et al. 2016). Because of this, the centrosome is the main microtubule-organizing center (MTOC) of animal cells (Bornens 2002; Doxsey 2001; Lüders and Stearns 2007). Centrosomes are important for several processes like cell polarity, cell migration, signal transduction pathways, chromosome segregation in mitosis and cilia formation (Conduit, Wainman, and Raff 2015; Loncarek and Bettencourt-Dias 2018; Mazo et al. 2016; Miller et al. 2009; Nigg and Holland 2018). Additionally, centrosomes are fundamental in mammalian cells for the timing of mitosis and the proper position and formation of the bipolar mitotic spindle.

1.2.2 The centrosome cycle

The centrosome duplicates only once per cell cycle, what is called the centrosome cycle (Figure 5) (Banterle and Gönczy 2017; Kochanski and Borisy 1990; Meraldi and Nigg 2002; Nigg and Holland 2018). The centrosome number and structure are strictly controlled during each cycle to ensure a successful bipolar spindle formation and chromosome segregation in mitosis (Fujita et al. 2016). Various studies showed that centrosome duplication defects occur in diverse human diseases, including cancer (Fujita et al. 2016; Meraldi and Nigg 2002). Each cell contains a pair of centrosomes. Dependent on the cell cycle phase one centrosome consist out of one or two centrioles. After mitotic exit in telophase/early G1 phase the protease separase aided by polo kinase PLK1 cleaves the orthogonal connection between the two centrioles (mother and daughter), called centriole disengagement, to ensure a new round of centriole duplication (Fujita et al. 2016; Lee and Rhee 2012). Afterwards the daughter centriole from the last cell cycle can assemble a new pro-centriole during the upcoming S phase (Meraldi and Nigg 2002). G1 cells carry two centrosomes each harboring one centriole surrounded by the PCM. Because of the semiconservative duplication mechanism and the cell cycle dependent maturation, the two G1 centrioles are distinct (Meraldi and Nigg 2002). Only the older mother centriole carries DA and SDA, respectively. The daughter centriole gains these structures after passing the upcoming mitosis (Nigg and Stearns 2011). During the entire interphase, cells contain only one main MTOC consisting of the two centrosomes linked together via a proteinaceous linker, known as the centrosome linker, and a network of interdigitating microtubules (Nigg and Stearns 2011; Panic et al. 2015).

At the G1/S phase transition the scaffold-based duplication mechanism is initiated by the recruitment of the Polo-like kinase 4 (PLK4) to the outside wall of the two mother centrioles by the centrosomal proteins CEP152 and CEP192 (Arquint and Nigg 2016; Kratz et al. 2015). Centriole duplication happens during S-phase controlled by PLK4 together with STIL as key regulators to secure correct cartwheel formation and centriole number by controlling that only one cartwheel on each centriole is formed

(Arquint and Nigg 2016; Kratz et al. 2015; Ohta et al. 2018). SAS-6, which is recruited by STIL, is accumulating in the typical nine-fold symmetry to start building the cartwheel structure, to create a platform to assemble MTs to form the wall of the new pro-centriole (Kratz et al. 2015). The newly formed centriole is assembled at the existing mother centriole in an orthogonally position and then elongate until the beginning of mitosis (Bettencourt-Dias et al. 2005; Habedanck et al. 2005; Kleylein-Sohn et al. 2007; Takao et al. 2019; Yamamoto and Kitagawa 2019). CPAP, SPICE1 and CEP120 are important proteins to ensure the correct length of the newly formed daughter centrioles.

Newly formed centrioles gradually convert into centrosomes through the recruitment of PCM proteins and so gain the ability for MT nucleation and assembly of a daughter centriole (Fu et al. 2016; Izquierdo et al. 2014; Meraldi and Nigg 2002) after complete centriole-to-centrosome conversion with the centriole disengagement in early G1 phase of the next cell cycle. This process is called centrosome maturation and is initiated by PLK1 that promotes Aurora A kinase recruitment to the centrosomes for the accumulation of PCM proteins (Fujita et al. 2016).

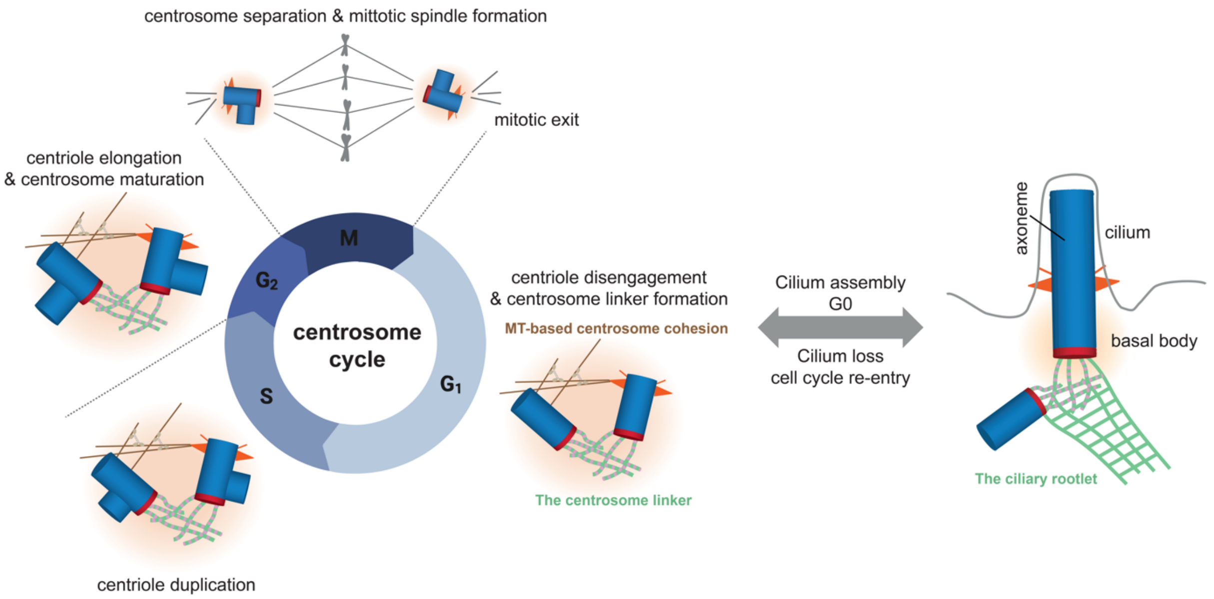

Figure 5 Schematic view of the centrosome cycle. Like DNA the centrosome duplicates once per cell cycle. The tight, orthogonal connection between the mother and the daughter centriole is lost, when a cell enters interphase, but the centrosome cohesion keeps them into one MTOC. Centrosome duplication and PCM recruitment to the newly formed centrosome happens during S to G2 phase. The centrosome linker is mostly dissolved in late G2/prophase to allow mitotic spindle formation. When a cell exits mitosis, centriole disengagement happens. At this point of the cell cycle daughter centrioles are mainly matured into a centrosome meaning that they have gained MT nucleation and centriole duplication ability.

Centrosome separation happens at the G2/M transition by the kinase Nek2 (Never in mitosis A-related kinase 2) (Fry et al. 2012; A M Fry, Meraldi, and Nigg 1998; Moniz et al. 2011) that inactivates centrosome cohesion. In late G2 phase Nek2 kinase can phosphorylate several centrosome linker proteins, including C-Nap1, Rootletin and CEP68, resulting in dissolution of the physical linkage between the two centrosomes (Panic et al. 2015). Afterwards the MT-based forces maintain the proximity of the two centrosomes until the SDAs become disassembled by Nek2 kinase, leading to subsequent separation of the two centrosomes. To ensure proper mitotic spindle formation the kinesin motor protein Eg5 (KIF11, kinesin-5 family) pulls the two centrosomes further apart to opposite directions to form the spindle poles of the mitotic spindle (Hata et al. 2019; Remo et al. 2020; Sawin et al. 1992).
At mitotic exit, cytokinesis divides the cytoplasm and the centrosome into two daughter cells. A new cell and centrosome cycle can start underlining that the semiconservative duplication process of the centrosomes is tightly synchronized with the cell cycle (Figure 5).

Cilia are membrane-bound MT-based structure present in various cell types in mammals and are important for cell signaling and motility. In quiescent/G0 cells a matured mother centriole can associates with the plasma membrane to build a basal body competent for cilium formation (Figure 5) (Fu, Hagan, and Glover 2015). In contrast to the basal body the axoneme of the cilium is consisting of MT duplets not triplets. A major structural component of the cilium is the ciliary rootlet, which is based on Rootletin, a protein what is also associated with centrosome linker filaments (Yang et al. 2002).

1.2.3 Centrosome aberrations in human diseases

Structural and numerical centrosome aberrations are found in a variety of human diseases such as cancer, neurodevelopmental disorders and ciliopathies (Jaiswal and Singh 2021; Nigg and Holland 2018). The most studied and best described development disorders are autosomal recessive primary microcephaly (MCPH) disorders, where infants are born with smaller brain and head size (Jaiswal and Singh 2021). Because of the diverse function of cilia in cells, faulty cilia formation, organization or function can cause severe disorders like retinal dystrophy, neurocognitive defects, infertility or respiratory problems (Jaiswal and Singh 2021).

In cycling cells centrosome number and duplication is tightly controlled and synchronized with the cell cycle. Multi-ciliated epithelial cells are one exception because they generate hundreds of centrioles that convert to basal bodies for multiple cilia formation (Nigg and Holland 2018).
Although it has been shown that cells can divide in the absence of centrosome, there are essential for proper spindle position and the timing of mitosis. The consequence of improper spindle formation and chromosome mis-segregation is a prolonged mitosis which is leading to cell cycle arrest or cell death via USP28-53BP1-p53-p21 pathway activation (Figure 6) (Nigg and Holland 2018). Therefore, p53 deficient cancer cells often fail to respond to centrosome loss and cannot sense numerical centrosome irregularities in the cell (Goundiam and Basto 2021).
The opposite defect is the accumulation of extra centrosomes, termed centrosome amplification, caused by dysregulation of centrosome duplication, cell cycle arrest or failed cell division. Centrosome amplification is observed in tumorigenesis and metastasis and is associated with chromosomal instability (CIN) and cancer progression (Figure 6) (Conduit et al. 2015; Ganem, Godinho, and Pellman 2009; Godinho and Pellman 2014; Jaiswal and Singh 2021). While facing high risk of multipolar spindle formation and mitotic failure, cancer cells cluster and organize centrosomes into a pseudo-bipolar spindle, bypassing the spindle assembly checkpoint and so avoiding cell cycle arrest or death (Godinho, Kwon, and Pellman 2009; Kwon et al. 2008; Remo et al. 2020). A well-studied centrosome clustering mechanism is provided by the minus-end-directed kinesin motor protein HSET (KIFC1, a member of Kinesin-14 family) (Ganem et al. 2009; Kwon et al. 2008; Marthiens, Piel, and Basto 2012; Vitre et al. 2020). The CEP215-HSET complex was shown to be crucial for centrosome clustering and so ensures cancer cell survival and tumor progression (Chavali et al. 2016). HSET promotes pseudo-bipolar spindle formation in cells with centrosome amplification via MT bundling and sliding resulting in spindle pole focussing (Kwon et al. 2008). Several other factors including the SKA1, 2, 3 kinetochore complex, SAC components and the anaphase-promoting complex (APC/C) are also shown to be important for the pseudo-bipolar spindle formation (Drosopoulos et al. 2014; Ganem et al. 2009; Kwon et al. 2008).
In the recent years centrosome amplification has been associated with different kind of tumors like colorectal, bone, breast or kidney and their progression (Jaiswal and Singh 2021; Remo et al. 2018).

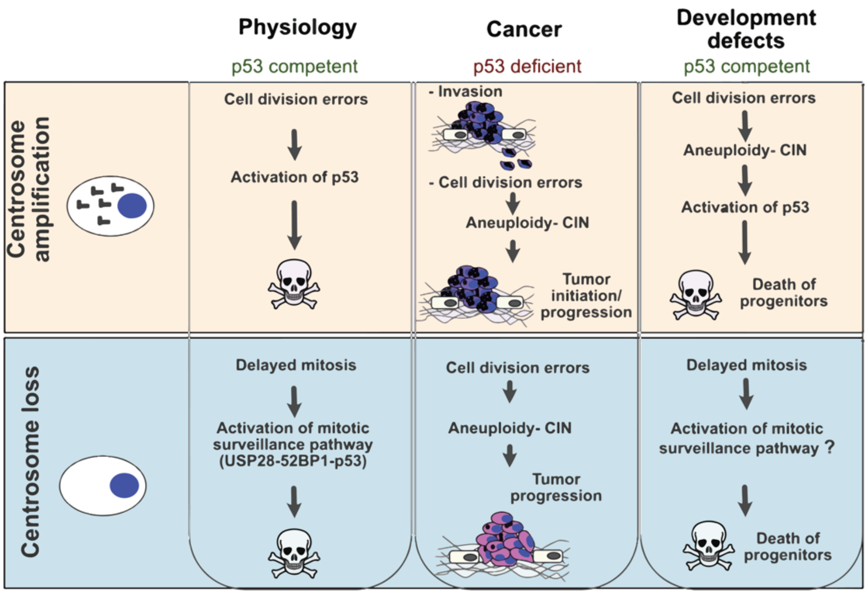

Figure 6 Centrosome aberrations in cancer. Dependent on the p53 status, the cell can respond differently to numerical centrosome aberrations (amplification or loss). Centrosome amplification is a commonly found feature in different cancer cells and tumors. Figure is adapted and modified from Goundiam & Basto, 2021.

1.3 The centrosome cohesion

During interphase the two centrosomes are joined together via centrosome cohesion. The current understanding of centrosome cohesion includes two different pathways: the centrosome linker and MT-based cohesion (Figure 7). The cooperative work of these two pathways is crucial to keep the centrosome close together until centrosome separation in late G2 to guarantee correct spindle formation and timing during mitosis.

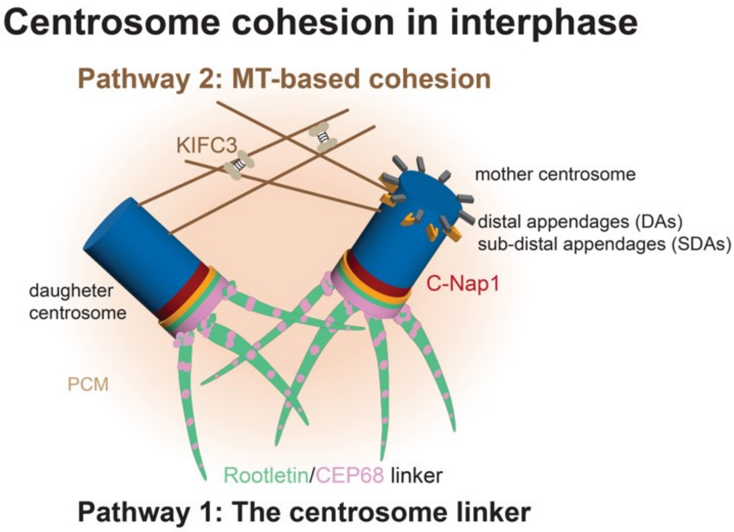

Figure 7 Centrosome cohesion during interphase. The linkage between the two centrosomes is known as centrosome cohesion. Two pathways contribute to the centrosome cohesion: the centrosome linker and the microtubule-based cohesion. These two pathways function redundantly to keep the centrosomes together in interphase (Remo et al., 2020).

1.3.1 The centrosome linker

The centrosome linker is a proteinaceous network creating a physical attachment between the proximal ends of both centrioles. The best described and most studied centrosome linker proteins are C-Nap1 (encoded by *CEP250*) and Rootletin (encoded by *CROCC*) (Bahe et al. 2005; Flanagan et al. 2017; Panic et al. 2015; Remo et al. 2020; Vlijm et al. 2018). C-Nap1 forms a ring like structure at the proximal end of both centrioles and organizes the Rootletin/CEP68 filaments (Bahe et al. 2005; Vlijm et al. 2018). In late G2 Nek2 kinase efficiently phosphorylates C-Nap1, Rootletin and CEP68 to dissolve the centrosome linker, which then leads to centrosome separation. Afterwards the two centrosomes can move apart to form the two poles of the mitotic spindle (Agircan, Schiebel, and Mardin 2014; Panic et al. 2015). Over the time many different proteins were proposed as potential centrosome linker candidates, like LRRC45, CEP215, Centlein, CEP85, DVL-2, CCDC102B and β-Catenin, but their role and exact function and the structure of the centrosome linker is still unclear (Bahe et al. 2005; Bahmanyar et al. 2008; Cervenka et al. 2016; Chen et al. 2015; Fang et al. 2014; Graser, Stierhof, and Nigg 2007; He et al. 2013; Xia et al. 2018).

The assembly and disassembly of the centrosome linker are tightly synchronized with the centrosome cycle. After centriole disengagement at mitotic exit, the orthogonal connection between the two centrioles is lost, making it possible to re-establish the filamentous centrosome linker structure between the two proximal ends (Figure 8A). First, C-Nap1 is recruited to the proximal ends of both centrioles via its binding partner CEP135 (Hardy et al. 2014; Kim et al. 2008). This interaction is essential to anchor the centrosome linker fibres to the centrioles and ensure the physical connection.

As describe above C-Nap1 is acting like a platform that anchors centrosome linker proteins to the proximal end of centrioles. Rootletin and CEP68 were discovered as the main structural components that form the linker filaments. STED super resolution microscopy made it possible to resolve the highly ordered interdigitating network of Rootlein/CEP68 fibres (Vlijm et al. 2018). The large coiled-coil protein Rootletin can build thin filaments via self-assembly, which get bundled with the help of CEP68 to thick repetitive filaments creating the basis for the fibrous centrosome linker structure (Figure 8B) (Agircan et al. 2014; Mahen 2018; Vlijm et al. 2018).

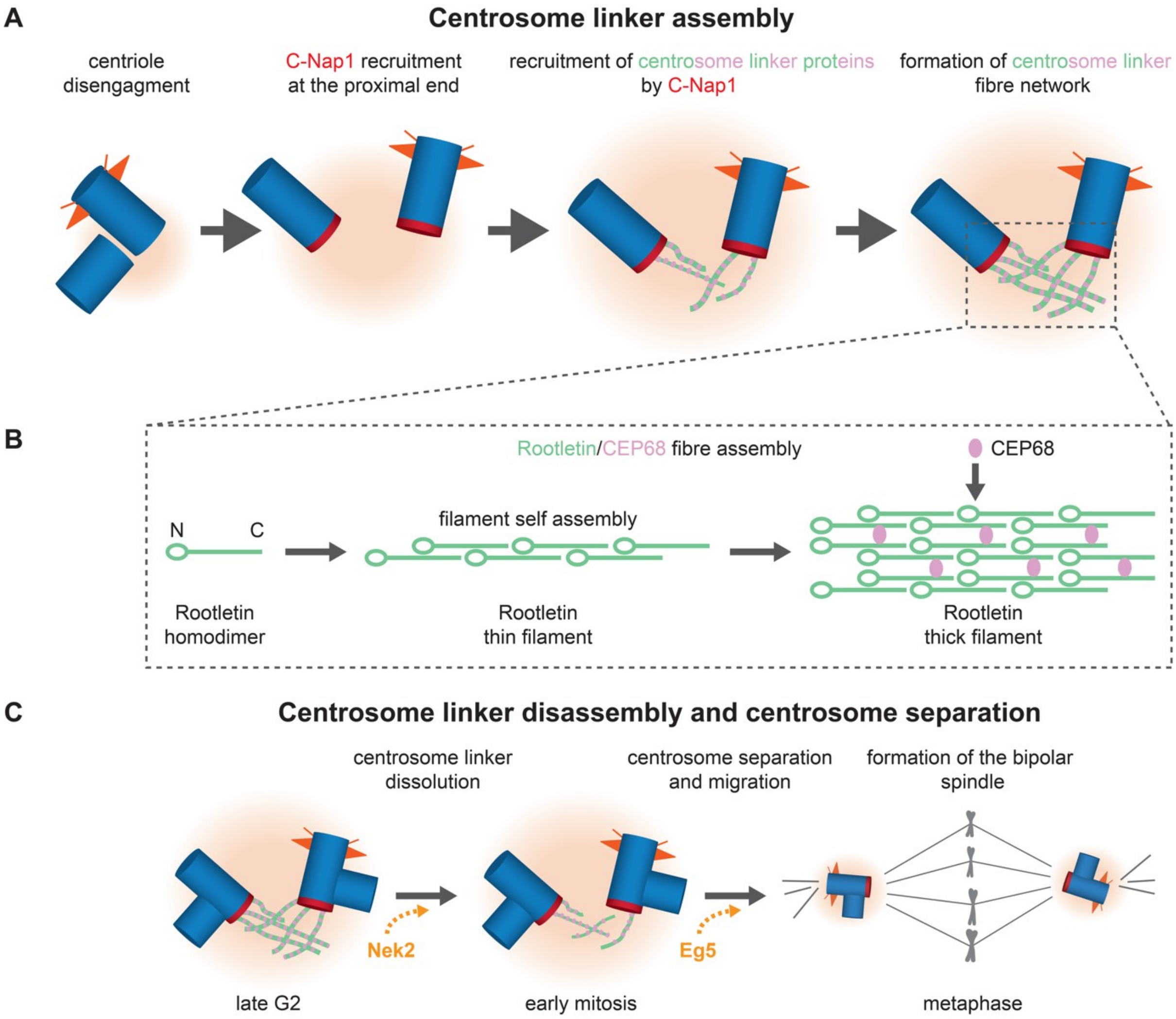

Figure 8 Structure and function of the centrosome linker. A, B The centrosome linker re-assembles after centriole disengagement in early G1 phase (A). CEP135 recruits C-Nap1 to the proximal ends of the centrioles (A) to initiate Rootletin/CEP68 fibre assembly (B). **C** Centrosome linker disassembly followed by centrosome separation happens at the onset of mitosis. Afterwards Eg5-dependent forces move the two centrosomes apart to form the mitotic spindle.

The centrosome linker connects the two centrosomes throughout the entire interphase until late G2 phase. Rootletin/CEP68 filaments interdigitate and most likely low affinity interactions between the filaments join both centrosomes together. Nek2 kinase, the key player for linker dissolution, gets activated and recruited to the centrosome via the mammalian sterile 20-like kinase (Mst2) kinase (component of the Hippo pathway (Mardin et al. 2010)) and phosphorylates several linker proteins including C-Nap1, Rootletin and CEP68 (Figure 8C) (Agircan et al. 2014; Andrew M Fry et al. 1998; Mardin et al. 2011; Meraldi and Nigg 2001). The interaction between CEP135 and C-Nap1 is lost after Nek2-dependent phosphorylation. Afterwards the linker starts to disassemble triggering centrosomes separation and movement (Hardy et al. 2014). The motor protein Eg5 pulls the two centrosomes apart to form the poles of the mitotic spindle (Figure 8C).

The timing of centrosome linker disassembly is important for correct spindle formation and efficient chromosome segregation. Usually, centrosome separation and migration to the spindle poles is happening before NEBD, called the prophase pathway (Kaseda, McAinsh, and Cross 2012; Remo et al. 2020). However, if this mechanism fails, the cells can follow a second route, the prometaphase pathway. Here the centrosome separation occurs after NEBD, which demands a difficult and complex cooperation between forces created by kinetochore-MT and actomyosin-based mechanisms (Kaseda et al. 2012; Rattner and Berns 1976; Rosenblatt 2005; Rosenblatt et al. 2004; Toso et al. 2009; Waters, Cole, and Rieder 1993)

1.3.2 MT-based cohesion pathway

Previous studies showed that the two centrosomes stay in proximity also after the centrosome linker is dissolved in late G2 (Hata et al. 2019; Panic et al. 2015). Furthermore, similar observations were reported in linker deficient cells leading to the hypothesis of alternative centrosome cohesion pathways based on MTs (Panic et al. 2015). Recent work discovered the minus-end directed tetrameric motor protein KIFC3 (kinesin family member C3) as main actor in the MT-based centrosome cohesion (Hata et al. 2019). During interphase KIFC3 works on interdigitating MTs derived from the SDAs of the mother centriole and the PCM of the daughter centriole. The cross-linking of MTs generates forces that pull the two centrosomes together (Dang and Schiebel 2022; Hata et al. 2019). After centrosome linker disassembly via Nek2 at the onset of mitosis, the KIFC3 dependent MT pathway counterbalances the pushing forces created by Eg5 and so perhaps ensures proper timing of centrosome movement to the spindle poles followed by spindle formation (Hata et al. 2019). Later on, Nek2 kinase also dissolve the SDAs and so disrupt the MT-based cohesion via KIFC3 activity resulting in centrosome separation (Hata et al. 2019; Remo et al. 2020; Sawin et al. 1992). The role of other proteins, like actin, as alternative centrosome cohesion pathways remain still unclear and need further investigation (Dang and Schiebel 2022).

Ninein, a MT minus-end associated centrosomal protein (Bouckson-Castaing et al. 1996; Mogensen et al. 2000), is associated with the SDAs of the mother centriole downstream of CEP128. The function of the coiled-coil protein Ninein as MT anchor and nucleator was linked to the MT-based cohesion pathway (Bouckson-Castaing et al. 1996; Delgehyr, Sillibourne, and Bornens 2005; Mogensen et al. 2000). Recently it was shown that Ninein also localizes at the proximal end of centrioles (Bouckson-Castaing et al. 1996; Mazo et al. 2016; Ye et al. 2014), but its function there is still unclear and not described yet. This study sheds light on the potential centrosome linker function of Ninein at the proximal ends of centrioles downstream of C-Nap1.

1.3.3 The function of the centrosome linker

Although it is clear that the centrosome linker needs to be resolved to form the bipolar mitotic spindle, the overall functions of centrosome cohesion, especially the centrosome linker, is still not completely understood. Beside the migration defects in RPE1 C-Nap1 KO cells that show a slower behaviour compared to WT, the separated centrosomes caused Golgi disorganisation with two distinct Golgi stacks found in the cells (Panic et al. 2015). Studies in *Dictyostelium discoideum* showed evidence that the position of the centrosomes can influence the direction of movement in migrating cells (Ishikawa-Ankerhold et al. 2022; Ueda et al. 1997). This suggests that the lack of spatial organisation in centrosome linker-deficient cells could cause not only slower migration but also influence the direction. The opinions in the field about the centrosome linker function in ciliogenesis are contradictory. Conroy and colleagues claimed that the centrosome linker is directly involved in primary cilium formation (Conroy et al. 2012). Later it was shown that the centrosome linker does not appear to be important for cilium formation but for the overall cellular organization of cilia (Graser et al. 2007; Mazo et al. 2016; Panic et al. 2015). It is still not completely clear how centrosome linker defects influence cilium formation, but Rootletin at the ciliary rootlets ensures the long-term stability of the cilium and is especially important in highly specialized sensory cells like hearing cells (Yang et al. 2002).

1.3.4 Centrosome linker dysfunction in human genetic disorders

The timing of centrosome separation is crucial for correct spindle assembly and chromosome segregation. Defects in the centrosome linker resulting in premature centrosome separation can impact the cell behaviour during interphase as well as mitotic spindle formation and cell division. It has been shown that deletion of C-Nap1 in mice alters centrosome cohesion causing defects in spermatogenesis and in the end male infertility (Dang, Martin-Villalba, and Schiebel 2022; Floriot et al. 2022). The loss of the centrosome linker showed a defective E-cadherin-based cortical polarity which is crucial during spermatogenesis for correct spindle orientation and successful asymmetric division to ensure the preservation of the germ stem cell pool (Dang et al. 2022). Furthermore, Ninein was reported to have a regulatory function in brain development by influencing the asymmetric stem cell division and the self-renewing ability of progenitor cells (Shinohara et al. 2013; Wang et al. 2009; Zhang et al. 2016). Besides of development defects, genetic alterations in centrosome linker proteins can cause diverse human diseases including cancer, MCPH, microdeletion syndrome or Alzheimer's disease (Dang and Schiebel 2022). For example, C-Nap1 and CROCC mutations are detected in patient with Usher syndrome, where the vision and hearing are impacted (Fuster-García et al. 2018). Furthermore, mutations in the centrosome linker gene of Rootletin (*CROCC*) is associated with aggressive colorectal cancer (Remo et al. 2018, 2020). Figure 9 shows an overview of different diseases associated with mutations or defects in centrosome linker proteins. The impact of centrosome cohesion dysfunction in human diseases still needs more investigation and clarification. Further insides would provide a deeper understanding about the physiological consequences of genetic defects in the centrosome linker and the potential drug or medical treatments.

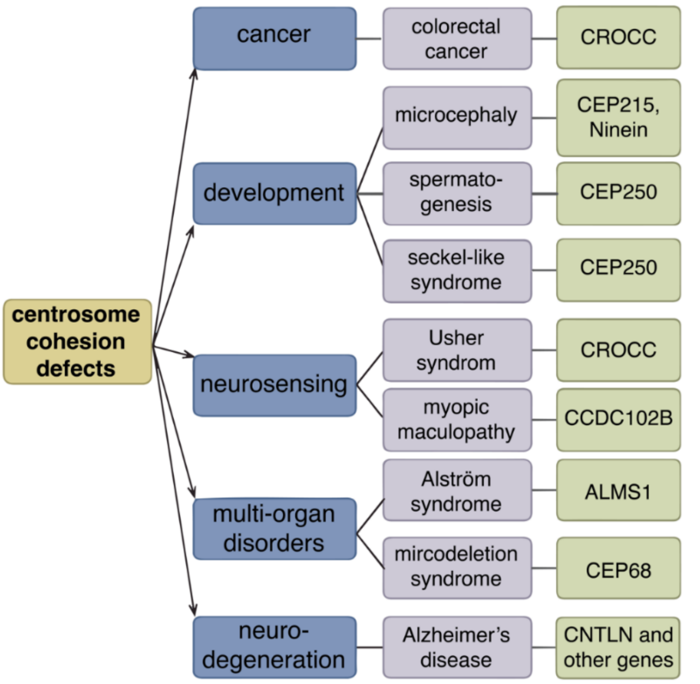

Figure 9 Schematic overview of centrosome cohesion related human diseases. Defects or mutations in the centrosome linker are associated with several human diseases and disorders. Adapted from Dang & Schiebel, 2022. Summary based on Dang et al., 2022; Floriot et al., 2015; Fonseca et al., 2015; Fuster-García et al., 2018; Hearn, 2019; Hohman et al., 2017; Hosoda et al., 2018; Jiang et al., 2022; Knorz et al., 2010; Marshall et al., 2015; Remo et al., 2018, 2020; Zheng et al., 2016.

2 Aim

Centrosome cohesion provided by the centrosome linker joins the two interphase centrosomes into one microtubule organizing centre (MTOC). Studies of the centrosome linker have mainly focused on identifying linker protein candidates. Despite the growing knowledge regarding centrosome linker components, linker diversity across different cell types and the function of the linker in cells with centrosome amplification, an important feature of many cancer cells, remain unexplored.

Ninein is a MT minus-end associated centrosomal protein at the SDAs of the mother centriole that functions in MT anchoring. Previous studies showed a second pool of Ninein localized at the proximal end of centrioles, however, the function at this position was still unclear. Here, I identified Ninein as the first centrosome linker protein with a dual function in centrosome cohesion, that organizes subdistal appendage MT and functions in the centrosome linker pathway downstream of C-Nap1. The aim of this study was to analyse cell type-dependent functions of centrosome linker components, including Rootletin/CEP68 and Ninein. To reach this goal, siRNA depletion and CRISPR/Cas9 based knock outs were used to characterize and validate the function of different centrosome linker proteins in distinct cell lines. Furthermore, not only fixed samples were analysed but also live cell imaging was performed. This shed light on the centrosome behaviour in living cells, especially in case of centrosome linker defects. STED super resolution microscopy was used to resolve the Rootletin filaments and to map different centrosome linker proteins at the proximal end of centrioles, including C-Nap1 and Ninein.

Additionally, this study asks fundamental questions about the role of centrosome cohesion in clustering supernumerary centrosome, occurring naturally in Caco-2 cells or after *PLK4* overexpression in RPE1 and HCT116 cell lines. Moreover, the impact of centrosome linker defects on nuclear envelope breakdown (NEBD), especially in the case of supernumerary centrosome, was investigated via live cell imaging.

Finally, this study uncovered an unknown role of centrosome cohesion in pseudo-bipolar spindle establishment and chromosome segregation in cells with multiple centrosomes.

3 Results

Parts of the results of this thesis were previously published in EMBO Journal (Theile et al. 2023). Dr. Xue Li and I were joint first authors of this manuscript. Dr. Xue Li performed the STED imaging and STED image analysis of Ninein and contributed to the siRNA and knockout experiments. The NEBD live cell imaging and analysis was performed in collaboration with Dr. Hairuo Dang. The radial scanning analysis was performed in collaboration with Dorothee Mersch and Prof. Dr. Simon Anders. If not stated differently, I performed the cell biology experiments and analysis.

3.1 Cell type-dependent centrosome linker diversity

3.1.1 Generation of HCT116 *CEP250* KO cell line

To compare and systematically analyse the different centrosome linker functions without siRNA depletion, several knockout (KO) cell lines were generated using CRISPR/Cas-9. During this study I knocked out the main centrosome linker gene *CEP250* coding for the protein C-Nap1 using the CRISPR/Cas-9 double cut strategy with a pair of two sgRNA (Figure 10A). The screening of the single clones was carried out using two different genomic PCRs. I designed one pair of primers to screen for the double cut in the genome and another pair for the presence of the wild type (WT) allele. Only clones with a double cut in both alleles (homozygous cut) were selected and further analysed. To validate the KO on the genomic level, PCR fragments of the selected clones were sent for DNA sequencing. The translated reading frame of clone #234 was checked for a frameshift and compared to the WT *CEP250* (Figure 10B). This analysis showed that in clone # the first 67 amino acids of C-Nap1 were as in the WT cell line but then were attached to five C-Nap1 unrelated amino acids (YGGRL) followed by a translational stop. Thus, of the 2442 amino acids of C-Nap1 only 67 were translated in the knockout clone #234.

For further validation on protein level an antibody against C-Nap1 (aa 2060-2068) was used to stain and quantify C-Nap1 intensity at the centrosome by indirect immunofluorescence (IF) (Figure 10C and D). I observed an intensity reduction by app. 80% in the HCT116 *CEP250* KO #234 clone. Additionally, there was no C-Nap1 band detectable by western blotting (Figure 10E). The KOs of the centrosome linker proteins Rootletin (encoded by *CROCC*) and Ninein (encoded by *NIN*) in RPE1 and HCT116 were generated by Dr. Xue Li, respectively (Theile et al. 2023).

To set a criterion for centrosome separation, a centrosome distance threshold of 2 µm for RPE1 (consistent with previous publications, (Bahe et al. 2005; Fang et al. 2014; Panic et al. 2015; Vlijm et al. 2018)) and 1 µm for HCT116 cells was used during this study. The lower threshold of 1 µm for HCT116 cells was used since the centrosome distance in centrosome cohesion-deficient cells (*CEP250* KO and Nocodazole) was about half of what I observed in RPE1 cells (Figure 10F). If not indicated differently interphase cells, excluding G2-cells via CENP-F staining, were analyzed during this study. CENP-F shows a cell cycle dependent localization pattern and therefore can be used to discriminate G2 from S and prophase cells.

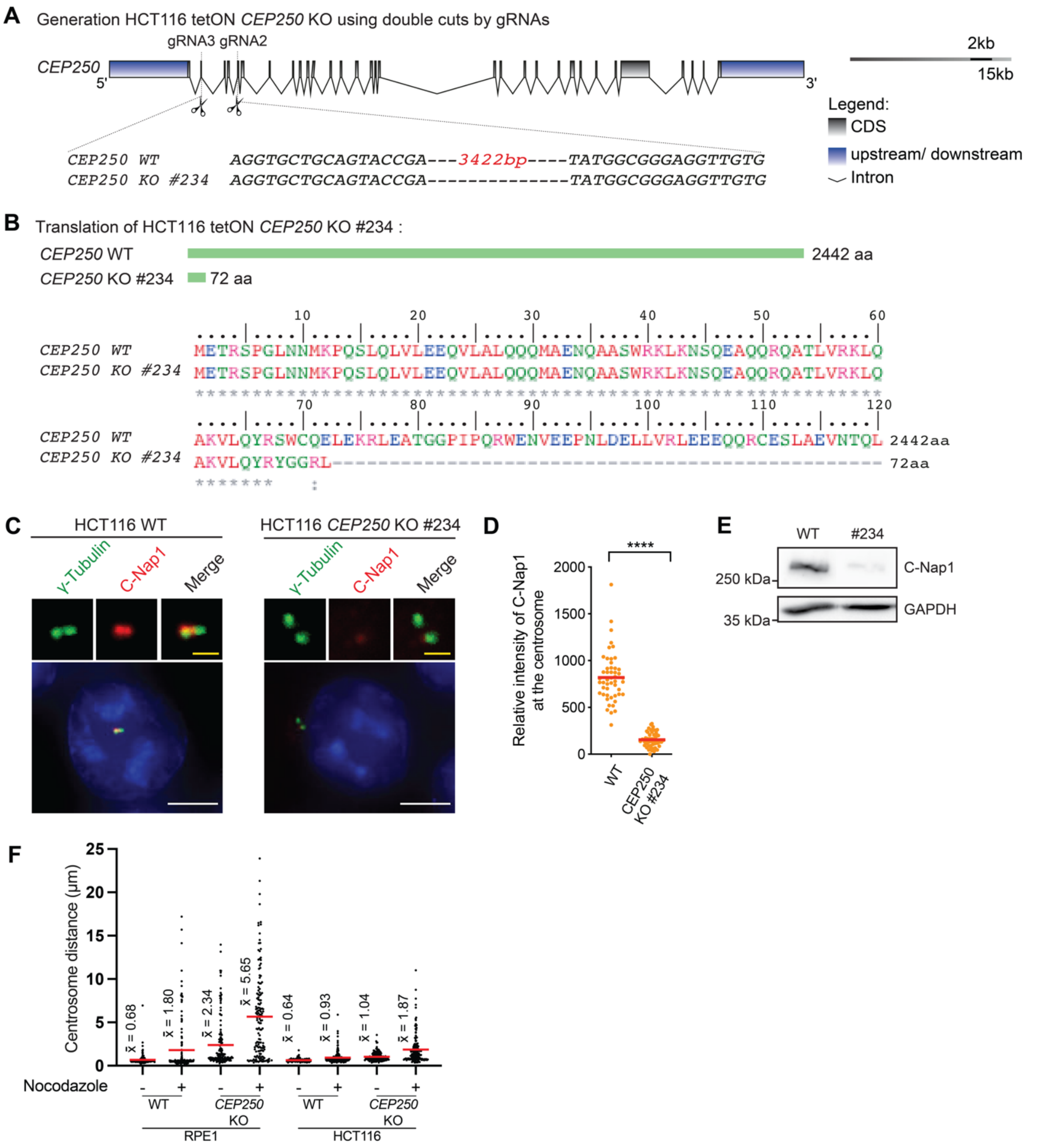

Figure 10 Generation and validation of HCT116 *CEP250* KO. A Scheme of *CEP250* gene and where the two selected gRNAs target in the gene. The gene structure was made using Exon-Intron Graphic Maker. **B** Comparison of the translation lengths between HCT116 tetON WT and *CEP250* KO #234 cells. **C** Fluorescent images of cells from HCT116 tetON WT and *CEP250* KO #234. White scale bars, 5 µm. Yellow scale bars, 2 µm. **D** Quantification of C-Nap1 intensity at the centrosome from HCT116 WT and *CEP250* KO #234. N = 50 cells; a representative dataset from 3 independent experiments is shown. Dot represents the relative intensity of C-Nap1 at the centrosome in each cell. Lines represent the mean. Unpaired t-tests. **** $p < 0.0001$. **E** Immunoblot of endogenous C-Nap1 in HCT116 WT and *CEP250* KO #234. GAPDH was used as loading control. **F** Centrosome distance (µm) in RPE1 WT and *CEP250* KO and HCT116 WT and *CEP250* KO, without and with MT depolymerization using the drug Nocodazole. N = 50 cells per experiment, n = 3 independent experiments. Mean ($\bar{x}$) is shown. (adapted from Theile et al., 2023)

3.1.2 Differences in the centrosome linker function of Rootletin and CEP68 in RPE1 and HCT116 cells

The current understanding of centrosome cohesion in mammalian cells includes two different pathways: the centrosome linker (pathway 1) and the MT-based cohesion (pathway 2) (Figure 11A). Figure 11A shows various strategies used during this study to impair centrosome cohesion by blocking one or both pathways.

The best described and most studied centrosome linker proteins are C-Nap1 (encoded by *CEP250*), Rootletin (encoded by *CROCC*) and CEP68 (Bahe et al. 2005; Flanagan et al. 2017; Andrew M Fry et al. 1998; Mayor et al. 2000; Panic et al. 2015; Remo et al. 2020; Vlijm et al. 2018). C-Nap1 forms a ring like structure at the proximal end of both centrosomes and organizes the Rootletin/CEP68 filaments to mediate the linkage between the two centrosomes (Vlijm et al. 2018). While the function of C-Nap1 as universal anchor of linker proteins at centrosomes is well established in several cell lines, functional analysis of the Rootletin and CEP68 containing filaments was mainly performed in U2OS cells (Bahe et al. 2005; Graser et al. 2007). To obtain deeper insights into the general function of the Rootletin/CEP68 linker, I analysed their role in RPE1 and HCT116 cells (Figure 11). The drug Nocodazole was used additionally to the siRNA-based depletion (for depletion efficiencies see Theile et al., 2023) to disrupt MTs. This drug treatment impacts the MT-based pathway that takes over centrosome cohesion when the centrosome linker is abolished (Figure 11A).

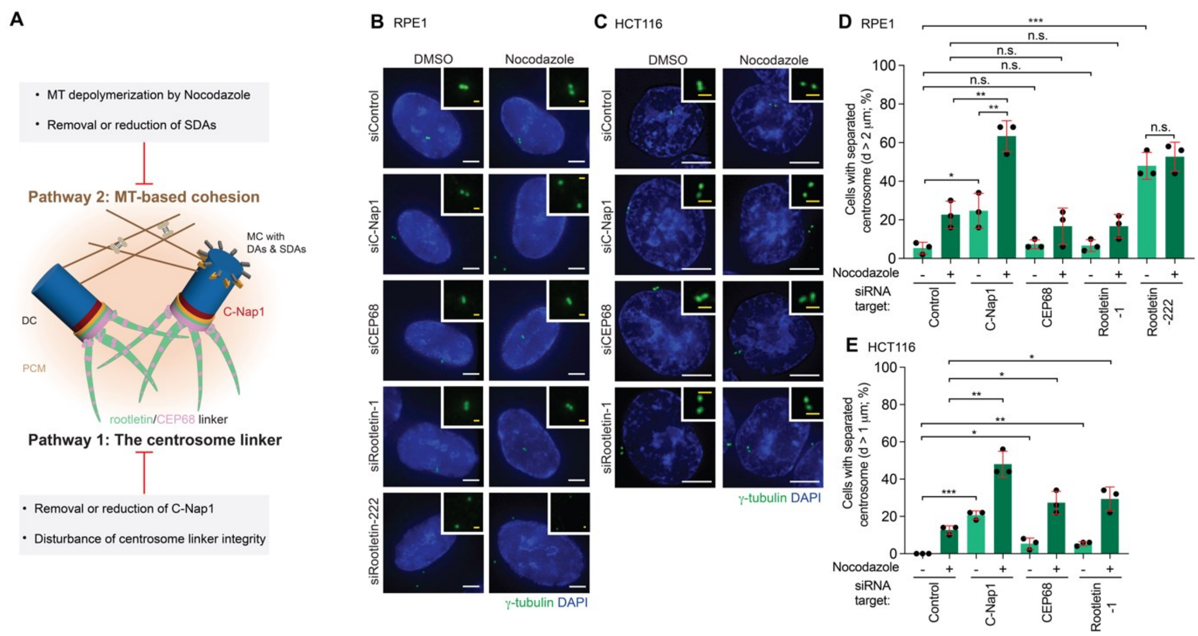

Figure 11 The role of linker proteins for centrosome cohesion in RPE1 and HCT116 cells. A Model of the centrosome cohesion in interphase. Two pathways contribute to the centrosome cohesion: the centrosome linker and the MT-based cohesion. **B, C** Representative fluorescent images of centrosomes in RPE1 (B) and HCT116 (C) cells under siRNA depletion condition using the indicated siRNAs, without and with MT depolymerization by Nocodazole. γ-tubulin was used to mark centrosomes and DNA was stained with DAPI. The box in the right-hand corner shows the centrosome signals of the cell in the main panel. Scale bars in white: 5 µm. Scale bars in yellow: 1 µm. **D, E** Quantification of cells with separated centrosomes (centrosome distance > 2 µm for RPE1 cells and > 1 µm for HCT116 cells) from RPE1 (B) and HCT116 (C) cells. N = 50 cells per analysis, n = 3 independent experiments. Bar and error represent mean and SD. Unpaired t-test. n.s.: not significant p > 0.05, * p < 0.05, ** p < 0.01, *** p < 0.001. **B-E** adapted from Theile et al., 2023; performed together with Dr. Xue Li.

Depletion of C-Nap1 triggered efficient centrosome separation in RPE1 cells, in particular when Nocodazole impaired the MT-based cohesion function (Figure 11B and D). In contrast, siRNA depletion of CEP68 and Rootletin (siRootletin-1) did not increased centrosome separation in RPE1 cells, even when the MT-based cohesion pathway was disrupted (Figure 11B and D). In previous studies about the role of centrosome linker candidates Rootletin was depleted by the siRNA siRootletin-222 (Bahe et al. 2005; He et al. 2013). Surprisingly, siRootletin-222 treatment led to very profound centrosome separation that was not increased by the additional treatment with Nocodazole (Figure 11B and D). This behavior suggested that siRootletin-222 affected both the centrosome linker and the MT centrosome cohesion pathways, probably as a consequence of an off-target effect. To verify this notion, I performed Rootletin siRNAs depletion and Nocodazole treatment in RPE1 *CROCC* KO cells (Figure 12). The siRootletin-1, like the siControl, had little impact on centrosome separation in RPE1 *CROCC* KO cells even when MTs were depolymerized with

Nocodazole (Figure 12A and B). In contrast, treatment of RPE1 *CROCC* KO cells with siRootletin-222 led to an efficient centrosome separation phenotype that was not enhanced by Nocodazole (Figure 12). These results indicate that the commonly used siRootletin-222 affects centrosome cohesion by an off-target effect. Therefore, I used siRNA Rootletin-1 throughout this study. Furthermore, the siRNA results showed that the centrosome linker in RPE1 cells could function independently of Rootletin. In HCT116 cells depletion of C-Nap1, CEP68 and Rootletin resulted in an increase in centrosome separation, however, more prominently when cells were treated with Nocodazole indicating that MT-based centrosome cohesion was very efficient in these cells (Figure 11C and E). This suggests that the C-Nap1-Rootletin/CEP68 centrosome linker pathway is functional in HCT116 but not in RPE1 cells. In addition, a robust MT centrosome cohesion pathway could mask centrosome linker defects in HCT116 cells.

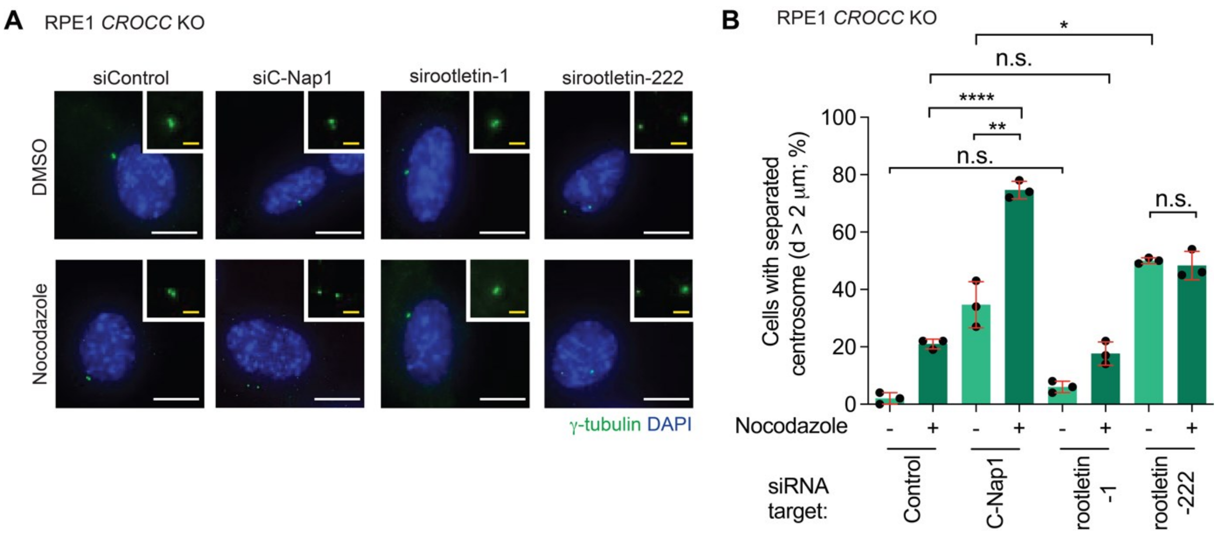

Figure 12 Verification of the off-target effect of siRootletin-222 in centrosome cohesion. A Representative fluorescent image of centrosomes in RPE1 *CROCC* KO under depletion of siControl, siRootletin-1 and siRootletin-222, without and with Nocodazole. White scale bars, 10 µm. Yellow scale bars, 2 µm. **B** Quantification of cells with separated centrosomes (centrosome distance > 2 µm) from RPE1 samples (A). N = 50 cells per experiment, n = 3 independent experiments. Bar and error represent mean and SD. Unpaired t-tests. n.s.: not significant p > 0.05, * p < 0.05, ** p < 0.01, **** p < 0.0001. (adapted from Theile et al., 2023)

3.1.3 The Rootletin centrosome linker contributes differently to centrosome cohesion across distinct cell lines

To confirm the outcome from siRNA-based depletion experiments in RPE1 and HCT116 cells (Figure 11), I analyzed *CEP250* KO and *CROCC* KO in both cell lines for centrosome cohesion defects, respectively (Figure 13). Compared to RPE1 WT, Nocodazole triggered centrosome separation in 20% of HCT116 WT cells, whereas in RPE1 WT cells the drug had little impact on centrosome cohesion (Figure 13). This indicates that the centrosome linker is working very efficiently in RPE1 WT cells, whereas in around 1/5 of HCT116 WT cells centrosome cohesion is mainly based on the MT pathway. In line with the results using siRNA depletion, *CEP250* deletion increased centrosome separation in RPE1 cells to 28% and in HCT116 cells to 42% (Figure 13B and D). Inactivation of the MT pathway via MT depolymerization with Nocodazole in *CEP250* KO cells further enhanced centrosomes separation to 50% in RPE1 cells and to 63% in HCT116 cells (Figure 13B and D). Consistent with the siRNA depletion data in Figure 11, RPE1 *CROCC* KO did not show an increasement in centrosome separation even when Nocodazole was added (Figure 13A and B). Surprisingly, deletion of Rootletin in HCT116 cells triggered centrosome separation in around 17 % of the cells (Figure 13C and D). The centrosome disjunction was further increased from 17% to 31% after Nocodazole treatment. Interestingly, the centrosome separation in HCT116 *CROCC* KO cells was less than in HCT116 *CEP250* KO (Figure 13D). This observation is consistent with the model that C-Nap1 functions upstream of Rootletin in centrosome linker function and suggests that an additional protein besides Rootletin functions downstream of C-Nap1 in centrosome cohesion pathway. These data together with the siRNA depletion indicate cell type-dependent differences in centrosome cohesion and indicate a lack of centrosome cohesion function of Rootletin in RPE1 cells despite the formation of Rootletin/CEP68 filaments in this cell line (Vlijm et al. 2018).

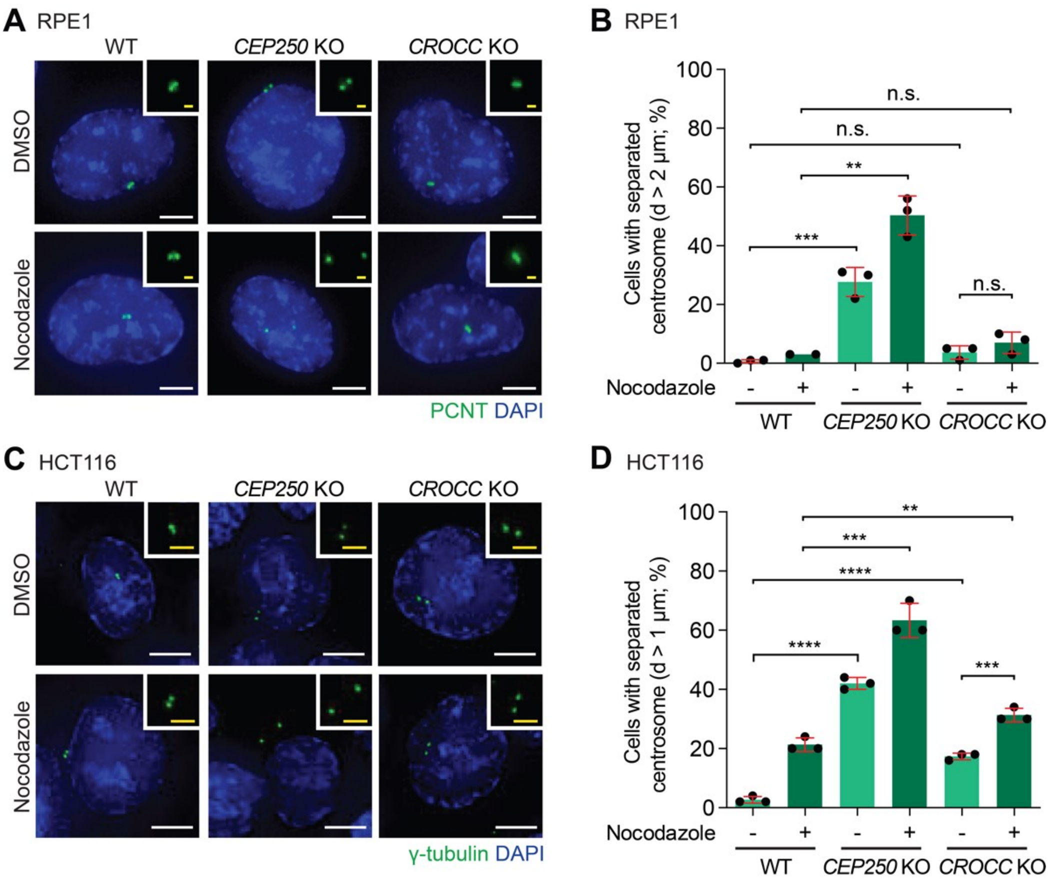

Figure 13 Cell-type dependent centrosome linker function in RPE1 and HCT116 cells. **A** Representative fluorescent images of centrosomes in RPE1 WT, *CEP250* KO and *CROCC* KO cells, without and with MT depolymerization using Nocodazole. Pericentrin (PCNT) was used as marker for centrosomes and DNA was stained with DAPI. The boxes in the right-hand corner show enlargement of the centrosome signals of the cell in the main panel. White scale bars, 5 µm. Yellow scale bars, 1 µm. **B, D** Quantification of cells with separated centrosomes (centrosome distance > 2 µm for RPE1 cells and > 1 µm for HCT116 cells) from RPE1 (A) and HCT116 (C) cells. N = 50 cells per experiment, n = 3 independent experiments. Bar and error represent mean and SD. Unpaired t-test. n.s.: not significant p > 0.05, ** p < 0.01, *** p < 0.001, **** p < 0.0001. **C** Representative fluorescent images of centrosomes in HCT116 WT, *CEP250* KO, *NIN* KO and *CROCC* KO cells, without and with MT depolymerization using Nocodazole. γ-tubulin was used to mark centrosomes and DNA was stained with DAPI. The boxes in the right-hand corner show enlargements of the centrosome signals of the cell in the main panel. White scale bars, 10 µm. Yellow scale bars, 2 µm. (adapted from Theile et al., 2023; performed together with Dr. Xue Li)

3.1.4 Actin does not play a role in centrosome cohesion in interphase

Recently, it was reported that F-actin has a function in centrosome clustering (Kwon et al. 2008), therefore I checked the impact of F-actin depolymerization on centrosome cohesion, especially in addition to centrosome linker deletion. Drug treatment with and without Nocodazole and Cytochalasin, that depolymerizes F-actin, of WT and *CEP250* KO RPE1 and HCT116 cells did not indicate such a function of F-actin (Figure 14). In conclusion, I could not observe a function of F-actin in centrosome cohesion in RPE1 cells neither HCT116 cells.

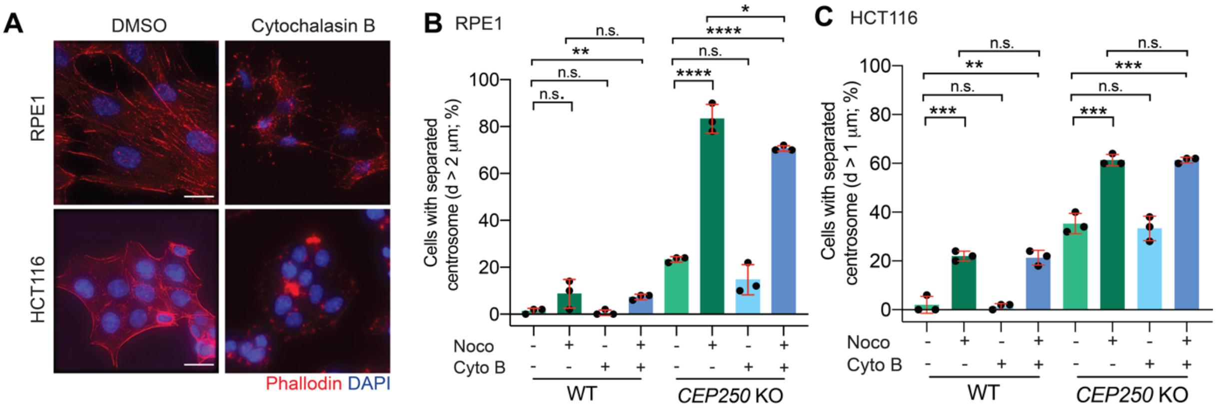

Figure 14 Actin does not play a role in centrosome cohesion in interphase. A Representative fluorescent images of RPE1 WT and HCT116 WT cells show that the actin cytoskeleton was disrupted upon Cytochalasin B (20 µM) treatment. Scale bars: 20 µm. **B, C** Quantification of cells with separated centrosomes (centrosome distance > 2 µm for RPE1 cells and > 1 µm for HCT116 cells) from RPE1 WT and *CEP250* KO (B) and HCT116 WT and *CEP250* KO (C) cells. Nocodazole was used to depolymerizes MTs, Cytochalasin B was used to inhibit actin filaments polymerization. N = 50 cells per experiment, n = 3 independent experiments. Bars and errors represent mean and SD. Unpaired t-tests. n.s.: not significant $p > 0.05$, * $p < 0.05$, ** $p < 0.01$, *** $p < 0.001$, **** $p < 0.0001$. (adapted from Theile et al., 2023)

3.2 Alternative centrosome linker pathways

3.2.1 Discovering Ninein as an alternative centrosome linker

In the past several proteins were identified as potential players in centrosome cohesion and therefore are candidates for centrosome linker proteins downstream of C-Nap1 (Bahe et al. 2005; Fang et al. 2014; He et al. 2013). However, the specific roles of these proteins in centrosome cohesion are not well understood. To gain a better understanding, we performed a siRNA-based mini screen depleting C-Nap1 (positive control), Ninein, CEP215 (also known as Cdk5RAP2) and LRRC45 (Leucine Rich Repeat Containing 45) in RPE1 WT cells (Figure 15A and B). Similar to C-Nap1 depletion, Ninein depletion led to ~30% of cells with separated centrosomes, while in the siControl centrosomes were separated in only 5% of the cells (Figure 15B, light green bars). Nocodazole further enhanced centrosome separation in C-Nap1 and Ninein-depleted cells (Figure 15B). In contrast, depletion of CEP215 and LRRC45 in RPE1 WT cells did not show an impact on centrosome separation (Figure 15B). These results indicate that Ninein could function in centrosome cohesion as centrosome linker protein.

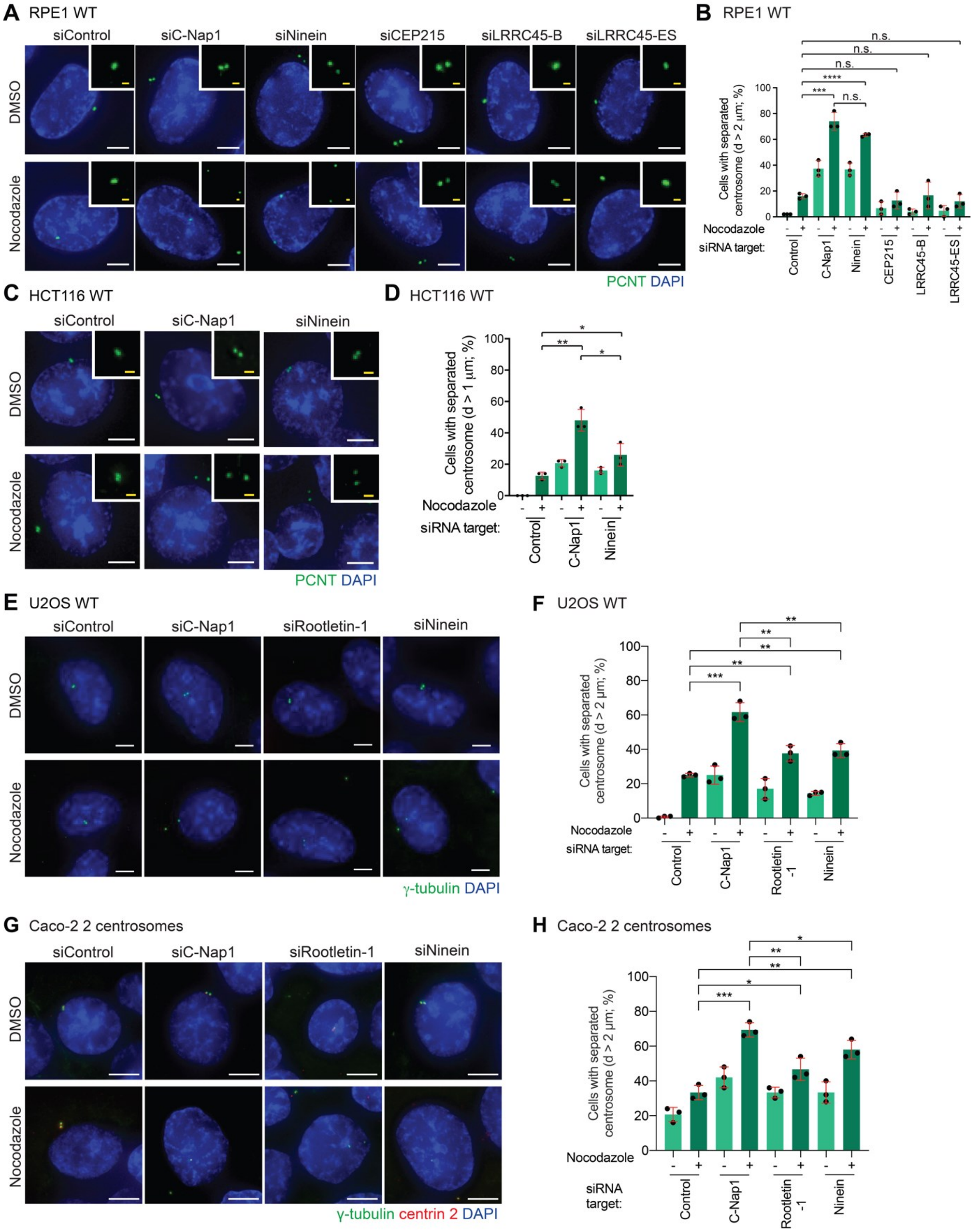

Figure 15 Ninein is a novel component of the centrosome linker. A-H (A, C, E, G) Representative fluorescent images of centrosomes in RPE1 (A), HCT116 (C), U2OS (E) and Caco-2 (G) WT cells with the indicated siRNA depletions, with and without MT depolymerization using Nocodazole. PCNT or γ-tubulin was used to mark centrosomes and DNA was stained with DAPI. The boxes on top show the centrosome signals of the cell in the main panel. Scale bars in white: 5 µm. Scale bars in yellow: 1 µm. (B, D, F, H) Quantification of cells with separated centrosomes (centrosome distance > 2 µm for RPE1 (B), U2OS (D) and Caco-2 (F) cells and > 1 µm for HCT116 (H) cells) from RPE1 (A), HCT116 (C), U2OS (E), and Caco-2 (G) cells with the indicated siRNA depletions, with and without MT

depolymerization using Nocodazole. N = 50 cells per experiment, n = 3 independent experiments. Bar and error represent mean and SD. Unpaired t-test. n.s.: not significant $p > 0.05$, * $p < 0.05$, ** $p < 0.01$, *** $p < 0.001$, **** $p < 0.0001$. (adapted from Theile et al., 2023, performed together with Dr. Xue Li.)

To analyse whether the function of Ninein in centrosome cohesion is cell-type specific, I depleted Ninein in HCT116 cells (Figure 15C and D). Similar to the results in RPE1 cells, depletion of Ninein in HCT116 led to a significant increase in centrosome separation, no matter whether MTs were depolymerized or not, confirming Ninein as potential centrosome linker protein (Figure 15C). Furthermore, to analyse the cell type-dependent differences in the Rootletin/CEP68 and Ninein centrosome linker functions I performed siRNA-based depletion in U2OS and Caco-2 cells, respectively (Figure 15E-H). A reduction of centrosome cohesion upon C-Nap1, Rootletin and Ninein depletion was also observed in U2OS and Caco-2 cells, similar to HCT116 cells (Figure 15C-H). Taken together, I observed that the centrosome cohesion function of Ninein is conserved in all tested cell lines.

3.2.2 Ninein plays a role in interphase centrosome cohesion and is independent of the Rootletin/CEP68 linker in HCT116 cells

To confirm the outcome of the siRNA depletion of Ninein, we generated and characterized CRISPR/Cas9 knockouts in *NIN* (encodes Ninein) in RPE1 and HCT116 cells (Figure 16A-D; (Theile et al. 2023)). In line with the pervious results using siRNA depletion (Figure 15), even without Nocodazole treatment, Ninein deletion showed a strong significant impact on centrosome separation compared to WT in RPE1 and HCT116 cells (Figure 16A-D). Interestingly, HCT116 *CEP250* KO cells had a stronger centrosome cohesion defect compared to HCT116 *NIN* KO and HCT116 *CROCC* KO cells (compare Figure 13D and Figure 16D). This observation is consistent with the notion that C-Nap1 functions upstream of Ninein and Rootletin in centrosome linker function and that Ninein and Rootletin could have partly overlapping functions independently from each other. To address this and to check if C-Nap1 can provide centrosome cohesion solely via phase separation, as suggested in a recent publication (Mahen 2022), I first analyzed C-Nap1 on centrosomes in RPE1 WT and *NIN* KO cells (Figure 16E). The loss of Ninein did not influence the localization and intensity levels of C-Nap1 at centrosomes in RPE1 cells. As showed before centrosome cohesion is similarly defective in RPE1 *CEP250* KO and *NIN* KO cells (compare Figure 13B and Figure 16C). Furthermore, depletion of C-Nap1 or Rootletin with siRNA in RPE1 *NIN* KO did not show an increase in centrosome separation (Figure 16F). These results together indicate that C-Nap1 requires Ninein for centrosome linker function in RPE1 cells and cannot function alone.

Knowing that there are cell type-dependent differences in the centrosome linker function and that Ninein and Rootletin both function in centrosome cohesion in HCT116 cells, I checked the interdependency of both linker branches in this cell line (Figure 16G-J). Taking advantage of the HCT116 knock-out cell lines in the *NIN* and *CROCC* genes, I measured the impact of Ninein and Rootletin loss on the centrosomal localization of Rootletin and Ninein, respectively (Figure 16G-J). Lack of one protein did not affect the intensity or localization of the other. Additionally, siRNA depletion of Rootletin in HCT116 *NIN* KO cells still increased the centrosome separation to a similar level like C-Nap1 depletion (Figure 16K). These observations indicate that the Rootletin/CEP68 and Ninein linker function in parallel and that the Rootletin linker is functional in the absence of Ninein.

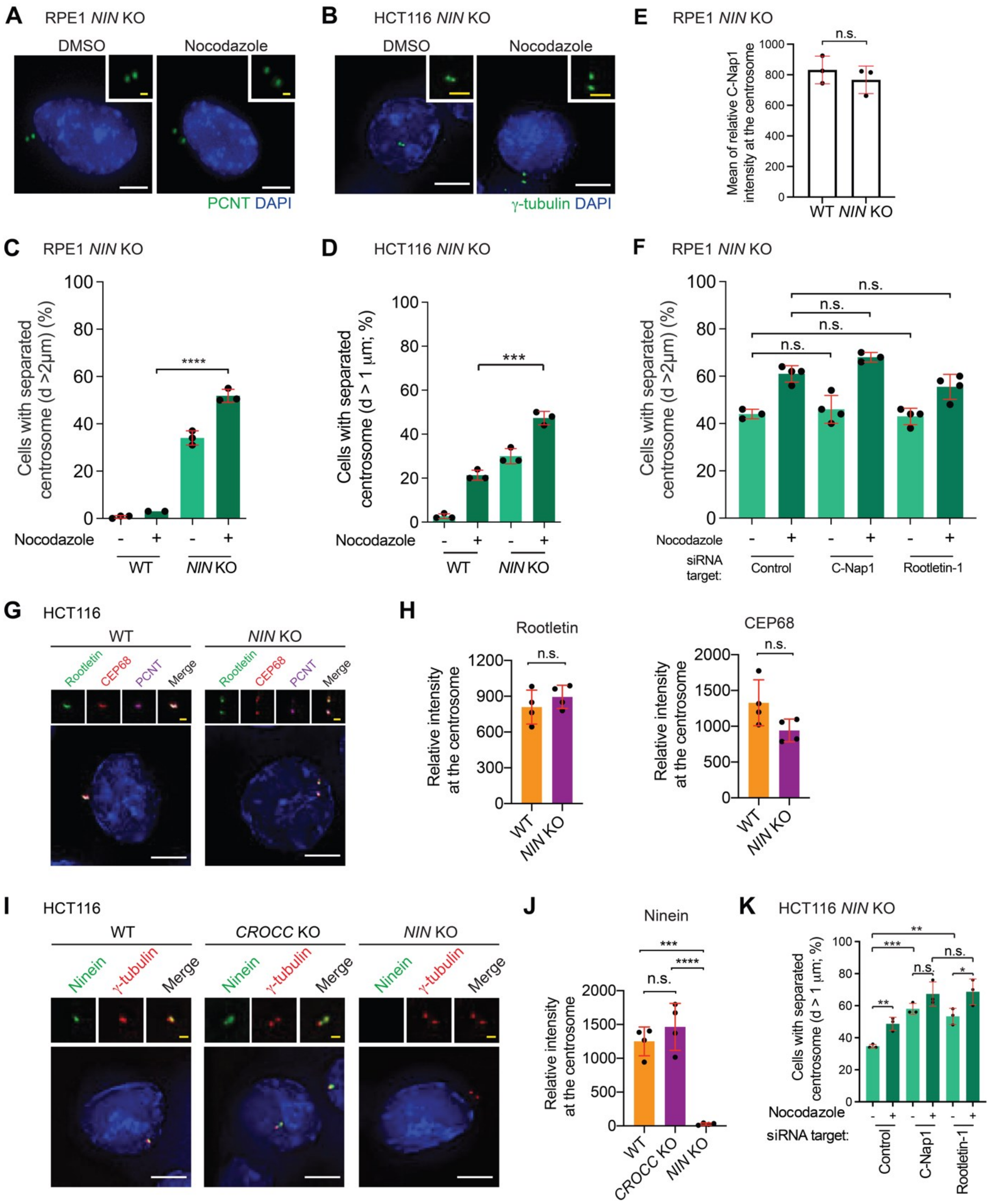

Figure 16 Ninein plays a role in interphase centrosome cohesion in RPE1 and HCT116. **A** Fluorescent images of centrosomes in RPE1 *NIN* KO, with and without MT depolymerization using Nocodazole. PCNT was used to mark centrosomes and DNA was stained with DAPI. The boxes on top show enlargement of the centrosome signals of the cell in the main panel. White scale bars, 5 µm. Yellow scale bars, 1 µm. **B** Fluorescent images of centrosomes in HCT116 *NIN* KO, without and with MT depolymerization using Nocodazole. γ-tubulin was used to mark centrosomes and DNA was stained with DAPI. The boxes on top show enlargement of the centrosome signals of the cell in the main panel. White scale bars, 10 µm. Yellow scale bars, 2 µm. **C, D** Quantification of cells with separated centrosomes (centrosome distance > 2 µm for RPE1 cells and > 1 µm for HCT116 cells) from RPE1 and HCT116 WT and *NIN* KO cells. N = 50 cells per experiment, n = 3 independent experiments.

Bar and error represent mean and SD. Unpaired t-tests. *** $p < 0.001$, **** $p < 0.0001$. **E** Quantification of cells with separated centrosomes (centrosome distance > 2 µm) in RPE1 *NIN* KO cells under siRNA depletion of siControl, C-Nap1 and Rootletin, without and with MT depolymerization using Nocodazole. N = 50 cells per experiment, n = 4 independent experiments, n = 3 for siControl w/o Noco and siC-Nap1 with Noco. Bar and error represent mean and SD. Unpaired t-tests. n.s.: not significant $p > 0.05$. **F** Quantification of C-Nap1 intensity at the centrosome from RPE1 WT and *NIN* KO. N = 50 cells; n = 3 independent experiments. Bar and error represent mean and SD. Unpaired t-tests. n.s.: not significant $p > 0.05$. **G** Fluorescent images of Rootletin and CEP68 in HCT116 WT and *NIN* KO cells using the indicated antibodies. DNA was stained with DAPI. The boxes on top show enlargement of the centrosome signals of the cell in the main panel. Scale bars in white: 5 µm; scale bars in yellow: 1 µm. **H** Quantification of relative Rootletin and CEP68 intensity at the centrosome in HCT116 WT and *NIN* KO cells (E). N = 50 cells per experiment, n = 4 independent experiments. Bar and error represent mean and SD. Unpaired t-test. n.s.: not significant $p > 0.05$. **I** Fluorescent images of Ninein in HCT116 WT, *CROCC* KO and *NIN* KO cells using indicated antibodies. DNA was stained with DAPI. The boxes on top show enlargement of the centrosome signals of the cell in the main panel. Scale bars in white: 5 µm; scale bars in yellow: 1 µm. **J** Quantification of relative Ninein intensity at the centrosome in HCT116 WT, *CROCC* KO and *NIN* KO cells (G). N = 50 cells per experiment, n = 4 independent experiments. Bar and error represent mean and SD. Unpaired t-test. n.s.: not significant $p > 0.05$, *** $p < 0.001$, **** $p < 0.0001$. **K** Quantification of centrosomes separation in HCT *NIN* KO cells with the indicated siRNA depletions, without and with MT depolymerization using Nocodazole. N = 50 cells per experiment, n = 3 independent experiments. Bar and error represent mean and SD. Unpaired t-test. n.s.: not significant $p > 0.05$, * $p < 0.05$, ** $p < 0.01$, *** $p < 0.001$. (adapted from Theile et al., 2023)

3.2.3 Lower expression levels in RPE1 compared to HCT116 cells probably explain lack of Rootletin linker function in RPE1 cells

To find an explanation for the significant differences observed in the Rootletin/CEP68 linker between RPE1 and HCT116 cells (Figure 11 and Figure 13), I investigated the protein levels of Rootletin and CEP68 in both cell lines (Figure 17). The indirect immunofluorescence signal of Rootletin and CEP68 at centrosomes in RPE1 cell was approximately 1.5 times lower than that observed in HCT116 cells (Figure 17A and B). Furthermore, the quantification of normalized immunoblots from total cell lysates revealed that Rootletin levels in RPE1 cells were 14 times and CEP68 levels 15 times lower than those in HCT116 cells (Figure 17C). In conclusion, the combination of lower expression of Rootletin and CEP68, along with reduced Rootletin/CEP68 levels at centrosomes, is likely a contributing factor to why the Rootletin linker does not play a major role in RPE1 cells.

To gain better insights about how Rootletin expression level influence centrosome cohesion, I generated a stable cell line containing a Doxycycline (Dox)-inducible Rootletin-FL construct in RPE1 *NIN* KO to check if Rootletin can rescue the centrosome separation phenotype of Ninein deletion (Figure 17D-F). Surprisingly, after successful expression of Rootletin in RPE1 *NIN* KO (Figure 17D and E), I could not observe a decrease in centrosome disjunction (Figure 17F), indicating that overexpression alone does not help Rootletin to gain a function in centrosome cohesion.

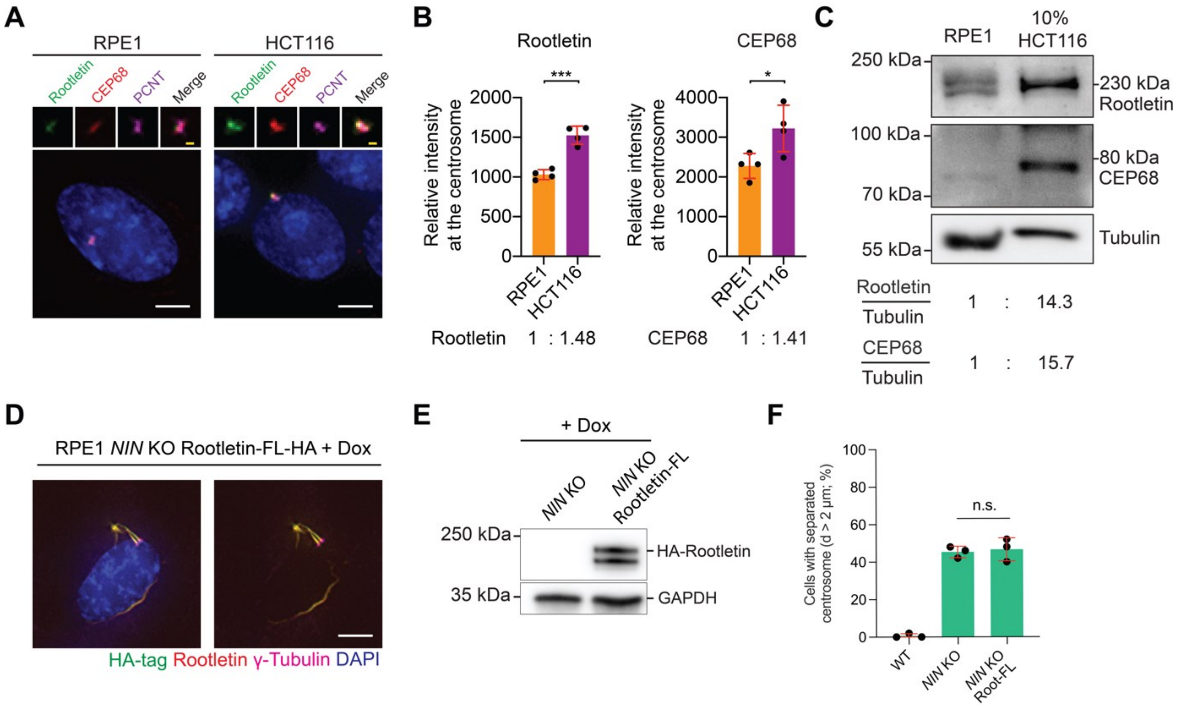

Figure 17 Reduced protein levels probably impair centrosome linker function of Rootletin/CEP68 in RPE1 cells. A Representative fluorescent images of RPE1 and HCT116 cells. Rootletin and CEP68 were stained, PCNT was used as centrosome marker and DNA was stained with DAPI. The boxes on top show the centrosome signals of the cell in the main panel. Scale bars in white: 5 µm. Scale bars in yellow: 1 µm. **B** Quantification of relative Rootletin and CEP68 intensity at the centrosome in RPE1 and HCT116 cells. Mean value of relative intensity at the centrosome from N = 50 in each replicate, n = 4 are shown. Bar and error represent mean and SD. Unpaired t-test. * $p < 0.05$, *** $p < 0.001$. **C** Abundance of Rootletin and CEP68 in RPE1 and HCT116 cells was examined by immunoblotting. Tubulin was used as loading control. Representative blot is shown. The original HCT116 protein sample was diluted 1:10. The relative abundance of Rootletin and CEP68 was normalized to the corresponding tubulin signal in each condition. **D** Representative fluorescent images of RPE1 *NIN* KO expression Rootletin-HA construct. The indicated antibodies were used for indirect fluorescent analysis. Scale bar: 5 µm. **E** Immunoblot of Rootletin-HA in RPE1 *NIN* KO and RPE1 *NIN* KO expressing the *Rootletin-HA* construct. GAPDH was used as loading control. **F** Quantification of cells with separated centrosomes in RPE1 WT, *NIN* KO and *NIN* KO expressing *Rootletin-HA* (Root-FL). N = 50 cells per experiment, n = 3 independent experiments. Bar and error represent mean and SD. Unpaired t-test. n.s.: not significant $p > 0.05$. **A-C** adapted from Theile et al., 2023.

3.2.4 Ninein has a similar function as C-Nap1 in interphase centrosome cohesion in RPE1 cells

To confirm the role of C-Nap1, Rootletin and Ninein in centrosome cohesion not only in fixed cells but also in living cells, I performed live cell imaging (Figure 18). After generating stable RPE1 WT, *CEP250* KO, *CROCC* KO and *NIN* KO cell lines continuously expressing γ-tubulin-mRuby2 as centrosome marker I added the SPY650-DNA probe to stain the DNA during time laps experiment. Over the 360 min of the live cell imaging the two centrosomes in RPE1 WT interphase cell stayed together (centrosome distance < 2 µm) (Figure 17A and B upper panel). Surprisingly, after Nocodazole addition centrosome separation increased in 27% of the WT cells at some point of the analysis, indicating the transient nature of the centrosome linker formation (Figure 17A and B lower panel). In 80% of the C-Nap1 deficient cells in the presence of Nocodazole both centrosomes were separated (Figure 17C and D upper panel). Furthermore, I could observe a back-and-forth movement between the two centrosomes, which was uncoupled after the Nocodazole treatment, indicating that the MT-based cohesion pathway could be responsible for this oscillating behaviour (Figure 17C and D lower panel). In line with the measurements in fixed RPE1 *CROCC* KO cells (Figure 13A and B), the centrosome stayed close together during the live cell imaging and the RPE1 *CROCC* KO cells behaved centrosome cohesion proficient, similar to WT cells (Figure 17E and F). In contrast, centrosomes in RPE1 *NIN* KO cells behaved similar to *CEP250* KO cells (Figure 17G and H). Nocodazole treatment also influenced centrosome movement in *NIN* KO cells indicating that the MT pathway was still active regardless of the lack of functional SDAs, probably because of MTs derived from the PCM.

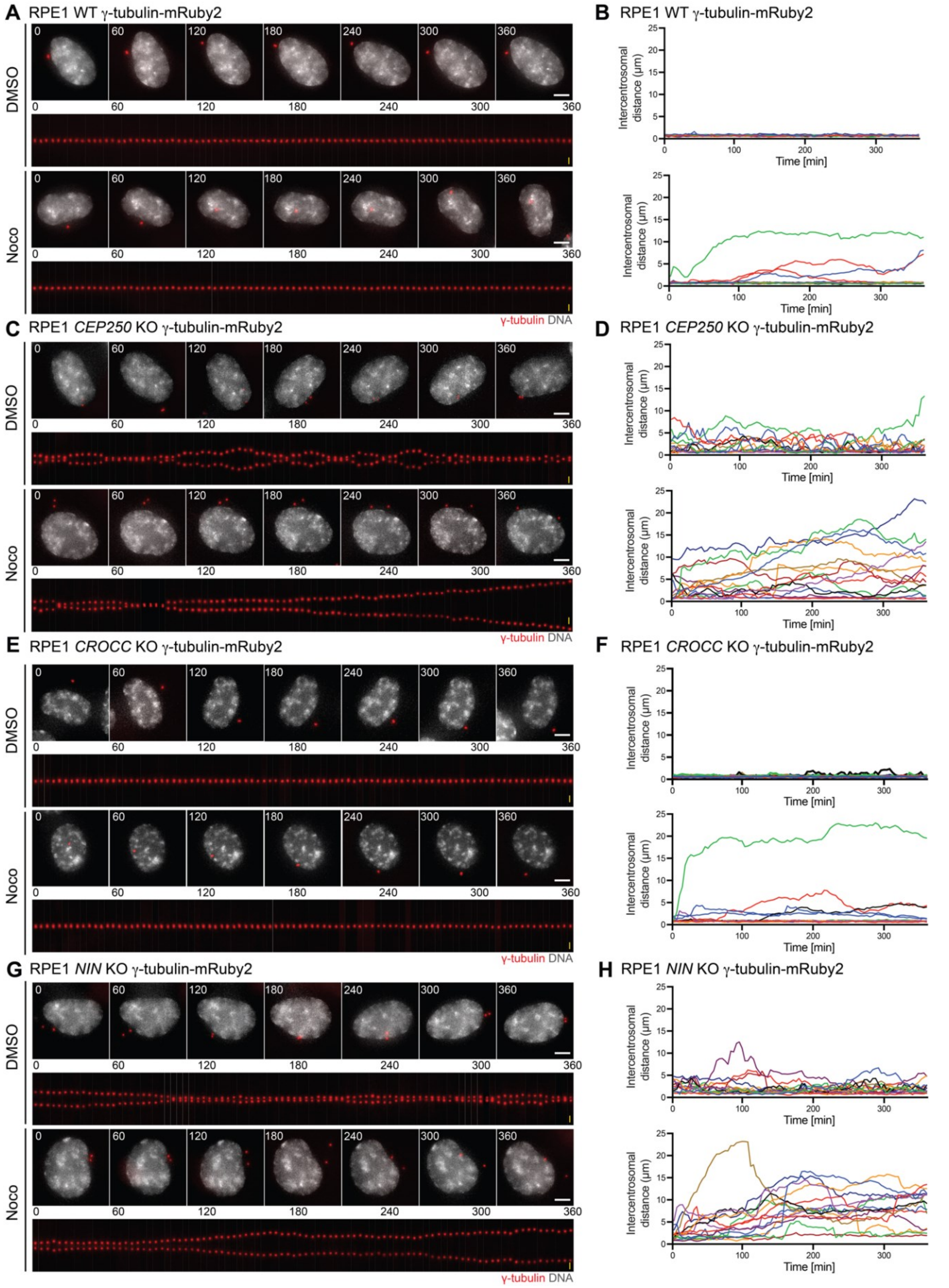

Figure 18 Ninein is a novel centrosome linker protein and functions in centrosome cohesion during interphase. A, C, E, G Time-lapse images (4 min interval) of RPE1 WT, *CEP250* KO, *CROCC* KO and *NIN* KO cells expressing γ-tubulin-mRuby2 (red) as marker for the centrosomes with and without Nocodazole treatment. Representative still images (top rows) and kymographs of centrosomes (bottom rows) are shown. The DNA was marked with SPY-DNA650 (grey). White scale bars, 5 µm. Yellow scale bars, 2 µm. **B, D, F, H** Intercentrosomal distances (µm) from (A), (C), (E) and (G) were plotted over time (n = 15 cells). **A-H** adapted from Theile et al., 2023.

3.3 Ninein plays a dual role in interphase centrosome cohesion

3.3.1 Ninein shows centrosome localizations corresponding to its dual function in interphase centrosome cohesion

Ninein was identified as a centrosome component that associates with the subdistal appendages where it stably anchors MTs to the mother centriole. Lately it was shown that Ninein is also localized at the proximal end of centrioles (Bouckson-Castaing et al. 1996; Mazo et al. 2016; Ye et al. 2014), where it could be involved in centrosome linker function. Indeed, fluorescence microscopy detected both pools of Ninein at the centrosome (Figure 19A). Ninein localized to the proximal end of both centrioles and was detected at the subdistal appendages of the mother centriole close to the signal of the distal appendage protein CEP164 (Figure 19A, upper panel). Since C-Nap1 is the known anchor protein of the centrosome linker and is believed to be the most upstream protein in the linker hierarchy, and CEP128 has been shown to be upstream of Ninein at the sub-distal appendages (Mazo et al. 2016; Panic et al. 2015), we checked the localization dependencies of Ninein at both sites in RPE1 *CEP250* KO and *CEP128* KO cell lines (Figure 19A). Ninein was no longer detectable at the proximal end of centrioles in *CEP250* KO cells (Figure 19A, middle panel) and was also not present at the subdistal appendages of the mother centriole in RPE1 *CEP128* KO cells (Figure 19A, lower panel). STED super resolution images of Ninein confirmed its dual localization at the centrosome and the dependence of the different Ninein pools on C-Nap1 and *CEP128*, respectively (Figure 19C and D). The Ninein pool at the subdistal appendages showed a ring-like appearance with a diameter similar to the CEP164 ring (Figure 19C, middle panel). To further analyze the proximal pool of Ninein and to check if Ninein directly connects both centrosomes together, we performed 3D STED in *CEP128* KO RPE1 cells where a series of STED images were taken, and a 3D model was reconstructed (Figure 19B). This showed a plate-like structure with a slightly wider width as the centriole wall, which was marked by polyglutamylated tubulin GT335 (acetylated tubulin highlights the centriole MTs). Different from Rootletin (Mahen 2022; Vlijm et al. 2018), apparently Ninein did not form filaments suggesting that Ninein itself does not link the two centrioles together, and probably serves as a scaffold downstream of C-Nap1 for the anchoring of other centrosome linker proteins (Figure 19D).

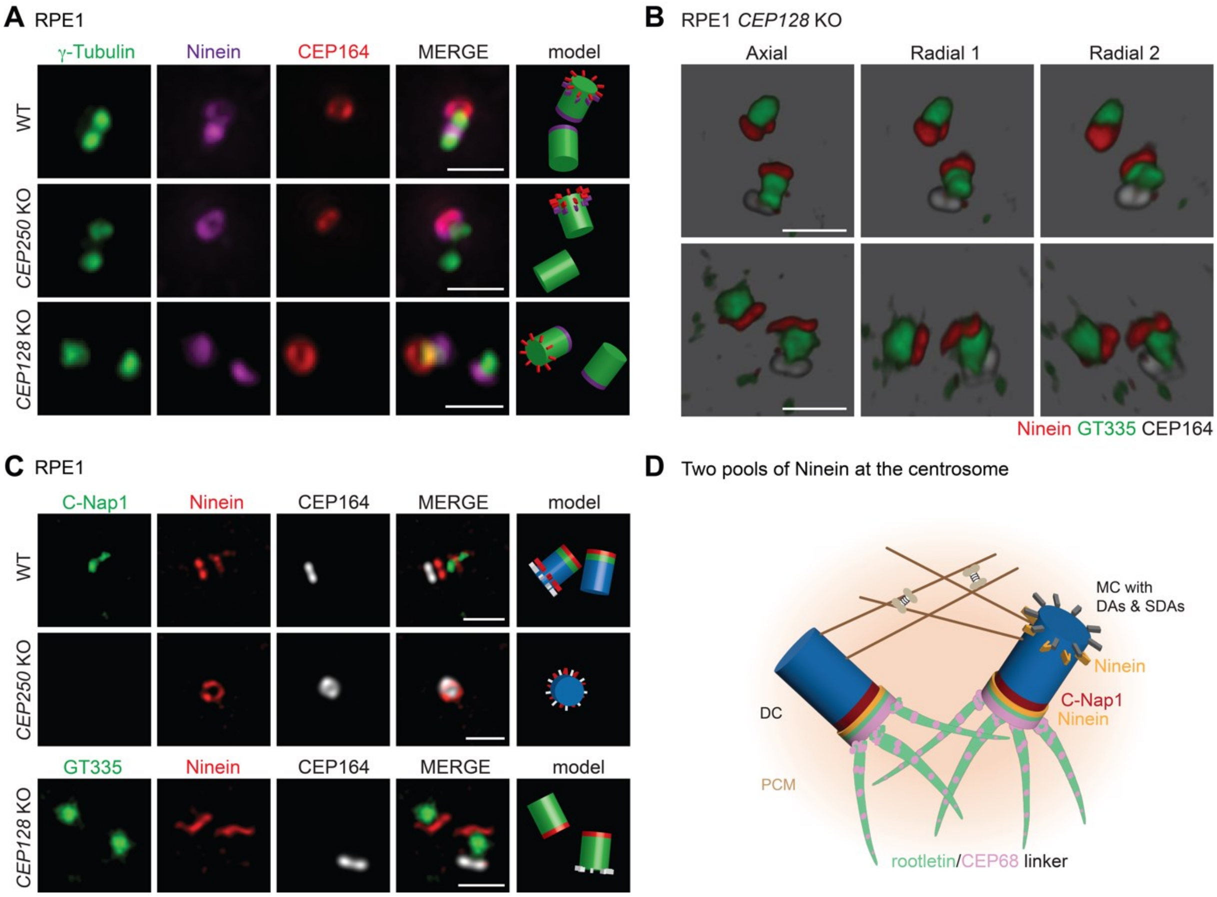

Figure 19 Ninein is a novel centrosome linker protein and shows dual localization at the centrosome. A Indirect immunofluorescence analysis of Ninein at the centrosomes in RPE1 WT, *CEP250* KO and *CEP128* KO cells. CEP164 marks the mother centriole, γ-tubulin was used as centrosome marker. The model panel illustrates the position of the centrioles and centriole appendages. Scale bars: 1 µm. **B** 3D reconstructed model of Ninein stained centrosomes from 3D STED images in RPE1 *CEP128* KO cells. Scale bars: 1 µm. **C** STED super resolution image and model of Ninein at the centrosome in RPE1 WT, *CEP250* KO and *CEP128* KO cells. CEP164, C-Nap1 and GT335 were used to mark the mother centriole, the proximal end of centrioles, and the centriole wall, respectively. The model panel illustrates the position of the centrioles and appendages (colour in model corresponds to the centrosome marker of the images on the left: Ninein is red; CEP164 white; C-NAP1 or GT335 are green). For WT and *CEP250* KO a blue centriole model was used for better illustration of the different positions. In CEP128 KO GT335 (green) was used to mark the centrioles. Scale bars: 1 µm. **D** Model of centrosome cohesion including Ninein's dual localization at the centrioles **A-C** adapted from Theile et al., 2023; performed by Dr. Xue Li.

To verify the function of Ninein in centrosome cohesion at both centriolar localizations, I performed siRNA depletion of C-Nap1 and Ninein in RPE1 *CEP250* KO (no Ninein pool at the proximal end) and *CEP128* KO (no Ninein pool at SDA) cells. In RPE1 *CEP250* KO cells, that are defective in centrosome linker formation and where centrosome cohesion depends on the MT pathway (Panic et al. 2015), siC-Nap1 had as expected no impact on centrosome distance and addition of Nocodazole strongly disjoined centrosomes (Figure 20A and B). In contrast, depletion of Ninein triggered a drastic increase in centrosome separation from 20% (siControl) to more than 60% even without Nocodazole treatment (Figure 20A and B) which is likely due to disruption of SDA MTs, confirming the role of Ninein in the MT centrosome cohesion pathway (Delgehyr et al. 2005; Mogensen et al. 2000). After depolymerization of all MTs via Nocodazole centrosome separation increased even further to 80% (Figure 20B). This indicates that in RPE1 *CEP250* KO cells about 2/3 of centrosome cohesion is provided by SDA-derived MTs and 1/3 probably by PCM MTs.

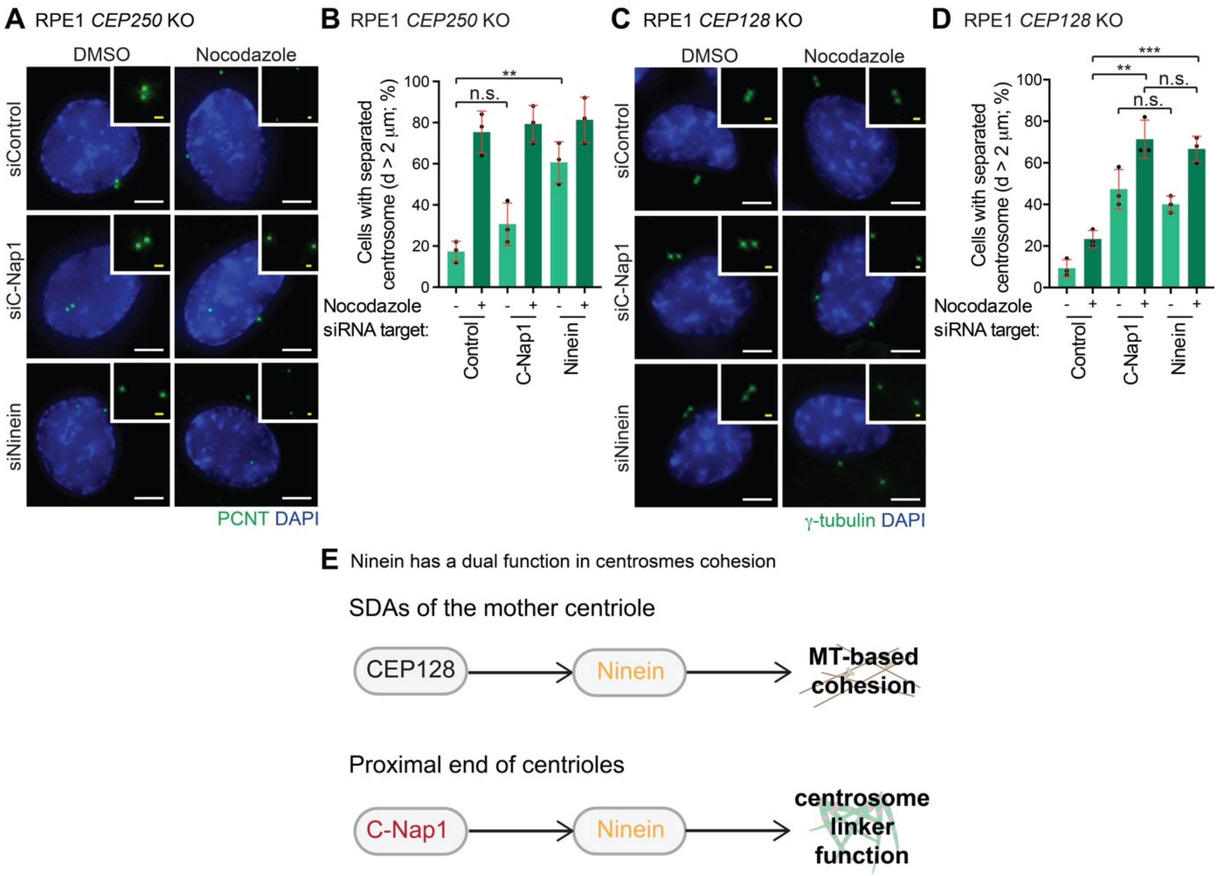

Figure 20 Ninein plays dual roles in interphase centrosome cohesion downstream of C-Nap1 and CEP128. A, C Fluorescent images of centrosomes in RPE1 *CEP250* KO and *CEP128* KO cells with the indicated siRNA depletions, without and with MT depolymerization using Nocodazole. PCNT or γ-tubulin was used to mark centrosomes and DNA was stained with DAPI. The box in the right-hand corner shows the centrosome signals of the cell in the main panel. Scale bars in white: 5 µm. Scale bars in yellow: 1 µm. **B, D** Quantification of cells with separated centrosomes (centrosome distance > 2 µm) for RPE1 *CEP250* KO (B) and *CEP128* KO (D) samples. N = 50 cells per experiment, n = 3 independent experiments. Bar and error represent mean and SD. Unpaired t-test. n.s.: not significant $p > 0.05$, ** $p < 0.01$, *** $p < 0.001$. **E** Summary of Ninein functions based on the dual localization. **A-E** adapted and modified from Theile et al., 2023.

Most interestingly, depletion of Ninein in MT linkage deficient *CEP128* KO cells, where centrosome cohesion is mainly dependent on the centrosome linker, increased centrosome separation from 10% to 40% (Figure 20C and D). This impact was comparable to the observation in response to C-Nap1 depletion (Figure 20D) and is consistent with the proposed centrosome linker function of Ninein downstream of C-Nap1 as indicted before (Figure 20E). Furthermore, the centrosome disjunction increased after Nocodazole treatment to 70% in C-Nap1 or Ninein depleted RPE1 *CEP128* KO cells, supporting the evidence of a role of PCM-organized MTs in centrosome cohesion.

Taken together, Ninein has a dual function in centrosome cohesion as centrosome linker component downstream of C-Nap1 and as MT anchor at SDAs downstream of *CEP128* in RPE1 cells (Figure 20E).

3.3.2 PCM-derived MT could play a role as additional centrosome cohesion pathway during interphase

Pericentrin (PCNT) is beside of CEP215 one of the major PCM components (Kim and Rhee 2014). It is not only required for centrosome maturation and proper bipolar spindle formation, but also for anchoring the γ-tubulin complexes at the centrosomes (Haren, Stearns, and Lüders 2009; Kim and Rhee 2014; Zimmerman et al. 2004).
The previous results showed evidence for a potential impact on centrosome cohesion of PCM-derived MTs (Figure 20). To collect further indications, I performed siRNA of PCNT in RPE1 WT and *NIN* KO cells (Figure 21), to check whether PCNT can enhance the centrosome separation phenotype especially after Ninein deletion. Depletion of C-Nap1 was used as positive control in WT and showed ~40% of centrosome separation which was even more enhanced to ~70% after Nocodazole treatment. Knock down of PCNT did not show an effect on centrosome cohesion compared to siControl in RPE1 WT. In line with previous results siC-Nap1 could not enhanced centrosome disjunction in RPE1 *NIN* KO cells. In contrast, depletion of PCNT enhanced centrosome separation to a similar level like RPE1 *NIN* KO with Nocodazole treatment. Surprisingly, Nocodazole did not show an impact on centrosome cohesion after siPCNT in RPE1 *NIN* KO, probably because PCM-derived MTs are absent now. These results indicate a potential role of PCNT and/or other PCM components in centrosome cohesion based on MTs from the PCM. Furthermore, the missing phenotype of PCNT depletion in RPE1 WT suggests a kind

of hierarchical function of the different pathways in centrosome cohesion, including the PCM-pathway besides the already known centrosome linker and MT-based cohesion pathway.

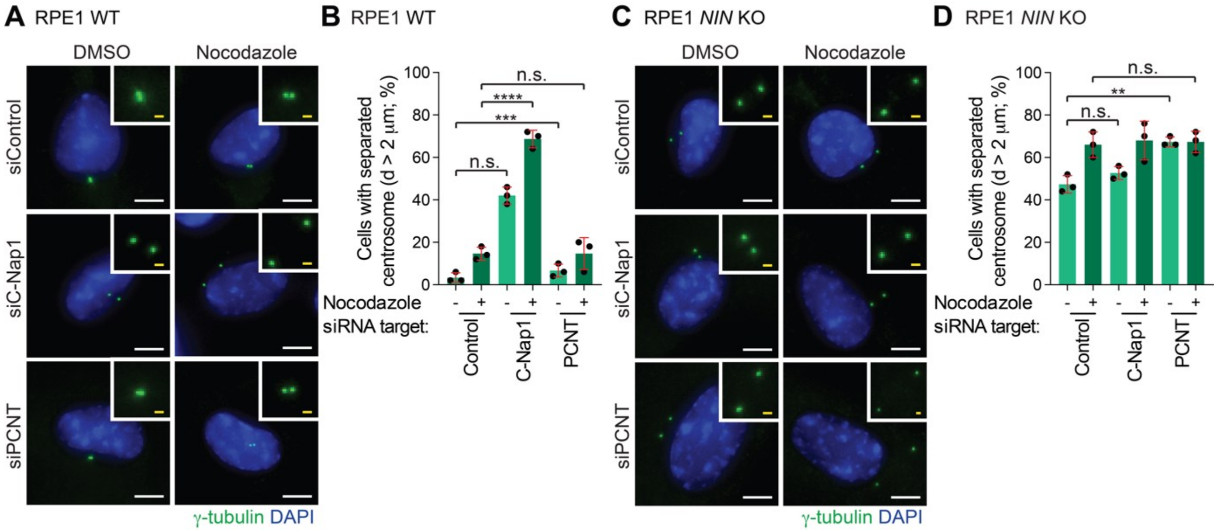

Figure 21 Pericentrin depletion impacts centrosome cohesion in RPE1 *NIN* KO cells. A-D (A, C) Fluorescent images of centrosomes in RPE1 WT and *NIN* KO cells with the indicated siRNA depletions, without and with MT depolymerization using Nocodazole. γ-tubulin was used to mark centrosomes and DNA was stained with DAPI. The box in the right-hand corner shows the centrosome signals of the cell in the main panel. Scale bars in white: 5 µm. Scale bars in yellow: 1 µm. (B, D) Quantification of cells with separated centrosomes (centrosome distance > 2 µm) for RPE1 WT (B) and *NIN* KO (D) samples. N = 50 cells per experiment, n = 3 independent experiments. Bar and error represent mean and SD. Unpaired t-test. n.s.: not significant $p > 0.05$, ** $p < 0.01$, *** $p < 0.001$, **** $p < 0.0001$. **A-D** adapted and modified from Theile et al., 2023.

3.4 MT dynamic is impaired in centrosome linker deficient RPE1 cells

3.4.1 C-Nap1 and Ninein have an impact on MT nucleation in RPE1 cells

In previous studies about Ninein the role in MT nucleation and anchoring at centrosomes was identified (Delgehyr et al. 2005). To test, if this function is only linked to the SDA pool of Ninein or is also related to the C-Nap1 anchored Ninein pool at the proximal end of centrioles, I performed a MT regrowth assay (Figure 22). First, MTs were depolymerized with cold treatment followed by re-nucleation after warming up the cells for ~15 sec (Würtz et al. 2022). During the treatment a limited number of MTs on the centrosomes formed that were afterwards analysed by fluorescence microscopy followed by a macro-based quantification in Fiji. Centrosomes in RPE1 WT and *CROCC* KO cells re-nucleated ~6 MTs per centrosome with a length of ~2.7 µm (Figure 22B). In contrast, the number of MTs per centrosome was reduced to ~4 and the length to ~2 µm in linker deficient RPE1

CEP250 KO and *NIN* KO cells (Figure 22B). The decreased number of nucleated MTs in *CEP250* KO was rescued by complementation with a constitutive expressed *CEP250* construct (Figure 22B and C). Furthermore, the rescue construct also restored centrosome cohesion in RPE1 *CEP250* KO cells to a similar level like RPE1 WT cells (Figure 22D). In conclusion, defects in the C-Nap1-Ninein-linker pathway decreases the ability of centrosomes to nucleate MTs. Rootletin deletion did not show an effect on MT nucleation underlining the missing function of Rootletin in RPE1 cells.

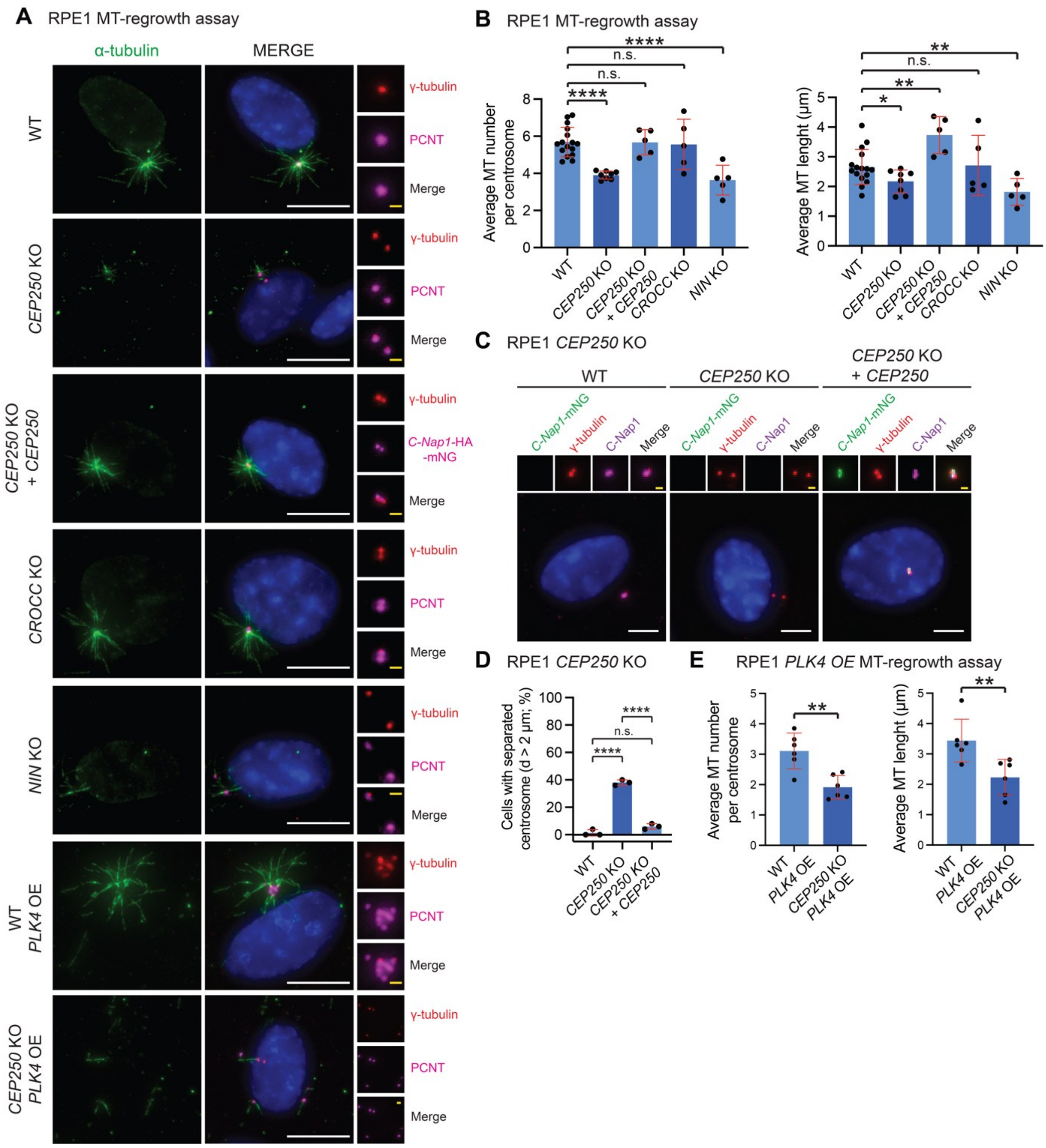

Figure 22 C-Nap1 and Ninein but not Rootletin play a role in MT nucleation. A Representative fluorescent images of MT asters nucleated from the centrosome (γ-tubulin)

after in vivo MT regrowth. The enlargements on the right show the centrosome signal of the cell in the main panel. Scale bars in white: 10 µm; scale bars in yellow: 1 µm. **B** Quantification of the average number (left) and length (right) of MTs re-nucleated from the centrosomes in (A). N = 50 cells per experiment, n ≥ 5 independent experiments. Bar and error represent mean and SD. Unpaired t-test. n.s.: not significant $p > 0.05$, * $p < 0.05$, ** $p < 0.01$, **** $p < 0.0001$. **C** Representative fluorescent images of RPE1 *CEP250* KO and *CEP250* KO expressing *CEP250-HA-mNeonGreen* (*CEP250* KO + *CEP250*). The indicated antibodies were used for indirect fluorescent analysis. Scale bars in white: 5 µm. Scale bars in yellow: 1 µm. **D** Quantification of centrosome separation from (C). N = 50 cells per experiment, n = 3 independent experiments. Bar and error represent mean and SD Unpaired t-test. n.s.: not significant $p > 0.05$, **** $p < 0.0001$. **E** Quantification of the average number (left) and length (right) of MTs re-nucleated from the centrosomes in (A) from RPE1 WT and *CEP250* KO cells with *PLK4* OE. N = 50 cells per experiment, n = 3 independent experiments. Bar and error represent mean and SD Unpaired t-test. ** $p < 0.01$. (adapted from Theile et al., 2023)

As described above, I also performed a MT-regrowth assay to analyse the nucleation ability of supernumerary centrosomes in RPE1 WT and *CEP250* KO after PLK4 overexpression (Figure 22E). In line with the observations in cells with two centrosomes, linker deficient *CEP250* KO cells with supernumerary centrosomes were less potent to re-nucleate MTs compared to WT centrosomes (Figure 22E). Interestingly, the number of nucleated MTs per centrosome were less in cells with supernumerary centrosomes irrespective of the linker status (compare Figure 22B and E), probably due to competition for MT assembly factors. This result confirmed that C-Nap1 decreases the MT nucleation ability of centrosomes.

3.4.2 The recruitment of γ-tubulin to centrosomes is decreased in RPE1 *CEP250* and *NIN KO* cells

To gain deeper insight into the MT nucleation function of the C-Nap1 anchored Ninein, I analysed the recruitment of the MT nucleator γ-tubulin to centrosomes (Figure 23). First, I analysed the localization and intensity levels of γ-tubulin in RPE1 WT, *CEP250* KO, *CEP250* KO + *CEP250*, *CROCC* KO and *NIN* KO cells (Figure 23A). As expected *CROCC* KO did not show in decrease in the γ-tubulin levels at the centrosomes (Figure 23A). In *CEP250* KO and *NIN* KO the γ-tubulin signal was decreased by app. 30% (Figure 23A). The *CEP250* construct was able to rescue the *CEP250* KO γ-tubulin recruitment defect. This result indicated that a fraction of γ-tubulin at centrosomes required C-Nap1 and Ninein but not Rootletin.

To ask the question which γ-tubulin pool (PCM or centriolar lumen pool) is influenced, I additionally performed expansion microscopy to check for defects at the inner pool of γ-tubulin (Figure 23B and C). I could not observe a difference in the length of the inner γ-tubulin pool after C-Nap1 or Ninein deletion (Figure 23C), indicating that the

PCM pool of γ-tubulin is influenced by defects in the centrosome linker, but the inner pool stays untouched.

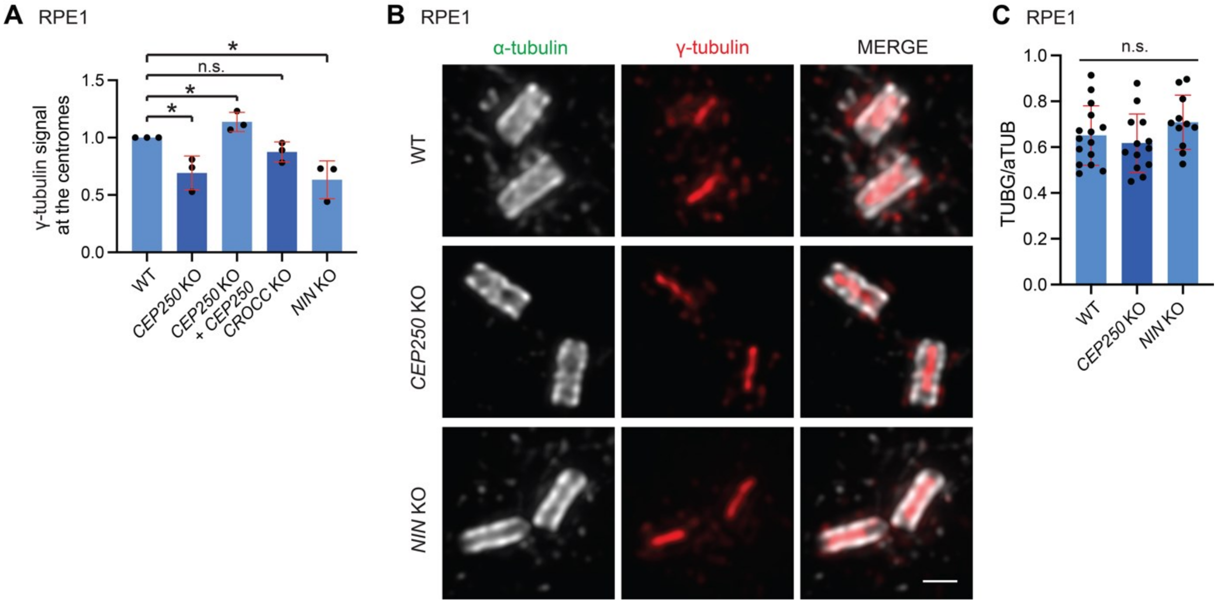

Figure 23 The level of γ-tubulin at the centrosomes is decreased in C-Nap1 and Ninein deleted cells, but the centriolar lumen pool stays untouched. A Quantification of relative γ-tubulin intensity at the centrosome in RPE1 cells. Mean value of relative γ-tubulin intensity at the centrosome is shown. N = 50 cells per experiment, n = 3 independent experiments. Bar and error represent mean and SD. Unpaired t-test. n.s.: not significant $p > 0.05$, * $p < 0.05$. **B** Representative expansion microscopy images (uExM, 4x expansion factor) from centrioles in RPE1 cells. Samples were stained with α-tubulin and γ-tubulin. Scale bar: 200 nm. **C** Quantification of the TUBG (γ-tubulin)/aTUB (α-tubulin) ratio (coverage) along the centrioles in RPE1 cells. n = minimum 10 centrioles. Unpaired t-test. n.s.: not significant $p > 0.05$ **A** adapted from Theile et al., 2023; **B, C** performed together with Aadyasha Mishra.

3.5 Centrosome cohesion is crucial for centrosome clustering during interphase

Centrosome clustering is an important mechanism that bundles supernumerary centrosomes during mitosis in cancer cells and therefore favours bipolar cell division and proper chromosome segregation (Karki, Keyhaninejad, and Shuster 2017; Kwon et al. 2008; Leber et al. 2010; Marthiens et al. 2012; Mountain et al. 1999; Pannu et al. 2015; Vitre et al. 2020). Microtubule motors including HSET (kinesin-14), kinetochore and spindle proteins have been shown working together in clustering extra centrosomes in mitosis (Karki et al. 2017; Kwon et al. 2008; Leber et al. 2010; Marthiens et al. 2012; Mountain et al. 1999; Pannu et al. 2015; Vitre et al. 2020).
Even though supernumerary centrosomes are also clustered in interphase (Godinho and Pellman 2014; Ring, Hubble, and Kirschner 1982), how supernumerary centrosomes are organized in interphase, the molecular key players and whether centrosome linker diversity is also reflected in this clustering mechanism is unknown.

3.5.1 Centrosome amplification induced by *PLK4* overexpression

To study the impact of the centrosome linker on centrosome clustering and organisation in interphase, I introduced centrosome overamplification by Dox-inducible *Flag-PLK4* OE in RPE1 and HCT116 cells with deletions in the centrosome linker genes *CEP250*, *NIN* and *CROCC* (Figure 24A and B). After 48 h of Dox induction of *Flag-PLK4*, 80% of cells showed overamplified centrosomes with a centrosome number between 6 to 11 independent of the cell line and the deleted gene (Figure 24C-F).

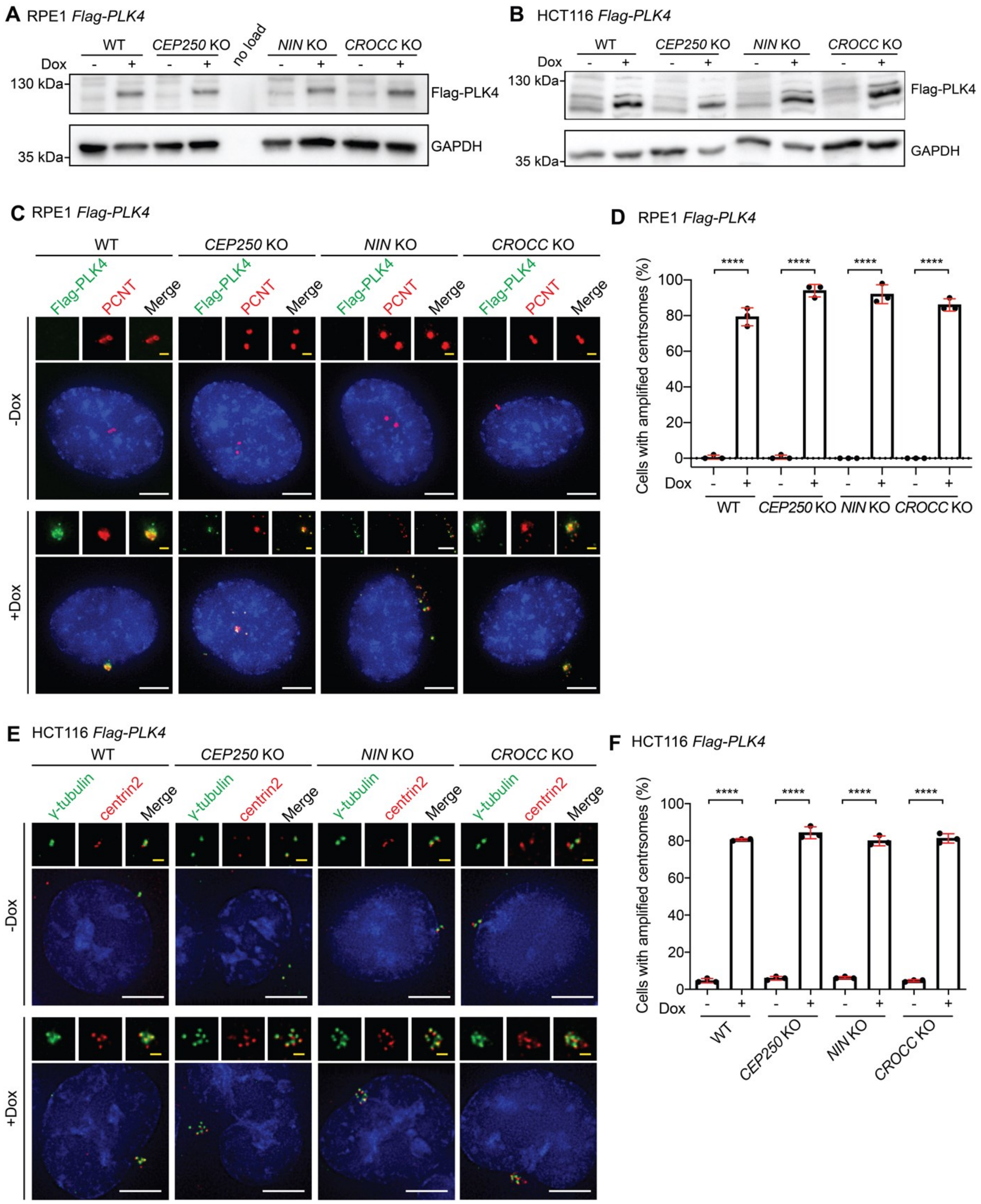

Figure 24 Confirmation of *PLK4* overexpression and supernumerary centrosome formation in RPE1 and HCT116 cells. A, B Immunoblot analysis of induced *Flag-PLK4* expression of Dox-inducible *Flag-PLK4* RPE1 WT, *CEP250* KO, *NIN* KO and *CROCC* KO cells (A) and HCT116 WT, *CEP250* KO, *NIN* KO and *CROCC* KO cells (B), with and without Dox. GAPDH was loading control. **C, E** Fluorescent images of centrosomes in Dox-inducible *Flag-PLK4* RPE1 and HCT116 WT, *CEP250* KO, *NIN* KO and *CROCC* KO cells, with and without Dox induction. The indicated antibodies were used. *Flag-PLK4* was stained with Flag antibodies. DNA was stained with DAPI. The boxes on top show enlargement of the centrosome signals of the cell in the main panel. Scale bars in white: 5 µm; scale bars in yellow: 1 µm. **D, F** Quantification of amplified centrosomes in cells from RPE1 (C) and HCT116 (E) cells, without and with Dox induction. N = 50, n = 3 independent experiments.

Dots represent the percentage of cells with amplified centrosomes in each sample. Bar and error represent mean and SD. Unpaired t-test. **** p < 0.0001. (adapted from Theile et al., 2023)

To exclude that centrosome amplification caused centriole fragmentation, I checked the co-localisation of the distal end markers Centrin2 and CEP97 with the PCM protein γ-tubulin, respectively (Figure 25).

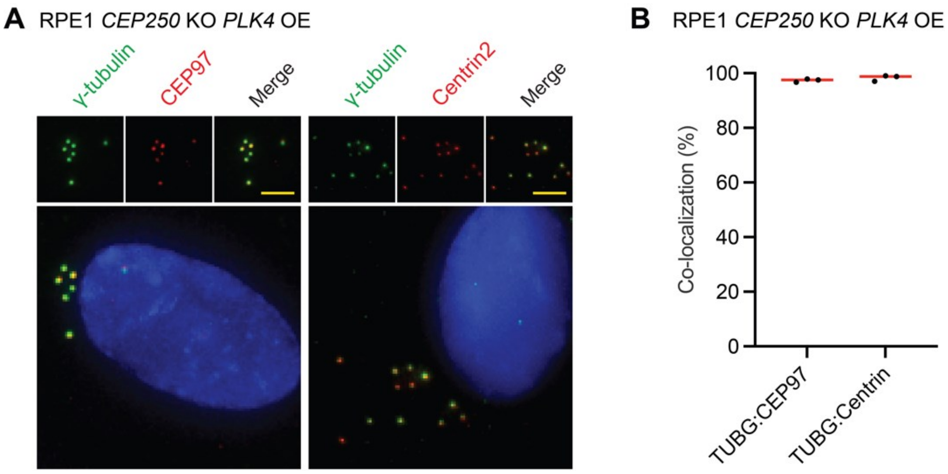

Figure 25 Centrosome amplification did not caused centrosome fragmentation. A Fluorescent images of CEP97 and γ-tubulin co-localisation, γ-tubulin and Centrin2 co-localisation in *Flag-PLK4* inducible RPE1 *CEP250* KO. Scale bars in white: 10 µm; scale bars in yellow: 5 µm. **B** Quantification of co-localisations of γ-tubulin, CEP97 and Centrin2 foci from (A). (adapted from Theile et al., 2023)

3.5.2 The centrosome linker including Ninein contributes differently to centrosome clustering

To understand, how supernumerary centrosome are clustered in interphase, I first investigated centrosome organisation and centrosome linker presence in Caco-2 cancer cells that show ~34% naturally centrosome amplification (Figure 26A and B). I measured the diameter of the smallest circle that included all amplified centrosomes of a cell, to judge centrosome distribution in cells with supernumerary centrosomes (Figure 26C).

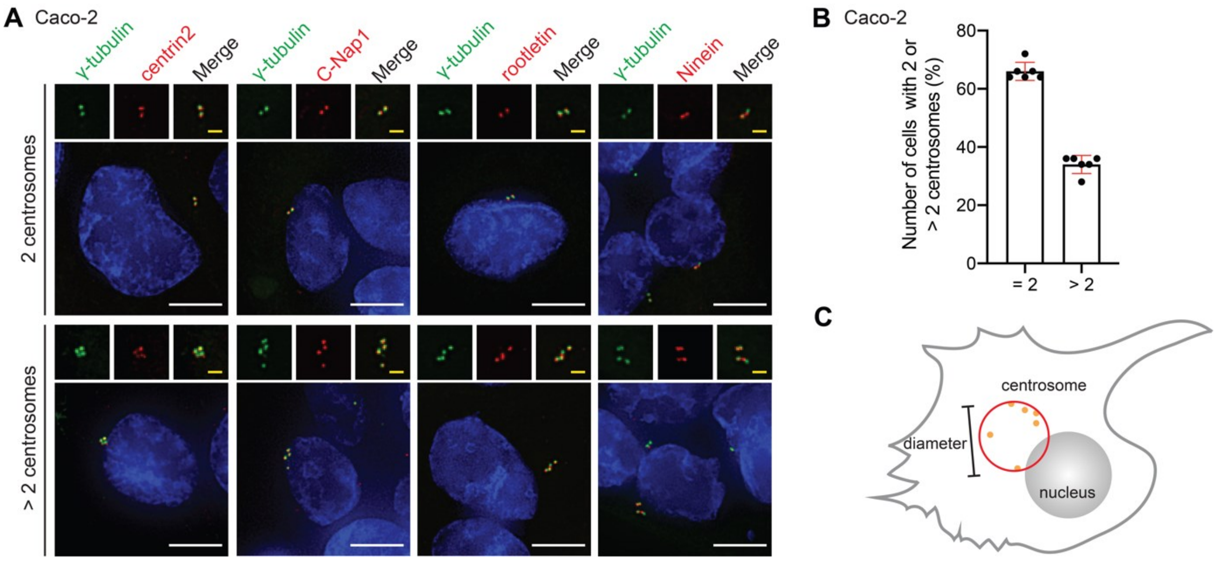

Figure 26 Centrosome organisation in Caco-2 cells with supernumerary centrosomes. **A** Fluorescent images of centrosomes and the centrosome linker proteins C-Nap1, Rootletin and Ninein in Caco-2 cells, with and without centrosome amplification. The enlargements on top show the fluorescent centrosome signals. Scale bars in white: 5 µm; scale bars in yellow: 1 µm. **B** Quantification of cells from (A). N = 50, n = 6 independent experiments. Dots represent the percentage of cells with or without amplified centrosomes in each sample. Bar and error represent mean and SD. **C** Model how to measure the diameter of amplified centrosomes. (adapted from Theile et al., 2023)

The siRNA depletion of C-Nap1, Rootletin and Ninein with and without Nocodazole treatment showed the importance of the centrosome linker and the MT pathway for the centrosome clustering during interphase in Caco-2 cells with supernumerary centrosomes (Figure 27A and B). RPE1 WT cells densely clustered centrosomes in mainly one spot, with a median diameter of 2.7 µm (Figure 27C and D). This increased to 9.1 µm after Nocodazole treatment (Figure 27D) indicating the importance of the MT-based cohesion pathway. In contrast, RPE1 *CEP250* KO and RPE1 *NIN* KO cells showed largely distributed centrosomes compared to WT, with a median diameter of ~13 µm without and even ~18 µm with Nocodazole (Figure 27D). Surprisingly, the median diameter of RPE1 *CROCC* KO cells treated with Nocodazole increased to 13.7 µm which is higher than what we observed in WT cells (9.1 µm) (Figure 27D). This could indicate a function of Rootletin in RPE1 cells with supernumerary centrosomes without MT-based cohesion. Also, in HCT116 WT cells amplified centrosomes were densely packed into one area (Figure 27E and F). In HCT116 *CEP250* KO, *NIN* KO and *CROCC* KO cells the centrosome distribution was increased with the strongest impact by *CEP250* KO followed by *NIN* KO and then *CROCC* KO (Figure 27E and F). Similar to RPE1 cells, HCT116 cells treated with Nocodazole showed enhanced distribution of supernumerary centrosomes indicating a role of the MT cohesion pathway in the clustering of amplified centrosomes (Figure 27F). However, the overall spatial centrosome distribution was less pronounced than in RPE1 cells (compare Figure 27D and F), maybe because of additional factors organizing supernumerary centrosomes in HCT116 cells.

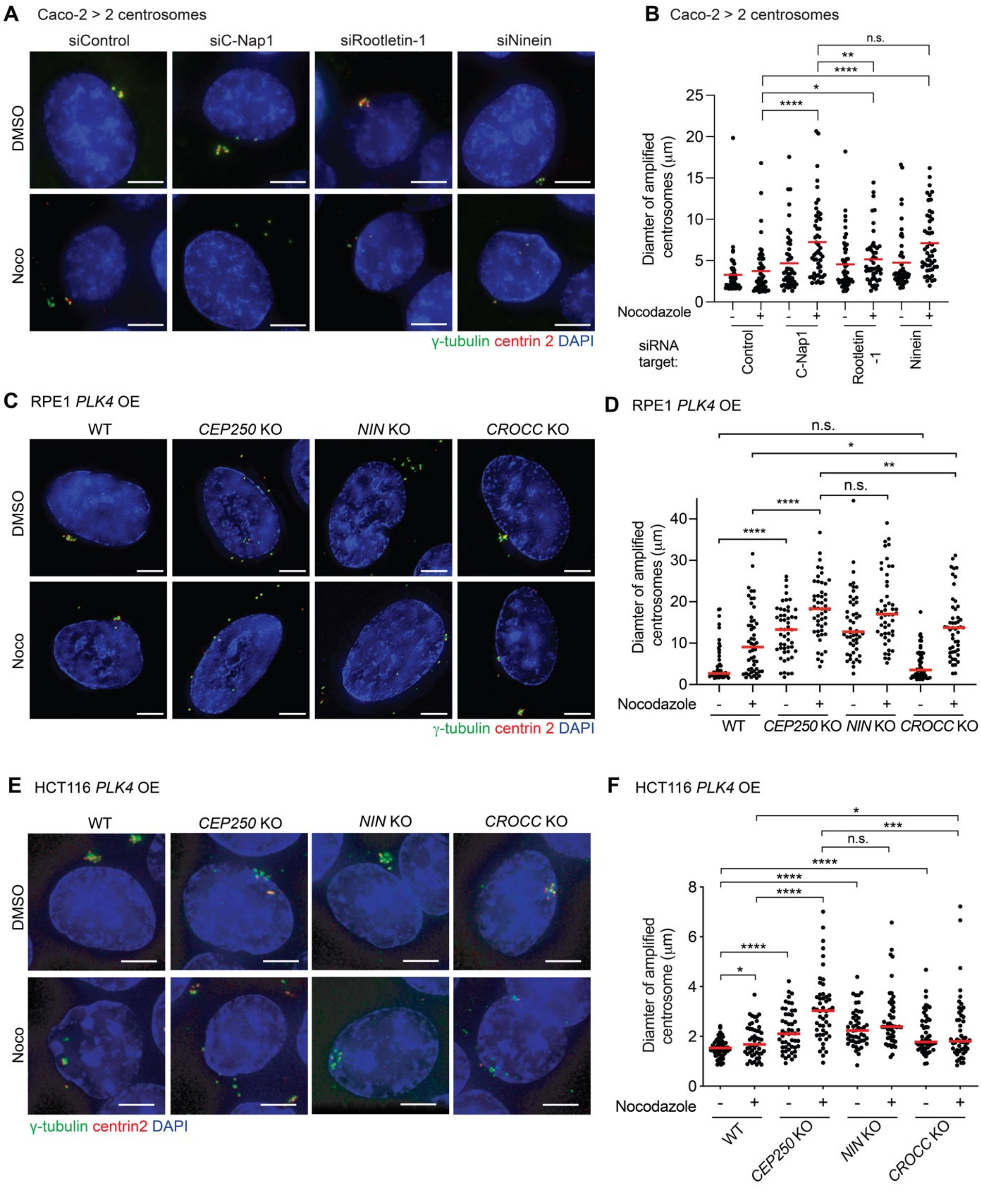

Figure 27 The centrosome linker clusters overamplified centrosomes during interphase. A Fluorescent images of centrosomes in Caco-2 cells with centrosome amplification under siRNA depletion condition using the indicated siRNAs, with and without MT depolymerization by Nocodazole. Scale bars: 5 µm. **B** Quantification of the diameter of

amplified centrosomes from (E). A representative dataset from six replicates (three replicates per experiment) are shown. N = 50 cells. Dots represent the diameter of amplified centrosomes in each cell with amplified centrosomes. Lines represent the median. Unpaired t-test. n.s.: not significant $p > 0.05$, * $p < 0.05$, ** $p < 0.01$, **** $p < 0.0001$. **C, E** Fluorescent images of centrosomes in Dox-inducible Flag-*PLK4* RPE1 and HCT116 WT, *CEP250* KO, *NIN* KO and *CROCC* KO cells upon 48 h induction, without and with MT depolymerization using Nocodazole. Scale bars: 5 µm. **D, F** Quantification of the diameter of amplified centrosomes from RPE1 (C) and HCT116 (E) cells as shown in Figure 26C in (E). A representative dataset from six replicates (three replicates per experiment) is shown. N = 50 cells. Dot represents the diameter of amplified centrosomes in each cell with amplified centrosomes. The red lines represent the median. Unpaired t-test. n.s.: not significant $p > 0.05$, * $p < 0.05$, ** $p < 0.01$, *** $p < 0.001$, **** $p < 0.0001$. (adapted from Theile et al., 2023; performed together with Dr. Xue Li)

I analysed centrosome clustering in a second way, by a radial scanning approach of the centrosome signal, to confirm the outcome of the median diameter analysis above. I quantified the fluorescence intensity outwards from the centre (brightest point) in a cell with clustered centrosome. In RPE1 WT and *CROCC* KO cells 50% of the maximum intensity (I_{50}) was reached within 3 µm, indicating that most centrosomes clustered together in one spot (Figure 28A and B). In contrast, in linker deficient RPE1 *CEP250* KO and *NIN* KO cells the centrosomes more dispersed in the cytoplasm, resulting in a diameter > 5 µm to reach 50% intensity (Figure 28A and B). In line with the median diameter analysis the MT depolymerization via Nocodazole treatment impacted centrosome distribution in all linker mutants. In consequence, I_{50} was reached further away from the centre, reflecting the even more dispersed supernumerary centrosomes (Figure 28A and B). I blotted the mean I_{50} and I_{70} values as a measure for the spatial centrosome distribution to compare the average of three experiments to simplify the presentation of the data (Figure 28B and C). As shown before, the Rootletin linker gained function upon centrosome amplification and Nocodazole treatment. However, the Rootletin linker branch seems to be the least important organizational element followed by C-Nap1 and Ninein. This suggests that it is mainly the C-Nap1-Ninein linker that clusters overamplified centrosomes in RPE1 cells consistent with what we have observed in RPE1 cells without centrosome amplification. Additionally, to the centrosome linker, the MT-based centrosome cohesion pathway is important to spatially organize supernumerary centrosomes in interphase.

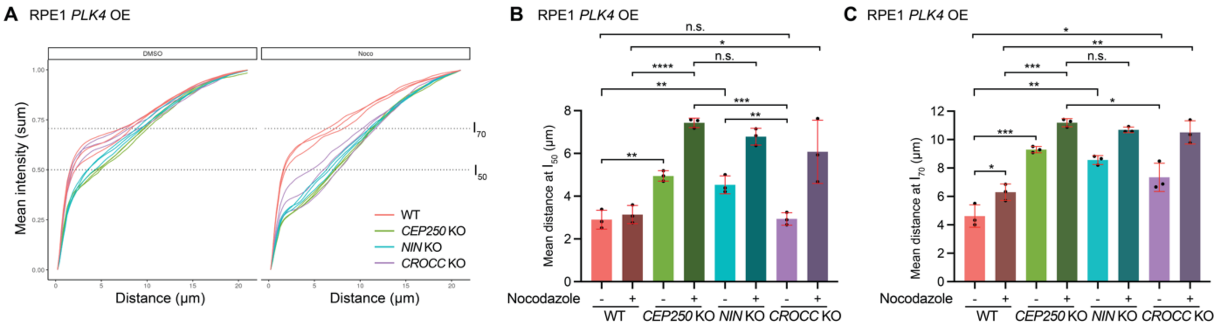

Figure 28 Radial scanning approach to analyse centrosome distribution in RPE1 cells with supernumerary centrosomes. A Mean intensity sum per replicate after radial scanning of the centrosome signal intensity from the brightest point outwards in Dox-inducible *Flag-PLK4* RPE1 WT, *CEP250* KO, *NIN* KO and *CROCC* KO cells upon 48 h Dox induction, with and without MT depolymerization using Nocodazole. The dotted line, named half intensity (I_{50}), represents the distance where 50% of the maximum intensity was reached. I_{70} is where 70% of the maximum intensity was reached. **B, C** The average of I_{50} (B) and I_{70} (C) values from (A). N ≥ 22 cells per replicate, n = 3 biological replicates. Bar and error represent mean and SD. Unpaired t-test. n.s.: not significant $p > 0.05$, * $p < 0.05$, ** $p < 0.01$, *** $p < 0.001$, **** $p < 0.0001$. (adapted from Theile et al., 2023; performed together with Dorothee Mersch and Prof. Dr. Simon Anders)

3.5.3 STED super resolution microscopy revealed Rootletin fibres between overamplified centrosomes

To gain a better understanding of the centrosome linker structure between overamplified centrosomes, I performed STED super resolution analysis with focusing on the Rootletin linker filaments (Figure 29). The Rootletin antibody Root-C1 was used to stain the Rootletin-fibres and γ-tubulin to mark the centrosomes. The STED analysis of Rootletin showed the filamentous Rootletin structure between two centrosomes in Caco-2, RPE1 and HCT116 cells (Figure 29). Based on the STED images, I could show that the Rootletin filamentous linker is also present between overamplified centrosomes in all cell lines (Figure 29). I noticed a denser Rootletin-fibre structure between centrosomes in HCT116 cells (Figure 29C) compared to RPE1 cells (Figure 29B), which may indicate formation of a stronger centrosome linker network consistent with our previous observation in HCT116 cells without centrosome amplification (Vlijm et al. 2018).

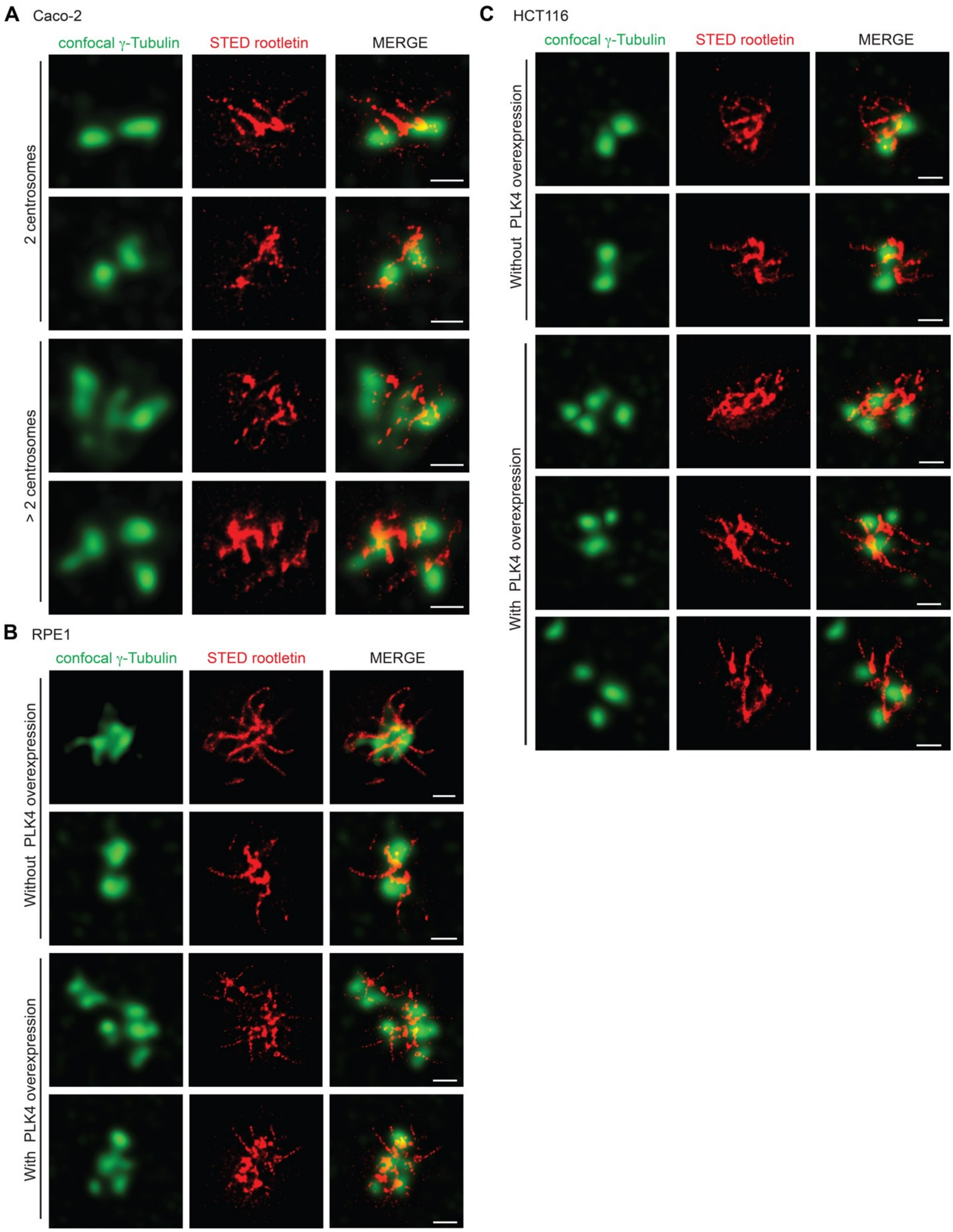

Figure 29 STED analysis of the Rootletin linker in cells without and with overamplified centrosomes. A STED super resolution image of the Rootletin linker between centrosomes in Caco-2 cells without and with natural centrosome overamplification. Scale bar: 500 nm. **B** STED super resolution image of the Rootletin linker between centrosomes in RPE1 WT (first panel) and Dox-inducible *Flag-PLK4* RPE1 WT cells without and with centrosome overamplification via *PLK4* overexpression. Scale bar: 500 nm. **C** STED super resolution images of the Rootletin linker between centrosomes in Dox-inducible *Flag-PLK4* HCT116 WT cells without and with centrosome amplification. Scale bar: 500 nm.

3.6 The influence of the centrosome linker on nuclear envelope breakdown (NEBD)

3.6.1 NEBD duration and metaphase is prolonged in centrosome linker deficient cells

In mammalian cells centrosomes are anchored to the nuclear envelope (NE) by MT/dynein interactors (Busson et al. 1998; Gönczy et al. 1999; Robinson et al. 1999). Previously, it has been shown that MTs derived from the centrosome can generate pulling forces to create mechanical tension in the nuclear lamina causing local NEBD (Beaudouin et al. 2002).

To understand the influence of the centrosome linker status especially in cells with supernumerary centrosomes on NEBD and the impact in mitosis we performed live cell imaging (Figure 30). We used RPE1 WT and *CEP250* KO cells with and without supernumerary centrosomes expressing γ-tubulin-mRuby2 as centrosome marker and LaminB1-mNeonGreen for the NE, respectively (Figure 30A). As described before, we added the SPY650-DNA probe to stain the DNA during the time laps experiment.

To gain deeper understanding of the events during NEBD we divided this phase into different time windows. The time before NEBD and NEBD preparation which starts with the appearance of the first NE fold close to centrosomes judge by the LamninB1 signal. The time point, where the first hole in the NE appears is called NEBD start. The NEBD end is reached as soon as the LaminB1 signal is dislocated from the nucleus. The sum of the time from the start to end of the NEBD is the NEBD duration. The overview of the different time windows analysed during mitosis is shown in Figure 30B.

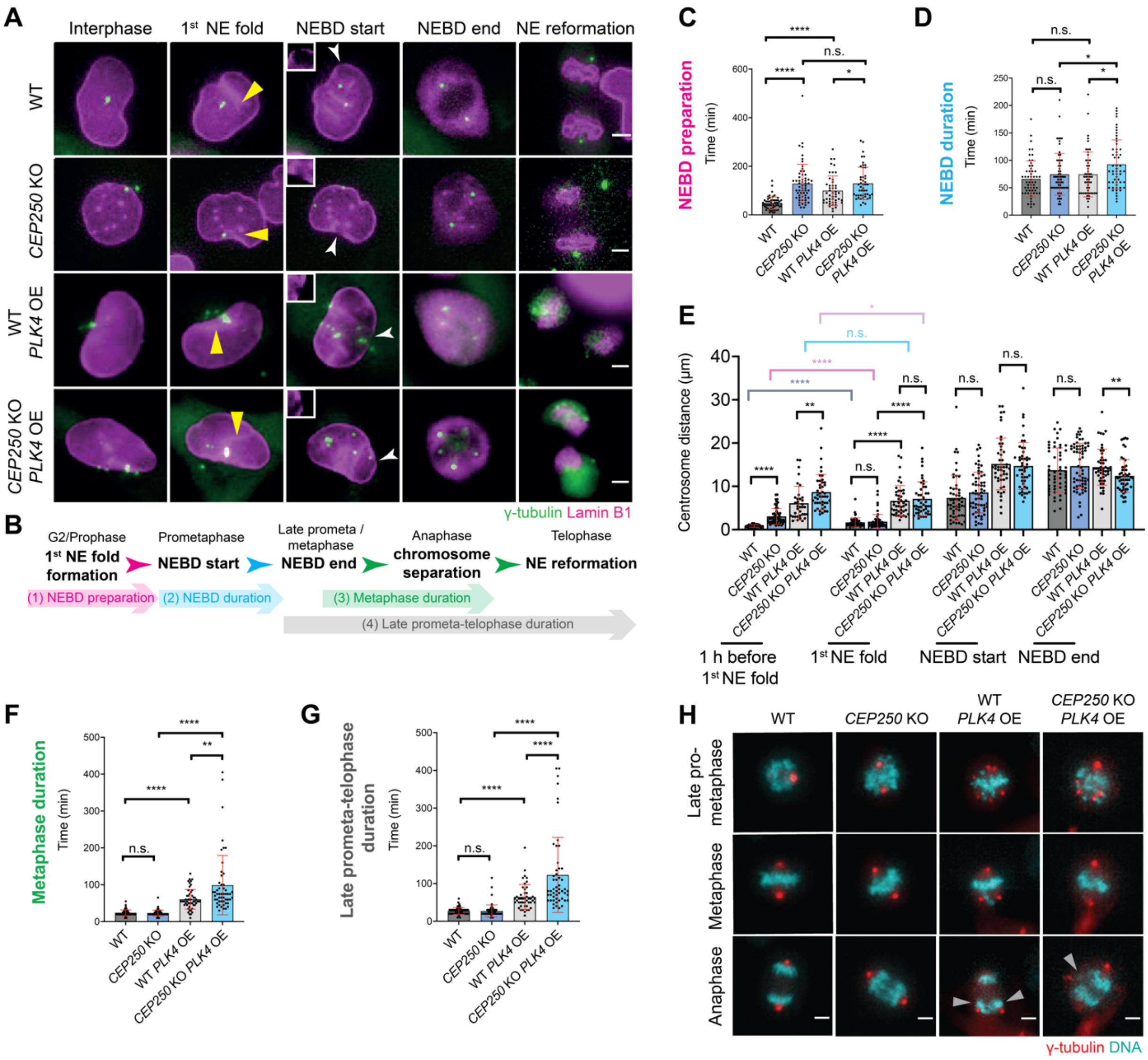

Figure 30 NEBD is delayed in linker deficient *CEP250* KO cells. A Representative images of live cell imaging analysis of RPE1 WT, *CEP250* KO, WT *PLK4* OE and *CEP250* KO *PLK4* OE cells expressing LaminB1-mNeonGreen (magenta) and γ-tubulin-mRuby2 (green) as markers for the NE and centrosomes, respectively. Yellow arrows indicate first NE fold. White arrows indicate first NE discontinuation. The inlet boxes show enlargement of first NE discontinuation. Scale bars: 5 µm. **B** Experiment design. Four critical time points were defined for the analysis: 1st NE fold formation close to the centrosomes; NEBD start (appearance of the first discontinuation in the NE); NEBD end (LaminB1 signal completely dispersed from the NE); NE reformation (reformation of LaminB1 signal around the chromosomes). The time between critical time points was analysed: (1) NEBD preparation time, (2) NEBD duration, (3) metaphase duration and (4) late prometa-telophase duration. **C** Quantification of NEBD preparation time. WT: n = 54 cells from 6 independent experiments, *CEP250* KO: n = 56 cells from 6 independent experiments, WT *PLK4* OE: n = 48 cells from 7 independent experiments, *CEP250* KO *PLK4* OE: n = 47 cells from 8 independent experiments. **D** Quantification of NEBD duration. WT: n = 54 cells from 6 independent experiments, *CEP250* KO: n = 56 cells from 6 independent experiments, WT *PLK4* OE: n = 48 cells from 7 independent experiments, *CEP250* KO *PLK4* OE: n = 47 cells from 8 independent experiments. **E** Quantification of centrosome distance (in case of WT *PLK4* OE and *CEP250* KO *PLK4* OE cells the centrosome distribution) at 1 h before 1st NE fold formation, 1st NE fold formation, NEBD start and NEBD end. WT: n = 54 cells from 6 independent experiments, *CEP250* KO: n = 56 cells from 6 independent experiments, WT

PLK4 OE: n = 48 cells from 7 independent experiments, *CEP250* KO *PLK4* OE: n = 47 cells from 8 independent experiments. **F** Quantification of metaphase duration. WT: n = 52 cells from 3 independent experiments, *CEP250* KO: n = 56 cells from 3 independent experiments, WT *PLK4* OE: n = 52 cells from 3 independent experiments, *CEP250* KO *PLK4* OE: n = 53 cells from 3 independent experiments. **G** Quantification of late prometa-telophase duration. WT: n = 54 cells from 6 independent experiments, *CEP250* KO: n = 56 cells from 6 independent experiments, WT *PLK4* OE: n = 48 cells from 7 independent experiments, *CEP250* KO *PLK4* OE: n = 47 cells from 8 independent experiments. **H** Representative images from live cell imaging analysis of WT, *CEP250* KO, WT *PLK4* OE and *CEP250* KO *PLK4* OE cells expressing γ-tubulin-mRuby2 (red) as a marker for the centrosomes. The DNA was marked by SPY-DNA650 dye (cyan). Gray arrows highlight chromosome segregation errors. Scale bars: 5 µm. Data information: In **C-G**, data are presented as mean ± SEM. N.s., not significant, *p<0.05, **p < 0.01, ***p < 0.005, ****p < 0.0001 (the Mann-Whitney test). (adapted from Theile et al., 2023, performed together with Dr. Hairuo Dang)

In RPE1 WT cells, the preparation for nuclear envelope breakdown (NEBD) took 50 min (Figure 30C), followed by a 70 min NEBD duration (Figure 30D). During this time, the two centrosomes remained in close proximity and stayed together until the first fold formation in the NE (1st NE fold, Figure 30E). With the start of the NEBD the two centrosomes subsequently separated and moved further apart to establish the mitotic spindle. In RPE1 cells lacking C-Nap1, centrosomes were already separated (>4 µm) before the 1st NE fold formation. Surprisingly, at the time point of the formation of the 1st NE fold the two centrosomes temporarily moved together (average distance approx. 1.8 µm) before their separation with NEBD (Figure 30E). In contrast to RPE1 WT cells, the time for NEBD preparation was prolonged in centrosome linker deficient *CEP250* KO cells compared to WT cells (>120 min vs. 50 min), suggesting a potential role of interphase centrosome cohesion in NEBD. In RPE1 *CEP250* KO cells with supernumerary centrosomes, not only the NEBD preparation but also the duration of the NEBD were further elongated compared to WT cells with additional centrosomes (Figure 30D). Important to note, the NEBD preparation is extended in RPE1 WT cells with centrosome amplification compared to RPE1 WT cells with 2 centrosomes (Figure 30C). In summary, in linker deficient RPE1 *CEP250* KO cells the NEBD preparation and duration are prolonged. This indicates that the centrosome linker status could be crucial for the applied forces to the NE and the subsequent NEBD in prometaphase, especially in the presence of supernumerary centrosomes.

To gain further insights into whether supernumerary centrosomes and/or defects in the centrosome linker influence the timing and accuracy of chromosome segregation, we investigated metaphase duration and the time interval from late-prometaphase (NEBD end) until NE reformation (telophase; Figure 30F-G). With an average metaphase duration of around 24 min RPE1 *CEP250* KO cells behaved like WT cells. The presence of supernumerary centrosomes extended metaphase to 60 min in RPE1 WT cells and to 111 min in *CEP250* KO cells (Figure 30F). A similar trend was observed when analysing the late prometaphase-to-telophase duration (Figure 30G). These results indicate that the presence of supernumerary centrosomes, coupled with a C-Nap1 defect, contributes to a delay in anaphase onset.

3.6.2 C-Nap1 deletion combined with centrosome overamplification activates the SAC

Previously, it was shown that supernumerary centrosomes impact kinetochore-MT attachments, which then fail to satisfy the SAC (Basto et al. 2008; Gergely and Basto 2008; Kwon et al. 2008; Yang et al. 2008). As demonstrated earlier, the RPE1 *CEP250* KO cells with supernumerary centrosomes showed a delay in the metaphase-anaphase transition (Figure 30F ang G), raising the question of whether supernumerary centrosomes contribute to SAC activation. To test this hypothesis, I checked the levels of two different SAC proteins by analysing the kinetochore signal of BUB1 and MAD1 relative to the centromere protein CENP-C (Etemad et al., 2019) (Figure 31A and B). In RPE1 WT cells with supernumerary centrosomes the BUB1 and MAD1 signal at kinetochores were increased (Figure 31B). Defects in the centrosome linker in *CEP250* KO cells in addition with centrosome amplification even further increased the SAC-protein levels at kinetochores (Figure 31B). In line with the normal metaphase-to-anaphase transition in RPE *CEP250* KO cells with two centrosomes, I observed only a slight increase in MAD1 but not BUB1 signal intensity at kinetochores compared to WT cells. This together suggests that the C-Nap1 defect, in combination with supernumerary centrosomes prolong SAC activity.
The outcome of the NEBD analysis is summarized in the model in Figure 31C.

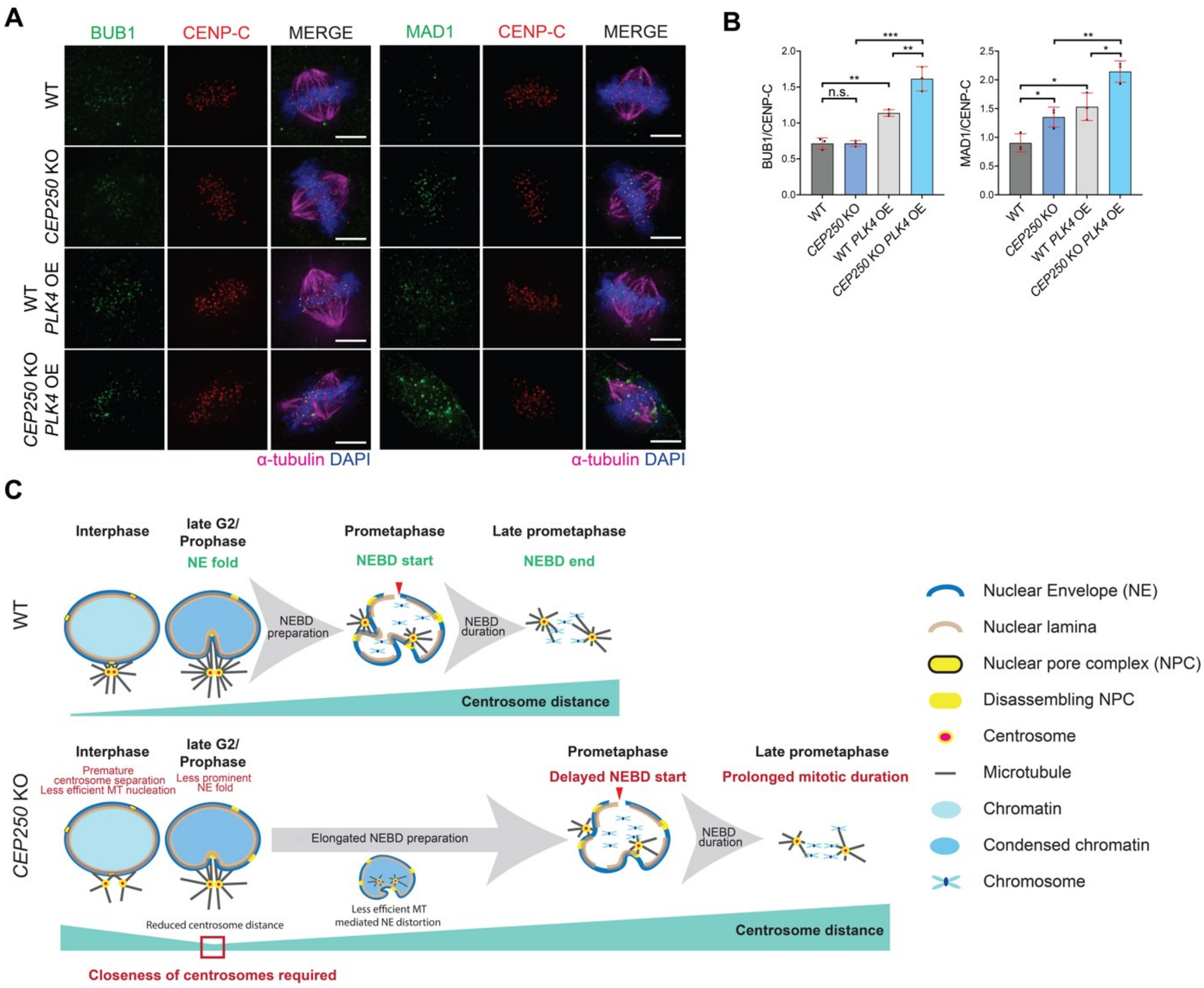

Figure 31 SAC activation is caused by centrosomes overamplification and *CEP250* deletion. A Fluorescent images of RPE1 WT, *CEP250* KO, WT PLK4 OE and *CEP250* KO *PLK4* OE cells. BUB1 and MAD1 were stained by IF to analyse the signal distribution or accumulation/persistence. CENP-C was used as centromere marker, α-tubulin to visualize the mitotic spindle and DNA was stained with DAPI. Scale bars: 5 µm. **B** Quantification of BUB1 and MAD1 signal intensity from (A) normalized to the corresponding CENP-C signal. N ≥ 46 cells, n = 3 independent experiments. Bar and error represent mean and SD. Unpaired t-test. n.s.: not significant $p > 0.05$, * $p < 0.05$, ** $p < 0.01$, *** $p < 0.005$. **C** Schematic diagram showing the proposed model for NEBD elongation in *CEP250* KO cells. Besides the premature centrosome separation, the less efficient MT nucleation ability might be one reason for delay in NEBD preparation causing a prolonged mitotic duration. (adapted and modified from Theile et al., 2023)

3.7 The impact of the centrosome linker on mitotic spindle formation in cells with supernumerary centrosomes

Based on our finding that the centrosome linker clusters supernumerary centrosome in interphase cells (Figure 27), I hypothesized that the centrosome linker may have an impact on spindle formation and chromosome segregation in mitosis. Analysis of RPE1 metaphase cells with and without centrosome linker function and carrying multiple centrosomes showed a slight increase (from 18% to 23%) in multipolar spindle formation when *CEP250* was deleted compared to the WT control (Figure 32A and B). This impact was not observed in RPE1 *NIN* KO and *CROCC* KO cells (Figure 32B) indicating that C-Nap1 functions as major factor under this experimental condition. This spindle abnormality resulted in an increased occurrence of mis-segregated chromosomes in RPE1 *CEP250* KO cells (Figure 32C and D). The absence of an enhanced phenotype in RPE1 *NIN* KO and *CROCC* KO cells likely reflects the functional redundancy of Ninein and Rootletin in RPE1 cells with supernumerary centrosomes. In HCT116 cells with centrosome overamplification I observed multipolar spindle formation with a similar frequency independent of the centrosome linker status probably due to the strongly pronounced MT cohesion pathway (Figure 32E and F).

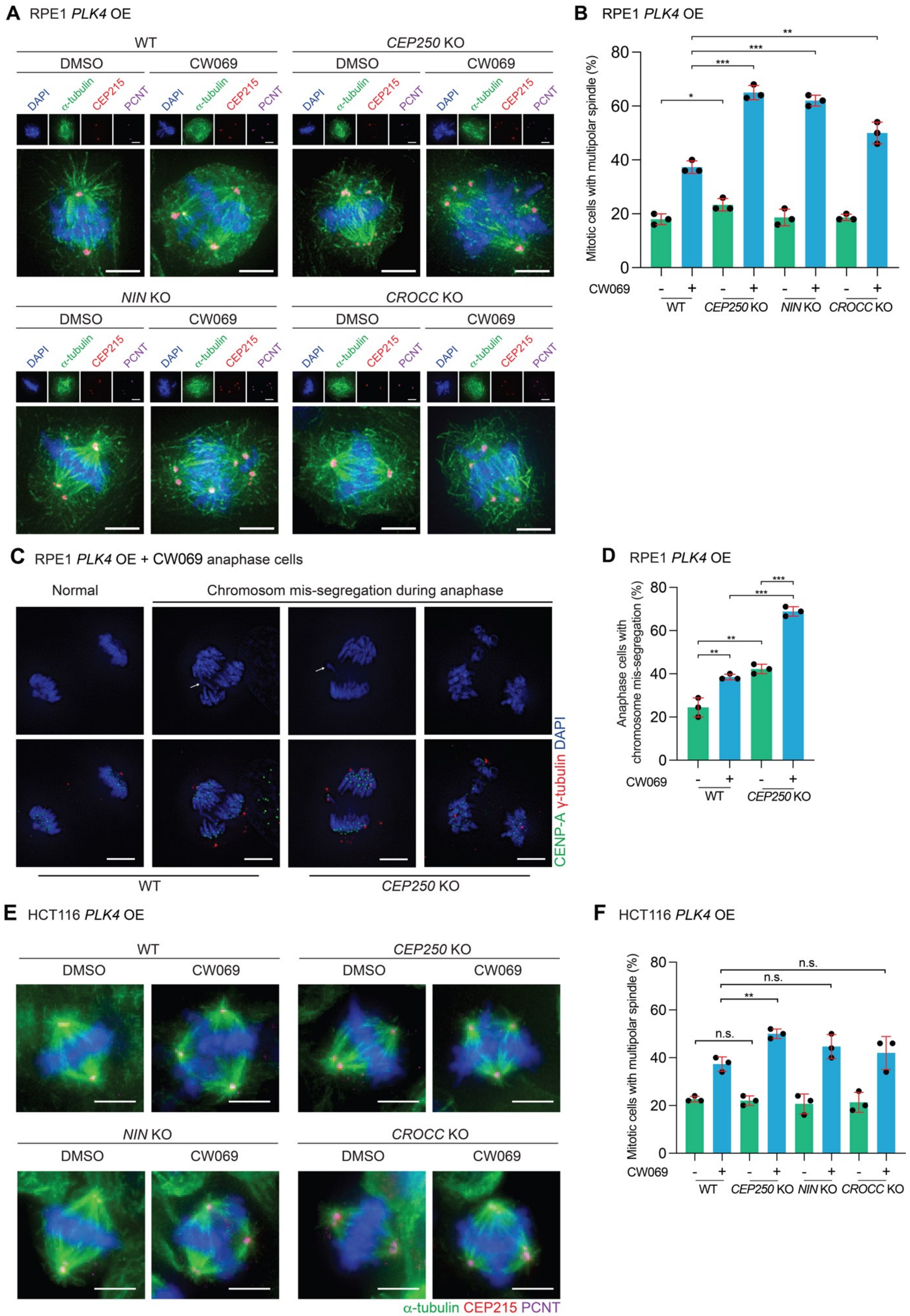

Figure 32 Impact of centrosome linker defects in RPE1 and HCT116 cells with amplified centrosomes in mitosis. A Fluorescent image of mitotic spindles in Dox-

inducible *Flag-PLK4* RPE1 WT, *CEP250* KO, *NIN* KO and *CROCC* KO cells upon 48 h Dox induction (*PLK4* OE). The chemical CW069 was used to partially inhibit HSET. DMSO was used as solvent control. White scale bars: 5 µm. **B** Quantification of mitotic cells with multipolar spindle from (A). N = 50 cells per experiment, n = 3 independent experiments. Bar and error represent mean and SD. Unpaired t-test. * $p < 0.05$, ** $p < 0.01$, *** $p < 0.001$. **C** Fluorescent images of RPE1 anaphase cells with supernumerary centrosomes (red; γ-tubulin) upon 48 h of *Flag-PLK4* Dox induction and CW069 treatment with and without chromosome mis-segregation. DNA was stained with DAPI. White arrows show lagging and bridging chromosomes. Scale bars: 5 µm. **D** Quantification of anaphase cells from (A) with chromosome mis-segregation (lagging, bridging or multipolar anaphase) in *Flag-PLK4* inducible RPE1 WT and *CEP250* KO upon 48 h Dox induction and with or without HSET inhibitor CW069 treatment. N = 45 cells per experiment, n = 3 independent experiments. Bar and error represent mean and SD. Unpaired t-test. ** $p < 0.01$, *** $p < 0.001$. **E** Fluorescent image of mitotic spindles in Dox-inducible Flag-PLK4 HCT116 WT, *CEP250* KO, *NIN* KO and *CROCC* KO cells upon 48 h Dox induction (*PLK4* OE). CW069 was used to partially inhibit HSET. Scale bars: 5 µm. **F** Quantification of mitotic cells with multipolar spindle in Dox-inducible *Flag-PLK4* HCT116 WT, *CEP250* KO, *NIN* KO and *CROCC* KO cells upon 48 h Dox induction. HSET was inhibited by CW069 addition. DMSO was added as solvent control. N = 50 cells per experiment, n = 3 independent experiments. Bar and error represent mean and SD. Unpaired t-tests. n.s.: not significant $p > 0.05$, ** $p < 0.01$. (adapted from Theile et al., 2023)

I ask the question whether a stronger impact of the centrosome linker on mitotic spindle formation could be masked by the kinesin HSET that normally cluster multiple centrosomes during mitosis. Previously, it was demonstrated that suppressing HSET, either by CW069 inhibition or siRNA depletion impacts the formation of pseudo-bipolar spindles and chromosome mis-segregation in cells with supernumerary centrosomes (Chavali et al. 2016; Karki et al. 2017; Kwon et al. 2008; Watts et al. 2013). To test the hypothesis that C-Nap1 becomes important for mitotic spindle formation and maybe cooperates with the HSET-dependent clustering mechanism in RPE1 cells with supernumerary centrosomes, I incubated the cells for a relatively short time (30 min) with CW069 for partial inhibition of HSET. I observed pseudo-bipolar spindles and multipolar spindles in all RPE1 metaphase cells with centrosome overamplification upon HSET inhibition independent of the centrosome linker status (Figure 32A and B). When I quantified the frequency of multipolar spindles, I observed a striking increase from ~20% to ~65% in RPE1 cells with deletion of *CEP250* or *NIN*, and ~50% in cells without Rootletin (Figure 32B). An increase from 18% to 38% of cells with multipolar spindles was also observed upon HSET inhibition in RPE1 WT cells what was, however, not as high as in linker deficient cells.

Furthermore, HSET inhibition also increased the frequency of multipolar spindle formation in HCT116 *CEP250* KO compared to HCT116 WT cells with centrosome overamplification (Figure 32E and F). Surprisingly, in contrast to RPE1 cells, I could not observe this rise in multipolar spindle formation in HCT116 *NIN* KO and *CROCC* KO cells (Figure 32F). This reduced impact could indicate the functional redundancy of Ninein and Rootletin in HCT116 with supernumerary centrosomes.

I next asked whether these defects in the formation of pseudo-bipolar spindles impact correct chromosome segregation in anaphase. Indeed, I observed an increase in mis-segregated chromosomes from ~24% to ~39% in RPE1 WT cells with supernumary centrosomes in response to HSET inhibition (Figure 32D). Strikingly, RPE1 *CEP250* KO cells showed already ~40% mis-segregated anaphase chromosomes and the additional inhibition of HSET increased the defects to >70% (Figure 32D). Thus, the kinesin motor HSET clustering mechanism and the centrosome linker are major factors that ensure proper mitotic chromosome segregation in cells with centrosome amplification. Furthermore, these results suggest that the centrosome linker contributes to centrosome clustering in mitosis and helps to form a bipolar spindle particularly when the HSET clustering mechanism is defective.

Finally, I confirmed the cooperation between C-Nap1 and HSET in RPE1 cells with supernumerary centrosomes by live cell imaging (Figure 33). Centrosomes were marked by γ-tubulin-mScarlet-I and DNA was stained with the SPY650-DNA probe prior live cell imaging. Besides of HSET inhibition with CW069 I used siRNA for 30 h to deplete HSET during the time laps experiment (Figure 33A-E). Both treatments increased the number of RPE1 WT cells with multipolar spindles from ~28% to ~45% (CW069 treatment) and ~57% (siHSET), respectively. In RPE1 *CEP250* KO cells I observed an increase from 40% to 75% for inhibition with CW069 and 80% for HSET depletion (Figure 33F and G).

In conclusion, these results suggest that the centrosome linker contributes to pseudo-bipolar spindle formation especially when the HSET clustering mechanism failed or is partially defective.

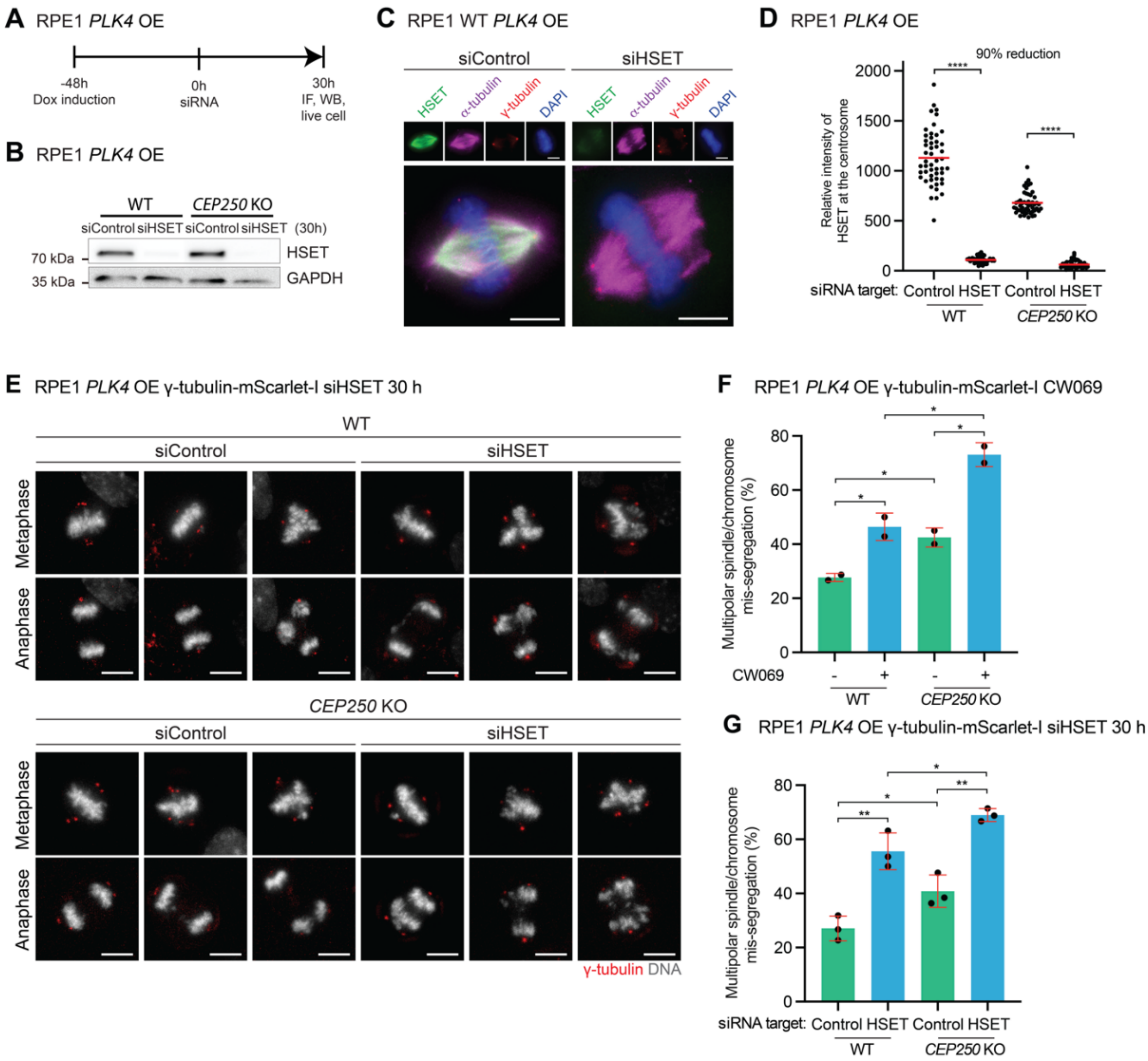

Figure 33 The centrosome linker impairs pseudo-bipolar spindle formation, especially in the absence of HSET. A Experimental design of siHSET (30 h) live cell analysis. **B** Immunoblot of HSET in RPE1 WT and *CEP250* KO cells with *PLK4* OE after 30 h siRNA treatment. GAPDH was used as loading control. **C** Representative fluorescent images of HSET signal at mitotic spindles in Dox-inducible *Flag-PLK4* RPE1 WT cells after siControl and siHSET (30 h). γ-tubulin was used as centrosome maker, α-tubulin to visualize the spindle and DAPI to stain DNA. Scale bars: 5 µm. **D** Quantification of relative HSET intensity at the metaphase spindle from (G). N = 50 cells; a representative dataset from 2 independent experiments is shown. Dot represents the relative intensity of HSET at the metaphase spindle in each cell. Mean is showed in red. Unpaired t-tests. **** $p < 0.0001$. **E** Time-lapse analysis of RPE1 WT *PLK4* OE and *CEP250* KO *PLK4* OE cells expressing γ-tubulin-mScarlet-I (red) as markers for the centrosomes followed by 30 h siHSET. The DNA was marked with SPY-DNA650 (grey). (E) shows representative still images of live cell imaging analysis. Scale bars: 10 µm. **F** Quantification of multipolar spindle/chromosome mis-segregation of Dox-inducible *Flag-PLK4* RPE1 WT and *CEP250* KO cells upon 48 h Dox induction expressing γ-tubulin-mScarlet-I (red) as markers for the centrosomes with or without CW069 treatment. The DNA was marked with SPY-DNA650 (grey). WT *PLK4* OE: N_{DMSO} = 28 cells, N_{CW069} = 40 cells, *CEP250* KO *PLK4* OE: N_{DMSO} = 26 cells, N_{CW069} = 31 cells; from 2 independent live cell experiments. Bar represents mean. Unpaired t-test. * $p < 0.05$. **G** Quantification of multipolar spindle/chromosome mis-segregation from (E) in RPE1 WT *PLK4* OE and *CEP250* KO *PLK4* OE with siControl and siHSET for 30 h. WT *PLK4* OE: $N_{siControl}$ = 59 cells, N_{siHSET} = 59 cells, *CEP250* KO *PLK4* OE: $N_{siControl}$ = 45 cells, N_{siHSET} = 32 cells; from 3 independent experiments. Bar and error represent mean and SD. Unpaired t-test. * $p < 0.05$, ** $p < 0.01$. (adapted from Theile et al., 2023)

4 Discussion

4.1 The Rootletin/CEP68 centrosome linker does not play a role in interphase centrosome cohesion in RPE1 cells

The centrosome linker together with the MT-based cohesion is important to keep the two interphase centrosomes into one MTOC. In this study, I discovered the cell type-dependent function of the previously described Rootletin/CEP68 linker (Bahe et al. 2005; Vlijm et al. 2018). Furthermore, the results support the universal function of the most studied centrosome linker protein C-Nap1 as the main anchor point of centrosome linker proteins at the proximal end of centrioles. The Nocodazole treatment of RPE1 WT cells showed little impact on centrosome separation indicating that centrosome cohesion is mainly provided by the centrosome linker in this cell line. In contrast, in HCT116 cells centrosome cohesion in around 20% of the cells is probably based solely on MTs. C-Nap1 depletion triggered efficient centrosome separation in all tested cell lines, especially after Nocodazole treatment, underlying the key function of C-Nap1 as main centrosome linker protein (Figure 11, Figure 13 and Figure 15). Surprisingly, I could not observe an impact of neither Rootletin depletion nor deletion in RPE1 cells on centrosome separation showing that the centrosome linker in this cell line functions without Rootletin. The previous observed function of Rootletin in RPE1 cells was highly likely caused by an off-target effect of the used siRNA (siRootletin-222), which I confirmed by depleting Rootletin in RPE1 *CROCC* KO (Figure 12).

Analysis of centrosome separation in in HCT116, U2OS and Caco-2 revealed a clear function of Rootletin in centrosome cohesion (Figure 15). Notable, the impact of Rootletin depletion on centrosome cohesion was not as significant as C-Nap1 depletion, going in line with the model that C-Nap1 functions upstream of Rootletin and potential other centrosome linker proteins.

To understand the functional variation of Rootletin/CEP68 in RPE1 and HCT116 cells I examined protein and intensity levels by immunoblot and immunofluorescence, respectively. Both analyses showed a significant decrease of Rootletin in RPE1 cells compared to HCT116 cells (Figure 17), indicating that the lower expression could be one reason for the lack of function in RPE1 cells. Surprisingly, Rootletin overexpression in RPE1 *NIN* KO did not decrease centrosome separation, indicating that Rootletin overexpression alone is insufficient to gain centrosome linker function (Figure 17). Maybe additional factors, such as protein modifications, co-expression of additional linker proteins, are needed or Rootletin fibres are important for other, currently unknown, processes around centrosome cohesion.

This analysis showed for the first-time cell type-dependent centrosome linker diversity among different cell lines. The Rootletin/CEP68 linker displayed variable functions in centrosome cohesion in distinct cell lines. Most notably, Rootletin showed no measurable role in RPE1 cells regardless of the Rootletin/CEP68 filament formation in this cell line as long as centrosomes were not amplified (Vlijm et al. 2018). These data raise the important question of potential alternative linker proteins, that support centrosome cohesion in RPE1 cells and function additional to Rootletin in other cell lines.

4.2 Ninein is a novel centrosome linker protein and has a dual function in centrosome cohesion

In this study, I discovered a new role of the centrosomal protein Ninein as a component of the centrosome linker (Figure 15). Different from most centrosome linker proteins that localize only at the proximal end of centrioles, Ninein also associates with the SDAs of the mother centriole. Although the localization of Ninein at the proximal end of centrioles has been described previously (Mazo et al. 2016), its function at this location was first identified during this study.

The fact that Ninein depletion promoted centrosome disjunction in RPE1 *CEP128* KO cells, which are defective in the MT centrosome cohesion pathway and mainly depend on the centrosome linker for cohesion emphasizes the important role of Ninein as centrosome linker component (Figure 20). Analysis of Ninein localization dependency at the proximal end of centrioles showed that it required C-Nap1 as anchor point and forms a plate-like structure at centrioles as detected by STED super resolution microscopy (Figure 19) and so suggests that Ninein functions rather as a docking hub than as a filament. Furthermore, Ninein depletion caused centrosome separation to a similar level like C-Nap1 depletion in RPE1 cells. Recently, it was proposed that C-Nap1 solely can achieve centrosome cohesion by liquid phase transition (Mahen 2022). The depletion data of Ninein in RPE1 cells and the observation that C-Nap1 intensity levels at centrosomes are not affected by the loss of Ninein, argue against this hypothesis. However, if Ninein promotes the C-Nap1

phase transition is still unclear. These results together indicate that C-Nap1 requires Ninein for centrosome linker function in RPE1 cells and cannot function alone.
The further analysis of this study showed that the centrosome cohesion function of Ninein is conserved in all tested cell lines. To gain deeper insights into the interdependency of the Rootletin and the Ninein linker, I performed corresponding experiments in HCT116 cells, where both linker branches are functional. However, I could not observe an impact of Ninein deletion on centrosomal Rootletin/CEP68 or vice versa in HCT116 cells (Figure 16). Additionally, depletion of Rootletin in HCT *NIN* KO further increased centrosome separation to a similar extend as C-Nap1 depletion. Presently it is unknown how the C-Nap1-Ninein platforms on the proximal ends connect the two centrosomes together. The involvement of CEP215 and LRRC45 was excluded by a mini-siRNA screen (Figure 15A and B). Further studies are needed to identify the centriole connecting elements in RPE1 cells. Taken together, Ninein is the prominent centrosome linker element in RPE1 cells that function in parallel with Rootletin/CEP68 in the other cell lines.

The centrosome linker is dissolved at the onset of mitosis by Nek2 kinase (Agircan et al. 2014; Bahe et al. 2005; Fang et al. 2014; Andrew M Fry et al. 1998). Centrosome cohesion is then shortly provided by the KIFC3/MT based pathway until the outward directed forces on centrosomes by the tetrameric kinesin motor Eg5 (activated by CDK1-Cyclin B) drive the two centrosomes apart (Hata et al. 2019). The balance between the opposing KIFC3/Eg5 forces determines the timing of the spindle assembly. Whether Ninein is phosphorylated by Nek2 is currently unknown but interestingly the SDAs are also modified by Nek2 in prophase raising the possibility that Ninein could be a Nek2 substrate (Hata et al. 2019; Spalluto, Wilson, and Hearn 2012; Viol et al. 2020). The impact of the cell type-dependent centrosome linker diversity on the timing of centrosome resolution is still unclear and needs further investigation. This, along with other factors, such as Nek2 activity, could give an explanation why cells follow the prophase or prometaphase pathway in the case of centrosome separation (Hata et al. 2019; Kaseda et al. 2012; Nam, Naylor, and van Deursen 2015; Rattner and Berns 1976).

4.3 Alternative centrosome cohesion pathways

The current knowledge about centrosome cohesion includes two pathways: the centrosome linker and the KIFC3/MT-based cohesion, where MTs derived from the SDAs of the older mother centrosome and PCM MTs of the younger centrosomes are crosslinked by KIFC3. The observation that Nocodazole addition increased centrosome separation in RPE1 *NIN* KO (Figure 21C and D), provides evidence for a function of PCM-PCM-derived MTs (Dammermann and Merdes 2002) in centrosome cohesion. In line with this hypothesis, PCNT depletion in RPE1 *NIN* KO cells increased centrosome separation to a similar level like Nocodazole treatment in the siControl depletion. Furthermore, I could not observe an enhancement in centrosome separation after addition of Nocodazole on top of PCNT depletion (Figure 21A and B) underlining the function of PCM-derived MT in centrosome cohesion. Surprisingly, depletion of PCNT in RPE1 WT did not show an effect on centrosome cohesion, independent of the MT-based cohesion status. This raises the question, if the centrosome cohesion during interphase could be hierarchically organized with the centrosome linker as the main pathway followed by the MT-based cohesion and the potential alternative pathway via PCM-derived MTs. Further investigations, including the depletion of other PCM proteins like CEP192, CEP152 or CEP215, are needed to get a clear understanding of alternative centrosome cohesion pathways and the potential key players. Additionally, the analysis of the centrosome distance instead of applying a threshold (> 2 µm for RPE1, > 1 µm for HCT116) to compare the percentage of cells with centrosome separation adds more information about the behaviour of the centrosomes during interphase. It could make it possible to identify trends by detecting smaller changes in the intercentrosomal distance.

4.4 Centrosome linker defects influence MT nucleation in RPE1 cells

Ninein was identified as novel MT minus-end associated centrosomal protein (Bouckson-Castaing et al. 1996; Mogensen et al. 2000). As describe above, beside the SDA pool, Ninein is also localized at the proximal end of the centrioles as part of the centrosome linker. In previous studies the function of MT nucleation and anchoring at the centrosomes was linked to the SDA pool of Ninein. I checked the possibility of an impact on MT nucleation in linker deficient RPE1 cells via MT-regrowth assay (Würtz et al. 2022). Going in line with the lack of linker function of

Rootletin in RPE1 cells, only deletion of C-Nap1 and Ninein showed an MT nucleation defect at the centrosomes (Figure 22). Furthermore, I observed a decreased γ-tubulin accumulation in *CEP250* KO and *NIN* KO cells, probably because of partial disruption of recruitment processes to the centrosome (Figure 23A). Analysis of the different γ-tubulin pools at the centrosome (PCM and centriolar lumen pool) showed, that the length of the inner pool of γ-tubulin is not affected in linker deficient cells (Figure 23C and D). Currently it is still unclear how C-Nap1 and Ninein influence γ-tubulin recruitment to the centrosomes and the impact on MT dynamics in detail. C-Nap1 could have an impact on PCM proteins, like CEP192, that are important for the localization of γ-tubulin ring complexes to the PCM in interphase (Schweizer et al. 2021). These abnormalities could be one of the reasons for the NEBD defects observed in Figure 30.

4.5 The centrosome linker clusters supernumerary centrosomes during interphase

Centrosome amplification is a prominent feature of many cancer cells. While facing high risk of multipolar spindle formation and mitotic failure, cancer cells can cluster and organize supernumerary centrosomes into pseudo-bipolar spindles, bypassing the SAC (Remo et al. 2020). A well-studied centrosome clustering mechanism is provided by the MT motor protein HSET (KIFC1, a member of Kinesin-14 family) (Ganem et al. 2009; Kwon et al. 2008; Marthiens et al. 2012). While the knowledge on centrosome clustering in mitosis is relatively advanced, it is unclear how cells bundle supernumerary centrosomes in interphase and whether this has an impact on spindle formation and chromosome segregation in mitosis.

The cell type-dependent differences of Rootletin and Ninein for centrosome linker function that I observed in cells with normal centrosome number, also exist in some extend in the clustering of overamplified centrosomes (Figure 27 and Figure 28). Surprisingly, I observed that Rootletin gained a centrosome linker function in RPE1 cells with supernumerary centrosomes, which was confirmed using two different analyses methods (Figure 27 and Figure 28). The similar trend between centrosome cohesion with and without centrosome amplification suggests that clustering of supernumerary centrosomes probably works in a comparable way like centrosome cohesion. Interconnecting filaments attached to the proximal end of the centrioles via

C-Nap1 and probably also via C-Nap1-Ninein link the two centrosomes together by transient attachments (Theile et al. 2023; Vlijm et al. 2018). This model is supported by STED analysis of the centrosome linker in RPE1, HCT116 and Caco-2 cells with supernumerary centrosomes (Figure 29). The achievement of a critical Rootletin fiber density after centrosome amplification could be one reason why the Rootletin linker gains a function in clustering supernumerary centrosomes during interphase.
Consistent with the previous results, MT nucleation is also decreased in C-Nap1 deficient cells with amplified centrosomes (Figure 22E). Interestingly, RPE1 cells with supernumerary centrosome nucleate less MTs compared to cells with two centrosomes irrespective of the centrosome linker status, probably because of competition for MT assembly factors.
In conclusion, the centrosome linker and the MT pathway function together in clustering supernumerary during interphase in RPE1, HCT116 and Caco-2 cells. Furthermore, a recently published pre-print showed similar data corresponding to the impact of the centrosome linker in centrosome clustering (Can Özcan et al. 2023). Additionally, Kalkan and colleagues showed that Nek2 mediates centrosome clustering through its function in centrosome separation. Decrease of Nek2 activity via KO or knock down supported centrosome clustering. In contrast, overexpression of Nek2 resulted in centrosome de-clustering and distribution (Kalkan et al. 2023). The MT defects in linker deficient cells are also observed after centrosome overamplification. This, together with other factors, like premature centrosomes separation, could cause defects in early mitosis and spindle formation.

4.6 The impact of centrosome linker defects on NEBD and mitotic spindle formation

In mammalian cells centrosomes are anchored to the NE in late G2/prophase and are important for the initiation of the NEBD via forces created by centrosomal MTs (Beaudouin et al. 2002; Busson et al. 1998; Gönczy et al. 1999; Robinson et al. 1999).
During live cell imaging *CEP250* KO cells showed a prolonged NEBD preparation phase independent of the centrosome number (Figure 30A-C). Interestingly, the separated centrosome in C-Nap1 deficient cells move together before NEBD start (Figure 30A-E). The centrosomes in RPE1 WT stay close together during interphase

until NE fold formation. Centrosome separation happens with the start of the NEBD. This observation indicates that the closeness is crucial to initiate NEBD via the first fold formation. Furthermore, the spatial centrosome organization on the NE may be relevant for the efficient NEBD. Important to note, NEBD preparation and duration were even further prolonged in RPE1 *CEP250* KO cells with amplified centrosomes, suggesting that the C-Nap1-dependent defects are enhanced through centrosome amplification (Figure 30A-D).

During NEBD, Lamin depolymerization via phosphorylation is crucial for the NE disassembly (Beaudouin et al. 2002) and is controlled via the Cdk2-CyclinB complex, but what is the function of the centrosome linker in these processes? Until now, the RanBP2–BICD2-dependent pathway and the Nup133-dependent tethering network are proposed to be important for centrosome anchoring to the NE and centrosome positioning at the G2/M transition (Bolhy et al. 2011; Splinter et al. 2010). However, currently it is not completely understood how the centrosomes are linked or attached to the NE and which role the centrosome linker plays in the centrosome-to-NE tethering. Furthermore, the correlation between centrosome separation and distance to the NE and the timing of NEBD is still unclear. The results suggest that a defined spatial organisation of the centrosomes around the nucleus is important for successful NEBD. MT, among others, have previously been reported to create tension in the nuclear lamina. Additionally, it was shown that centrosomal MTs interfere with the NE structure in late G2. This raises the questions which impact has the MT-based cohesion on these processes and how MT nucleation at the centrosomes happens before and at NEBD. The described movement closer together shortly before NEBD start in C-Nap1 deficient RPE1 cells could be MT-dependent. Further studies about the NEBD should include *CEP128* KO, *NIN* KO and *CEP250-CEP128* double KO to investigate the impact of the different cohesion pathways. Additionally, complementation/rescue experiments are important to proof the concept of linker-dependent early mitotic defects and to strengthen the outcome of this study.

Previously, it was shown that cells with amplified centrosomes fail to satisfy the SAC because of faulty kinetochore-MT attachments. (Basto et al. 2008; Gergely and Basto 2008; Kwon et al. 2008; Yang et al. 2008). In line with this notion, I observed intensity signal accumulation at kinetochores of the SAC proteins MAD1 and BUB1 in RPE1 WT cells with supernumerary centrosomes (Figure 31). This could be one reason for

the prolonged metaphase-to-anaphase transition in cells with amplified centrosomes, because the SAC stays longer active in these cells. Moreover, the deletion of C-Nap1 further increased the accumulation of the SAC proteins at kinetochores causing enhanced metaphase defects in RPE1 *CEP250* KO cells with multiple centrosomes (Figure 31).
As described above C-Nap1 deletion also reduced MT nucleation at the centrosomes independent of the centrosome number (Figure 22). This defect could be one reason for the observed NEBD delay and the prolonged metaphase-to-anaphase transition in linker deficient cells with supernumerary centrosomes. Moreover, these initial mitotic defects could cause the prolonged activation of the SAC which potentially can lead to multipolar spindle formation and mis-segregation of chromosome.

Centrosome clustering in mitosis groups supernumerary centrosomes into two defined units and so helps preventing multipolar spindle formation. The minus-end-directed motor proteins HSET and dynein together with other factors are important for clustering the multiple centrosomes into two poles and so enabling the cells to assemble a pseudo-bipolar spindle that can efficiently segregates the chromosomes (Krämer, Maier, and Bartek 2011; Kwon et al. 2008; Leber et al. 2010; Marthiens et al. 2012; Quintyne 2005).
I observed in RPE1 *CEP250* KO cells with supernumerary centrosomes an increase in multipolar spindles compared to RPE1 WT (Figure 32A and B), suggesting that the centrosome linker has an impact on mitotic spindle assembly in the presence of multiple centrosomes. Importantly, after HSET inhibition 40% of RPE1 cells with supernumerary centrosomes showed multipolar spindles and this number increased to 50-70% in *CEP250* KO, *NIN* KO and *CROCC* KO cells (Figure 32B). The defects in bipolar spindle formation were translated in anaphase chromosome mis-segregation (Figure 32C and D). HSET inhibition and impairment of the centrosome linker by C-Nap1 deletion had a nearly additive effect on chromosome mis-segregation raising the possibility that there are two independent pathways ensuring chromosome segregation in mitosis. It would be interesting to investigate if the PCM-pathway is also important for centrosome clustering because it was proposed that the HSET-CEP215 complex groups centrosome together during mitosis (Chavali et al. 2016). PCM defects could disrupt the HSET-based centrosome clustering mechanism but may also trigger centrosome distribution during interphase. Additionally, the decreased γ-tubulin at the centrosomes in RPE1 *CEP250* KO give

evidence to check other PCM components including CEP215. An initial lower recruitment of CEP215 to centrosomes in C-Nap1 deficient cells could explain the higher amount of multipolar spindle formation compared to WT, also when the HSET is not inhibited.

My results suggest that linker-deficient C-Nap1 cells show various mitosis-related defects (see model Figure 31C) but how does a defect in the centrosome linker during interphase influence mitotic spindle formation? Unfortunately, it is still unclear whether pre-mitotic centrosome distribution correlates with mitotic defects such as multipolar spindle formation or chromosome mis-segregation. The multiple centrosomes were quite dispersed in interphase RPE1 *CEP250* KO cells, which is different to the clustered situation of RPE1 WT cells. This makes bipolar spindle formation in linker deficient cells at the beginning of mitosis a more challenging task. In absence of HSET and centrosome linker defects, alternative cluster mechanisms may provided by dynein (Vitre et al. 2020) are functional but probably are in ~70% of cells insufficient to organize the multiple centrosomes into a pseudo-bipolar spindle (Figure 33). Interestingly, although the Rootletin based centrosome linker was not important for centrosome cohesion in RPE1 WT cells with normal centrosome number, it had an impact on mitotic spindle organization in cells with supernumerary centrosomes (Figure 32A and B). This goes in hand with the observation that Rootletin gained a centrosome linker function in interphase RPE1 cells with overamplified centrosomes (Figure 27 and Figure 28). In conclusion, these results indicate that the centrosome linker provides centrosome clustering until beginning of mitosis and contributes to pseudo-bipolar spindle formation especially in the absence of the HSET clustering mechanism.

5 Conclusion and future perspectives

From the observation that the two centrosomes are connected during interphase, through description of the main linker protein C-Nap1 as anchor for the highly organized network of Rootletin/CEP68 filaments to the recent discovery of the KIFC3/MT-based pathway, centrosome cohesion is a crucial factor for a successful centrosome cycle and important for cell division (Bahe et al. 2005; Hata et al. 2019; Mayor et al. 2000; Panic et al. 2015; Vlijm et al. 2018).

Over the years many proteins were proposed as potential centrosome linker candidates, however, the complete architecture, assembly, dissolution and function of the centrosome linker is still unclear. During this study I showed for the first time cell type-dependent centrosome linker diversity. The function of the centrosome linker protein Rootletin differs among cell lines, irrespective of the filament formation showed before (Vlijm et al. 2018). Further studies such as checking the filamentous structure in *NIN* KO cells or analysing the attachment to the nuclear envelope are needed to understand why and for what cells build up Rootletin/CEP68 fibers between the two centrosomes. One possibility could be the involvement in centrosome-to-NE tethering via Nesprin (Potter et al. 2017; Schneider et al. 2011).

Ninein was discovered as the first centrosome cohesion protein with a dual function as centrosome linker at the proximal end of centrioles downstream of C-Nap1 and as MT anchor at the SDAs downstream of CEP128. Furthermore, the centrosome linker function of Ninein was conserved in all tested cell lines pointing out the import role of Ninein in interphase centrosome cohesion. Currently, it is still unknown whether Ninein downstream proteins like CEP170, KIF2a or p150glued (Mazo et al. 2016) are involved in centrosome cohesion and which protein can form the filamentous structures for promoting the physical connection between the two proximal ends of the centrosomes. The STED analysis of Ninein suggests a plate-like structure near the C-Nap1 ring, proposing Ninein as docking hub for linker filaments rather than forming fibers by itself (Figure 34). Further investigations are needed to understand the missing parts and the structure of the C-Nap1-Ninein-dependent centrosome linker.

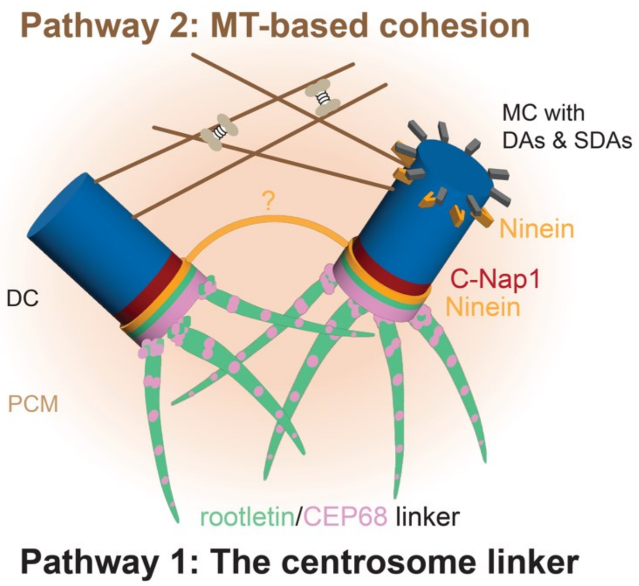

Figure 34 Model of the centrosome cohesion during interphase including the Ninein-dependent linker branch. Ninein shows a function in both centrosome cohesion pathways because of its dual localization at the proximal end and at the SDAs of the centrosomes. The structure and key components of the filaments anchored by the C-Nap1-Ninein linker is still unclear. The current understanding of centrosome cohesion during interphase includes two pathways, but the complexity and the presence of alternative pathways is still being investigated.

Additionally, the increase in centrosome separation after disruption of the MT-based pathway with Nocodazole in linker deficient *NIN* KO cells raises the question for potential alternative cohesion mechanism. Our current knowledge of centrosome cohesion includes two pathways: the centrosome linker and the KIFC3/MT-based cohesion. The data in this thesis showed evidence for the existence of another potential pathway based on MTs derived from the PCM of both centrosomes. Surprisingly, the depletion of one of the main PCM components PCNT not only showed centrosome cohesion defects but also proposed a hierarchy of the centrosome cohesion pathways. The centrosome linker seems the dominantly function element, followed by the KIFC3/MT-based and the PCM-MT-dependent pathways. The study of alternative linker pathways and the hierarchy in the centrosome cohesion is of strong interest to complete our view of interphase centrosome cohesion. First, it would be interesting to analyze more PCM proteins, including CEP152, CEP192 and Cdk5Rap2 and the influence on centrosome separation. Additionally, future studies should not only focus on centrosome separation but also include the analysis of the raw centrosome distance. The highest impact could be achieved by including 3D measurements and tracking centrosome movement in living cells.

Future studies should also focus on migration defects in linker-deficient cells. As previously reported, loss of C-Nap1 in RPE1 cells reduces migration speed compared to WT cells. In addition to studying cell migration in *NIN* KO, the effect of the centrosome linker on cell invasion, particularly in cells with centrosome amplification, awaits clarification. Furthermore, the recently described MTOC-first navigational migration (Kroll et al. 2023; Renkawitz et al. 2019) raises the question of whether centrosome cohesion influences not only the speed but also the pathfinding during migration. This could shed light on the behaviour of linker-deficient cells in complex environments and answer important questions about the impact on invasiveness, a crucial parameter in cancer research.

The discussed data above showed that C-Nap1 deficient cells not only have early mitotic defects like the prolonged NEBD preparation, but further it also gives evidence that centrosome cohesion is important for correct spindle formation and efficient chromosome segregation, especially in the case of supernumerary centrosomes. The additional disruption of the main clustering mechanism via HSET caused a further enhancement of the observed C-Nap1 related defects, suggesting an impact of centrosome cohesion in proper mitotic spindle formation. Currently it is still unknown how centrosome separation influences the connection and position to the NE and which proteins are involved. Analysis of the centrosome-to-NE distance in 2D and 3D including the impact of centrosome cohesion defects could shed light on these questions. The function of the centrosome linker in cells with supernumerary centrosome could be the basis to study the impact in cancer models and to search for potential therapeutic targets.

6 Material

6.1 Reagents, buffers and solutions

6.1.1 DNA analysis

Table 1 PCR reagents

Reagent	Used for
Q5® High-Fidelity DNA Polymerase (NEB)	high fidelity PCR reaction
***Taq* DNA Polymerase (NEB)**	PCR reaction (colony PCR)
Restriction enzymes (NEB)	Plasmid linearization, sticky end generation
Gel Loading Dye, Purple (6x) (NEB) or orange (Schiebel lab)	Load DNA samples in agarose gels
GeneRulerTM 1kb Plus DNA ladder (Thermo Fischer)	Reference ladder on agarose gels
T4 DNA ligase (NEB)	Ligation
T4 Polynucleotide Kinase (NEB)	5' phosphorylation, removal of 3' phosphoryl groups, DNA ligation
NEBuilder® HiFi DNA Assembly Master Mix (NEB)	DNA assembly
QuickExtract™ DNA extraction solution (Lucigen, Cat. #QE09050)	Mammalian genomic DNA extraction

Table 2 Plasmid purification

Buffer	Protocol	Storage
Minipreparation resuspension buffer (S1)	50 mM Tris pH 8.0 10 mM EDTA 100 µg/ml RNase A (DNase free)	4 °C
Minipreparation lysis buffer (S2)	200 mM NaOH 1% SDS	Room temperature
Minipreparation neutralization buffer (S3)	2.8 M K-Acetate, pH 5.1	4 °C
Midi preparation (for mammalian transfection)	See NucleoBond Xtra Midi kit for transfection-grade plasmid DNA (Macherey-Nagel Cat. #740410)	

Table 3 Agarose gel electrophoresis

Buffer	Protocol	Storage
10x TAE buffer	242 g Tris base 57.1 ml acetic acid 100 ml 0.5 M EDTA solution (pH 8.0) Bring up the volume to 1 l with ddH2O	Room temperature
1x TAE buffer	Diluted from the 10x TAE buffer	Room temperature
20x SB buffer (100 mM, pH 8)	38.17 g Sodium Borate decahydrate 33 g Boric acid Bring up the volume to 1 l with ddH2O	Room temperature
1x SB buffer	Diluted from the 20x SB buffer	Room temperature

6.1.2 Immunofluorescence

Table 4 Solutions for immunofluorescence

Buffer	Protocol	Storage
1x PBS	Diluted from the 10x PBS	Room temperature
Blocking buffer	10 % FBS + 0.01% Triton X-100	4 °C
3 % BSA	3 % BSA (w/v) in PBS	aliquots store at -20 °C

6.1.3 SDS-page and western blot

Table 5 Solutions for SDS-page and western blot

Solution	Protocol	Storage
0.5 M Tris-Cl pH 6.8 buffer (for separating gels)	Dissolve 60.57 g Tris base (in around 700 ml of ddH_2O) Adjust the pH to 6.8 with concentrated HCl. Bring up the volume to 1 l with ddH2O	Room temperature
2 M Tris-Cl pH 8.8 buffer (for stacking gels)	Dissolve 242.28 g Tris base in around 700 ml of ddH2O.	Room temperature

	Adjust the pH to 8.8 with concentrated HCl. Bring up the volume to 1 l with ddH_2O	
10% (w/v) SDS	Dissolve 10 g SDS (heat up to 60 °C) Bring up the volume to 100 ml with ddH_2O.	Room temperature
10% (w/v) APS	1 g Ammonium persulphate per 10 mL ddH_2O	aliquots store at -20 °C
1x SDS running buffer	Diluted from the 10x SDS running buffer	Room temperature
Coomassie Blue	0.25% Coomassie Blue 20% Ethanol 3% Acetic acid	Room temperature
10x Tris-Glycine buffer	30.275 g Tris base 144 g glycine 50 mL 20% SDS Bring up the volume to 1 l with ddH_2O	Room temperature
1x Transfer buffer	100 ml 10x Tris-Glycine buffer 200 ml Methanol Bring up the volume to 1 l with ddH_2O	Make before use
1x TBS	Diluted from the 10X TBS buffer	Room temperature
1x TBS-T	1x TBS 0.1% Tween 20	Room temperature
5% skimmed milk in 1X TBST	1x TBS-T 5% (w/v) skimmed milk For membrane blocking and secondary antibody dilution	4 °C
3% BSA in 1x TBST	1x TBS-T 3% (w/v) Bovine serum albumin (BSA) For primary antibody solution	4 °C, aliquots store at -20 °C

6.2 Antibodies

The abbreviation IF was used for immunofluorescence and WB for western blotting.

6.2.1 Primary antibodies

Table 6 Primary antibodies

Primary antibody	Species	Dilution	Source
Anti-BUB1	Rabbit	1:1000 IF	Bethyl (Catalog # A300-373A)
Anti-CENP-A	Mouse	1:600 IF	Enzo (ADI-KAM-CC006-E)
Anti-CENP-C	Guinea Pig	1:2000 IF	Biozol (MBL-PD030)
Anti-CENP-F (anti-mitosin)	Mouse	1:100 IF	BD (610768)
Anti-centrin 2	Rabbit	1:100 IF	Schiebel lab, polyclonal antibody
anti-Cep128	Rabbit	1:500 IF	Abcam (ab118797)
Anti-CEP164	Guinea Pig	1:1000 IF	(Schmidt et al. 2012)
Anti-CEP215	Rabbit	1:100 IF	Merck (06-1398)
Anti-CEP68 (R169)	Rabbit	1:800 IF 1:500 WB	(Graser et al. 2007)
Anti-CEP97	Rabbit	1:300	Bethyl (Catalog # A301-945A)
Anti-C-Nap1	Goat	1:1000 IF	(Panic et al. 2015)
Anti-C-Nap1	Mouse	1:100 IF 1:500 WB	BD (611374)
Anti-C-Nap1	Mouse	1:2 IF	(Fava et al. 2017)
Anti-C-Nap1	Rabbit	1:300 IF 1:1000 WB	(Hardy et al. 2014)
Anti-FLAG	Mouse	1:500 IF	Cell Signaling (81465)
Anti-FLAG	Rabbit	1:1000 WB	Proteintech (20543-1-AP)
Anti-GAPDH	Rabbit	1:5000 WB	Cell Signaling (2118)
Anti-GT335	Mouse	1:1000 IF	AdipoGen (AG-20B-0020)
Anti-HA (3F10)	Rat	1:500 IF 1:1000 WB	Merck (11867423001)
Anti-HSET	Rabbit	1:500 IF 1:1000 WB	Abcam (ab172620)
Anti-Lamin B1	Rabbit	1:1000 WB	Abcam (ab16048)
Anti-MAD1	Mouse	1:100 IF	Santa Cruz (sc-47746)
Anti-Myc (9E10)	Mouse	1;100 IF 1:500 WB	Merck (M4439)
Anti-Myc (9E10)	Mouse	1:100 IF	Santa Cruz (sc-40)

		1:100 WB	
Anti-Ninein (L79)	Rabbit	1:500 IF 1:1000 WB	(Mogensen et al. 2000)
Anti-Ninein (serum)	Rabbit	1:500 IF 1:1000 WB	(Mogensen et al. 2000)
Anti-PCNT	Rabbit	1:500 IF	Abcam (ab-4448)
Anti-PCNT	Guinea Pig	1:500 IF	Schiebel lab
Anti-Rootletin (C-terminal, root-C1)	Rabbit	1:100 IF 1:500 WB	Schiebel lab, polyclonal antibody Antigen: rootletin aa 1826-2017 (Panic et al. 2015)
Anti-Rootletin (C-terminal, root-C2)	Mouse	1:100 IF 1:500 WB	Monoclonal antibody Antigen: rootletin aa 1882-1917 Santa Cruz (sc-374056)
Anti-Rootletin (N-terminal)	Rabbit	1:100 IF	(Panic et al. 2015)
Anti-α-tubulin	Mouse	1:500 IF	Sigma Aldrich (T9026, DM1A)
Anti-α-tubulin	Mouse	1:500 IF	Proteintech (66031-1-Ig)
Anti-α-tubulin	Rabbit	1:500 IF	Proteintech (11224-1-AP)
anti-γ-tubulin	Mouse	1:500 IF	Abcam (TU-30, ab27074)
anti-γ-tubulin	Guinea Pig	1:50 IF	Schiebel lab

6.2.2 Secondary antibodies

Table 7 Secondary antibodies

Secondary antibody	Species	Dilution	Source
Anti-goat IgG Alexa Fluor 488/555/647	Donkey	1:500 IF	Thermo Fisher scientific
Anti-guinea pig IgG Alexa Fluor 488/555/647	Goat	1:500 IF	Thermo Fisher scientific
Anti-mouse Atto 594	Goat	1:100 IF	Sigma-Aldrich
anti-mouse HRP	Goat	1:5000 WB	Jackson ImmunoResearch
Anti-mouse IgG Alexa Fluor 488/555/647	Donkey	1:500 IF	Thermo Fisher scientific
Anti-mouse IgG STAR 520SXP/580/600/635P	Goat	1:100 IF	Abberior
Anti-rabbit Atto 594	Goat	1:100 IF	Sigma-Aldrich

anti-rabbit HRP	Donkey	1:5000 WB	Jackson ImmunoResearch
Anti-rabbit IgG Alexa Fluor 488/555/647	Donkey	1:500 IF	Thermo Fisher scientific
Anti-rabbit IgG STAR 580/600/635P	Goat	1:100 IF	Abberior
anti-rat HRP	Goat	1:5000 WB	Thermo Fisher scientific
Anti-rat IgG Alexa Flour 488/647	Donkey	1:500 IF	Thermo Fisher scientific
Rhodamine-Phalloidin	-	1:300 IF	Thermo Fisher scientific

6.3 siRNAs

Table 8 siRNAs

siRNA	Sequence (5'-3') / description	Source
siControl	D-001810-01-20	Dharmacon
siC-Nap1 (#3)	ON-TARGETplus, J-012364-07	Dharmacon
siCEP68	Sciencer® 136783	Ambion
siRootletin-1	Sciencer® 216869	Ambion
siRootletin-222	5′-AAGCCAGTCTAGACAAGGA-3′ (Bahe et al. 2005)	Dharmacon
siNinein	ON-TARGETplus, smart pool siRNA, L-019133-00	Dharmacon
siNinein#2	ON-TARGETplus, GEHC1-001585, 5′-CGGUACAAUGAGUGUAGAA-3′ (Mogensen et al. 2000)	Dharmacon
siCEP215	ON-TARGETplus, L-019154-00	Dharmacon
siLRRC45-B	5′-CCAACAGAACAAGUCCAUU-3′	(He *et al.*, 2013)
siLRRC45-ES	ON-TARGETplus, Smart pool, J-052082	Dharmacon
siHSET	ON-TARGETplus, Smart pool, L-004958-00-0005	Dharmacon
siEg5	Silencer® Select, 4390824	Ambion
siPCNT	ON-TARGETplus, Smart pool, L-012172-00-0005	Dharmacon

6.4 sgRNAs

Table 9 gRNAs for CRISPR/Cas9 Knock-out generation

Gene	gRNA	Target	Sequence (5'-3')	KO strategy
CEP250	gRNA3	Exon 2	AGGTGCTGCAGTACCGAAGC	Double cut
	gRNA2	Exon 5	ACGGTCGCCTTCTCAGTCTA	Double cut
NIN	gRNA2	Exon 3	CCAGCATGAGGCCCGACTCA	Single cut
CROCC	gRNA2	Exon 3	AATGGCGAGCTCATCGCGCT	Double cut
	gRNA4	Exon 6	AAGCGCCCTCATCCGGCTGG	Double cut

6.5 Plasmids

Table 10 List of Plasmids used in this study

Plasmid name	Application	Midi collection (Box-Position)
pX458	empty vector Knock out/Knock in human cells	135-14
pX458-*NIN*-gRNA2	*NIN* KO generation	149-38
pX458-*CEP250*-gRNA2	*CEP250* KO generation	166-31
pX458-*CEP250*-gRNA3	*CEP250* KO generation	166-32
pX458-*CROCC*-gRNA2	*CROCC* KO generation	149-55
pX458-*CROCC*-gRNA4	*CROCC* KO generation	149-57
pCMV-VSV-G	envelope vector	154-38
pRetroX-TRE3G	empty vector	120-75
pRetroX-TRE3G-*Flag-PLK4*	for *PLK4* OE to induce centrosome amplification	166-55 177-64
pQCXIZ-*TUBG1-mRuby2*	for live cell imaging	177-60 166-49
pQPXIP-*mNeonGreen-LaminB1*	for live cell imaging	166-73
pQPXIP-*TUBG1-mScarlett-I* #1	for live cell imaging	177-59
pQPXIP-*CEP250-HA-mNeonGreen* #2	for *CEP250* KO rescue	177-62
pQPXIP-*CEP250-HA-mNeonGreen* #14	for *CEP250* KO rescue	177-63
pQPXIP-*NIN-HA-mNeonGreen*	for *NIN* KO rescue	177-65

6.6 Cell culture

6.6.1 Cell lines

Table 11 List of human cell lines used in this study

Cell line	Source/reference
RPE1 tetON WT	Schiebel lab
RPE1 tetON *CEP250* KO #17	(Panic et al. 2015)
RPE1 tetON *CEP128* KO	RPE1 *CEP128* KO was received from (Mönnich et al. 2018), tetON promoter was integrated by Dr. Xue Li
RPE1 tetON *NIN* KO #14	Marko Panic, Stefanie Heinze and this study
RPE1 tetON *CROCC* KO #49	Generated in this study
HCT116 tetON WT	Schiebel lab
HCT116 tetON *CEP250* KO #234	Generated in this study
HCT116 tetON *CROCC* KO #79	Generated in this study
HCT116 tetON *NIN* KO #139	Generated in this study
RPE1 tetON WT Flag-PLK4	Generated in this study
RPE1 tetON *CEP250* KO #17 Flag-PLK4	Generated in this study
RPE1 tetON *NIN* KO #14 Flag-PLK4	Generated in this study
RPE1 tetON *CROCC* KO #49 Flag-PLK4	Generated in this study
HCT116 tetON WT Flag-PLK4	Generated in this study
HCT116 tetON *CEP250* KO #234 Flag-PLK4	Generated in this study
HCT116 tetON *NIN* KO #139 Flag-PLK4	Generated in this study
HCT116 tetON *CROCC* KO #79 Flag-PLK4	Generated in this study
RPE1 tetON WT TUBG1-mRuby2	Generated in this study
RPE1 tetON *CEP250* KO #234 γ--tubulin-mRuby2	Generated in this study
RPE1 tetON *NIN* KO #139 TUBG1-mRuby2	Generated in this study
RPE1 tetON *CROCC* KO #79 TUBG1-mRuby2	Generated in this study
RPE1 tetON WT TUBG1-mRuby2	Generated in this study

mNeonGreen-LaminB1	
RPE1 tetON *CEP250* KO #234 TUBG1-mRuby2 mNeonGreen-LaminB1	Generated in this study
RPE1 tetON WT Flag-PLK4 TUBG1-mRuby2 mNeonGreen-LaminB1	Generated in this study
RPE1 tetON *CEP250* KO #234 Flag-PLK4 TUBG1-mRuby2 mNeonGreen-LaminB1	Generated in this study
RPE1 tetON *CEP250* KO #234 C-Nap1-HA-mNeonGreen	Generated in this study
HEK293 T	Schiebel lab
HEK293 GP	Schiebel lab
U2OS tetON WT	Schiebel lab
Caco-2	Schiebel lab

6.6.2 Cell growth media

All Media and supplements used in this study were purchased from Thermo Fisher (Gibco) and Trypsin/EDTA from Sigma-Aldrich.

Table 12 Growth media

Medium/supplement	Description
DMEM-F12	growth medium for RPE1, HCT116 and HEK293
DMEM GlutaMax	growth medium for U2OS
DMEM-F12 w/o Phenolred	live cell imaging medium, FACS medium
OptiMEM	transfection medium
Trypsin/EDTA 0.05%	for trypsinisation
L-glutamine	for growth medium
penicillin/streptomycin	for growth medium

6.6.3 Human cell drugs and reagents

Table 13 Cells drugs and reagents

Drug/reagent	Description
Dox	for induction of gene expression using the TetON system (Takara Bio Clontech) 48 h induction for centrosome amplification in Flag-PLK4 cell lines: 1 µg/ml for RPE1; 2 µg/ml for HCT116
EdU	Click-iT EdU Cell Proliferation Kit for Imaging, Thermo Fischer) for labelling S and G2 cells
Nocodazole (Noco)	Before fixation, to depolymerize MTs 5 µM for 1 h at 37 °C
CW069	HSET inhibitor (Karki et al., 2017; Watts et al., 2013) fixed cells: 350 µM for 30 min at 37 °C live cell imaging: 25 µM
Cytochalasin B (Cyto B)	Before fixation, to depolymerize actin 20 µM for 1 h at 37 °C
DMSO	solvent control for Noco, CW069 and Cyto B

7 Methods

7.1 DNA engineering and cloning

7.1.1 PCR amplification

The plasmid backbone, gene fragments (template: Plasmid, G-Block, genomic DNA) or cDNA were amplified via PCR using Q5 High-Fidelity DNA Polymerase or *Taq* DNA Polymerase. Procedures were according to the manufacturer's protocols. The online NEB Tm calculator was used to calculate the annealing temperatures for the designed primers. PCR products were analysed via gel electrophoresis.

7.1.2 Mammalian cells genomic DNA purification

The QuickExtract™ DNA Extraction Solution (Lucigen) was used to extract genomic DNA, especially for single clone screening (96 well plate). The medium was removed, and cells were washed once with cold PBS. Afterwards 20-50 µl (depends on the cell confluence) of the DNA Extraction Solution were added on top of the cells. Samples were mixed at 700 rpm 10 min at 65 °C and then transferred to PCR tubes to run the following program:

65 °C 15 min
68 °C 15 min
98 °C 10 min
12 °C hold

Genomic DNA concentration was measured using Nanodrop. Afterwards the genomic DNA was analysed using PCR (see 7.1.1) or stored at -20 °C.

7.1.3 Linearized DNA purification (PCR purification and gel extraction)

The miniBio Column PCR Product Purification Kit (MiniBio) or miniBio Column DNA Gel Extraction Kit (MiniBio) were used to purify PCR products or extract DNA after gel electrophoresis. The protocols were provided with the purification Kits. Linearized DNA fragments were fused together using the NEBuilder® HiFi DNA Assembly Master Mix (NEB) following the manufacturer's protocol.

7.1.4 Plasmid transformation in bacterial cells and DNA purification

Competent *E.coli* DH5α were thawed on ice prior transformation. The plasmid and the bacteria were mixed and incubated for 30 min on ice. The heat shock was performed for 30 sec at 42 °C followed by 5 min incubation on ice and antibiotic resistance-dependent recovery at 37 °C. Afterwards the cells were plated before liquid culture.

DNA purification form small bacterial liquid cultures were performed using column free isopropanol purification (Mini preparation). *E.coli* culture (2 ml) were centrifuged at 14000 rpm, 4 °C for 1 min. The supernatant was discarded, and the pellets were resuspended in 250 µl cold S1 buffer followed by 250 µl S2 buffer to lyse the cells. The tube was inverted an incubated up to 5 min at room temperature (RT) before 300 µl S3 buffer was added for neutralization. Cell debris were centrifuged at 14000 rpm, 4 °C for 5 min. The supernatant was transferred into a new tube and 0.8 times the volume of Isopropanol was added. After mixing by vortexing, the samples were centrifuged at 14000 rpm, 4 °C for 10 min and the supernatant was discarded. DNA pellets were washed with 0.5 ml 70% Ethanol and centrifuge again for 5 min. Finally, most of the Ethanol was removed and the pellet was dissolved in nuclease-free water. DNA concentration was measured using Nanodrop after 5-10 min reconstitution.

The DNA purification from large cultures of *E.coli* culture (> 50 ml) were executed using NucleoBond Xtra plasmid purification Midi Kit (MACHEREY-NAGEL) following the manufacturer’s protocol.

7.2 Human cell culture and transfection

RPE1, HCT116, Caco-2 and HEK293 cell lines were cultured in Gibco DMEM/F-12 (Thermo Fisher). U2OS cells were maintained in DMEM/GlutaMAX™ medium (Thermo Fisher). Media were supplemented with 10% FBS, 1% penicillin/streptomycin and 1% L-glutamine. The cell lines were cultivated at 37°C with 5% CO2. Mycoplasma tests were carried out regularly and confirmed the absence of mycoplasma contamination in all used cell lines.

7.2.1 siRNA

The siRNA transfection was done using the Lipofectamine RNAiMAX (Thermo Fischer Scientific). The adapted procedure describe underneath is based on the manufacturer's protocol.

Table 14 Preparation of the siRNA master mix for 24 well

RNAiMAX mix	OptiMEM	25 µl
	RNAiMAX	1 µl
	→ mix and incubate for 5 min	
siRNA mix	OptiMEM	25 µl
	siRNA	0.5 µl
	→ mix and incubate for 5 min → afterwards mix with RNAiMAX mix (ratio 1:1) and incubate 5 min	
Add final mix per well		50 µl
Add cell suspension per well		450 µl

If not stated differently, a final siRNA concentration of 20 µM was used and the depletion was carried out over 72 h. 24 h after the siRNA treatment, the cells were split and seeded on coverslips (for IF) or expanded to 12 well (for WB). The cells were fixed or lysed after total 72 h of siRNA treatment.

7.2.2 Plasmid transfection

The Plasmid transfection in HCT116 cells was performed using the Lipofectamine LTX Kit (Thermo Fischer Scientific). The adapted procedure describe underneath is based on the manufacturer's protocol.

Table 15 Preparation of the Plasmid master mix for 6 cm dishes

Lipofectamine LTX mix	OptiMEM	375 µl
	Lipofectamine LTX Reagent	15 µl
	→ mix and incubate for 5 min	
PLUS-Plasmid mix	OptiMEM	375 µl
	PLUS Reagent	7.5 µl
	DNA/Plasmid	total 7.5 µg
	→ mix and incubate for 5 min → afterwards mix with Lipofectamine LTX mix (ratio 1:1) and incubate 5 min → add mix dropwise onto the cells	

HCT116 cells were seeded one day before transfection at a confluency of 25-30% (final confluence on transfection day should be around 50-60%) in 5 ml medium. Before adding the Plasmid master mix dropwise to the cells, 1 ml medium was removed. Medium was changed after 24 h and FACS sorting was carried out after 48 h post-transfection.

7.3 CRISPR/Cas9 genome editing

CRISPR-Cas9 knockouts (KO) were generated in accordance with established protocols (Ran et al. 2013; Shalem et al. 2014). 48 h after transfection cells were sorted using FACS to generate a GFP-enriched cell pool. After expanding, genomic DNA was extracted, and a pool-PCR was performed to check for the cut and potential KOs in the cell pool. In the case of a positive result (KO PCR product) single cells were sorted into 96 well plates using FACS. After 10 to 14 days cultivation the single clones were screened using genomic PCR followed by sequencing. To confirm and validate the outcome of the CRISPR-Cas9 KO IF and WB was performed.

7.3.1 sgRNA cloning

The gRNAs were selected from the CRISPR knockout (GeCKO) library (Shalem et al. 2014) or were designed using Benchling (https://benchling.com). The sgRNAs were cloned into the pSpCas9-2A-GFP (px458, Addgene, #48138) (Ran et al. 2013) vector. The empty vector way used as positive control for the transfection and the FACS sorting. Pre-test for cut efficiency and toxicity were performed in HEK293 cells. To delete a large genomic region usually two sgRNAs were used to generate a double cut in the genome.

7.3.2 Electroporation

The enhance the transfection efficiency in RPE1 cells electroporation was used instead of chemical transfection. The Neon Transfection Kit (Thermo Fischer) was used following the protocol from the manufacturers. For HCT gRNA transfection was performed as described in 7.2.2.

7.4 Generation of stable cell lines

The retroviral Tet-On 3G inducible expression system from Takara was used to establish Dox-inducible stable cell lines. RPE1 and HCT116 cells with the tetON system (namely, RPE1 tetON and HCT116 tetON) were created following the manufacturer's protocol. The genes of interest (GOI) were inserted into the pRetroX-TRE3G vector. To generate the retroviruses HEK293 GP were co-transfected using PEI (Polyethyleneimine) with the pRetroX-TRE3G vector (carrying the gene of interest) and the envelope vector pCMV-VSV-G (Addgene plasmid #8454). Subsequently, the cells were infected with the retrovirus-containing media to trigger the integration of the gene of interest into the genome. To establish the stable cell line the positive transduced cells were enriched through antibiotic selection or FACS sorting.

Table 16 Virus production and infection

Step	Reagents	6 cm dish (4 ml)	10 cm dish (10 ml)
HEK293 GP transfection	OptiMEM	800 µl	1 ml
	pCMV-VSV-G	6 µg	10 µg
	pRetroX-TRE3G + GOI	6 µg	10 µg
	PEI	15 µl	35 µl
Virus harvest	Virus	4 ml	10 ml
		➔ filter (0.45 µm) into a falcon	
	FBS	1 ml	2.5 ml
	medium	2 ml	5 ml
	Polybrene (Stock 4 mg/ml	1:1000 dilution (final conc. 4 µg/ml)	

HEK193 GP cells were seeded one day before transfection at a confluence of 25-30% (final confluency on transfection day should be around 50-60%). Before adding the Plasmid master mix dropwise to the cells, 1 ml medium was removed. Medium was changed after 24 h and the virus was harvested 48 h after transfection. Cells for virus infection need a 40% confluence at the first virus treatment. The virus was replaced three times every 4-6 h. 24 h after first virus infection cells were split.

7.5 Immunofluorescence

Cells were seeded on coverslips with a diameter of 12 mm or 15 mm. Prior indirect immunofluorescence staining, the samples were washed once with 1x PBS (except those after Noco, CytoB or CW069 treatment) and fixed with pre-cooled methanol for 5 min at -20 °C. CW069 treated samples were fixed first with 4% PFA for 10 min at RT, washed once with 1x PBS followed by a second fixation and permeabilization with cold methanol for 5 min at -20 °C. For the permeabilization and blocking the samples were incubated with 10% (v/v) FBS + 0.1% Triton X-100 at RT for 30 min. The primary antibodies were diluted in 3% (w/v) BSA and incubated with the samples for 1 h in a humid chamber. After three times washing with 1x PBS, the secondary antibodies, including DAPI to stain the DNA, were diluted in 3% BSA followed by 30 min incubation in a dark humid chamber. The stained coverslips were mounted on glass slide with Mowiol (Calbiochem) with and without PPD (p-phenylenediamine, 0.01%, anti-fading agent, Sigma) for conventional microscopy and with ProLong Gold Antifade Mountant or ProLong Glass Antifade Mountant (ThermoFischer) for STED microscopy. The Click-iTTM Plus EdU Alexa FluorTM 555/647 Imaging Kit (Thermo Fischer) was used together with CENP-F staining to specify S and G2 cells. The EdU staining was performed before the primary antibody incubation using the manufacturers protocol. To analyse the SAC proteins MAD1 and BUB1 samples were extracted 45 sec with 37 °C PEM (100 mM PIPES pH 7.0, 1 mM MgCl2, 5 mM EGTA, 0,1% Triton X-100) prior fixation.

7.6 Western blot

To harvest the protein samples for WB cells were washed once with cold 1x PBS on ice. Afterwards 4x Laemmli buffer with Benzonase (Merck, 1:1000 dilution) was added and cells were scratched off the plastic surface to collect them into a 1.5 ml Eppendorf tube. After 10 min incubation on ice samples were checked for low viscosity and then cell debris were spun down via centrifugation (16 000 rpm) at 4 °C for 15 min. The supernatant was collected into a new tube and boiled for 5 min at 95 °C. Protein samples were loaded and run on a SDS-PAGE (80V before entering separation gel, 100V-120V in the separation gel) and subsequently resolved. After the transfer to a methanol activated PVDF (Polyvinylidenfluorid) membrane, these were blocked in 5% skimmed milk in TBST (TBS, 0.1% Tween 20) for 30 min at RT.

The membrane was washed (3 times with TBST for 5 min), cut when required and incubated with the primary antibody (dilution in 3% BSA) at 4 °C on a rolling shaker overnight. The membrane was washed (3 times with TBST for 5 min), incubated with the secondary antibody dilution (5% skimmed milk in TBST) for 30 min at RT and afterwards washed again 3 times for 5 min with TBST. Prior WB imaging (Fujifilm LAS-4000 system) the membrane was developed using the Clarity and Clarity Max ECL WB Substrates (Bio-Rad).

Protein samples for mass spectrometry analysis were prepared as followed: RPE1 and HCT116 cells were harvest and count. A pellet with 2 x 10^7 cells was resuspended in 2.5 ml RIPA buffer (50 mM Tris-HCl, 150 mM NaCl, 5 mM EDTA, 1% Triton X-100, 0.1% SDS, 0.5% sodium deoxycholate, pH 8.0) supplemented with protease inhibitors (cOmplete™, Roche), 1 mM PMSF, 5 mM $MgCl_2$ and incubated for 5 min on ice. Benzonase Nuclease (Merck, final concentration: 180 U/ml) to degrade DNA was added and incubate for 30 min on ice (mix in between) or on a roller in a 4 °C cold room. Afterwards the cell suspension was centrifuged at 16,000 g for 45 min at 4 °C. The supernatant was aliquoted, snap-frozen in liquid nitrogen and stored at -80 °C. For reduction and alkylation, the chloroform/methanol precipitation (Wessel and Flugge 1984) and the 8 M Urea in-solution digestion was performed following the procedure of the ZMBH Core Facility for Mass Spectrometry & Proteomics (CFMP).

7.7 MT-regrowth assay

To induce depolymerization of the MT at the centrosome cells were placed on ice and incubated at 4 °C for 40 min (cold treatment). Subsequently, cells were washed with 1x PBS at 37 °C and then put on a pre-warmed metal rack (maintained at 37 °C) for 15 sec to induce MT re-growth. Pre-warmed CSK buffer (10 mM PIPES pH 7.0, 300 mM Sucrose, 100 mM $NaCl_2$, 3 mM $MgCl_2$, 10 mM EGTA, 0,5% Triton X-100) was used to extract and remove soluble non-polymerized components of the cytoskeleton. Afterwards cells were washed with 1x PBS and fixed with ice-cold methanol (−20 °C) followed by indirect immunofluorescence staining. The length and number of MTs per centrosome were quantified using the Fiji software (Schindelin et al. 2012).

7.8 Live cell imaging

In preparation for live cell imaging, cells were cultured in Ibidi µ-Slide 8-well slides (Ibidi) and labelled with SPY650-DNA dye (1:7000 dilution) for 2 hours prior imaging. Image acquisition was performed using the DeltaVision RT system. Z-stacks were captured with a 60x objective every 4 min over 16 h at 37 °C. Maximum intensity projections and/or deconvolution were created using SoftWoRx. The inter centrosomal distance was measured using Fiji. For the NEBD analysis, cells were observed over 24 h (imaging in 5 min intervals) using the 40x objective at 37 °C. Z-Stacks with a hight of 15 µm and an interspace between each stack of 1 µm were acquired through the live cell imaging. For all live cell experiments HEPES-buffered DMEM/F12 medium w/o phenol red was used.

7.9 Microscopy

The DeltaVision RT system (GE Healthcare), Cell Observer system (Zeiss), Nikon Ti2 inverted microscope, Olympus CellSens IX81 widefield microscope and Leica SP8 STED nanoscopy (Leica) were used in this study. The DeltaVision was used as conventional microscope for fixed cell samples and live cell imaging to perform quantitative analysis. Images obtained with the DeltaVision were projected and/or deconvolved using the softWoRx software provided by DeltaVision, and quantification was performed using Fiji. The Leica SP8 STED microscopy was used for super resolution imaging of fixed cell samples. Deconvolution was performed using Huygens Professional (Scientific Volume Imaging). Sample preparation and imaging were performed following the manufacturer’s protocols.

7.10 Analysis, software and macros

Image analysis was performed using Fiji. The inter-centrosomal distance was measured by hand with the line tool or semi-automated with the following macro:

```
macro "2D/3D distanceMeasure" {
    getDateAndTime(year, month, dayOfWeek, dayOfMonth, hour, minute, second, msec);
    print("--->");
    print("2D/3D distance Measurements");
    print("Date: " + (month+1) + "/" + dayOfMonth + "/" + year + " Time: " + hour + " : " + minute + " : " + second);
    run("Set Measurements...", "area redirect=None decimal=0");
    run("Clear Results");

    if (roiManager("count") > 0) {
        roiManager("deselect");
        roiManager("delete");
    }

    ImageTitle = getTitle();
    print("Image: " + ImageTitle);
    getDimensions(width, height, channels, slices, frames);
    print("Number of slices: " + slices);
    getVoxelSize(width, height, depth, unit);
    print("2D/3D distance (" + unit + "): ");

    run("Point Tool...", "type=Crosshair color=Magenta size=Medium auto-measure add");
    setTool("point");

    waitForUser("Mark as many centrosome pairs \nfor distance measurement by clicking.");
    count = getValue("results.count");

    for (i = 0; i < count; i += 2) {
        x1 = getResult("X", i);
        y1 = getResult("Y", i);
        x2 = getResult("X", i + 1);
        y2 = getResult("Y", i + 1);

        if (slices == 1) {
            z1 = 0;
            z2 = 0;
        } else {
            z1 = (getResult("Slice", i) * depth);
            z2 = (getResult("Slice", i + 1) * depth);
        }

        distance = sqrt(((x1 - x2) * (x1 - x2)) + ((y1 - y2) * (y1 - y2)) + ((z1 - z2) * (z1 - z2)));
        print(i / 2 + 1 + ", pair- " + distance);
    }

    IJ.renameResults("Results", "2D/3D Distance measurements " + ImageTitle + " Date: " + (month + 1)
    + "/" + dayOfMonth + "/" + year + " Time: " + hour + " : " + minute + " : " + second);
    print("<---");
}
```

To measurement the fluorescence intensity at the centrosome, maximum intensity and sum intensity projection were generated using the softWoRx software of the DeltaVision or with Fiji. To following macro was used to perform the analysis and to subtract the background signal from the relative intensity of the protein of interest:

```
macro "auto IF quantification [u]" {

//cricle size is dependent on centrosome distance!
//select one size for each experiment!
a=55 //inner circle size
b=60 //oute circle size
s = selectionType();

if( s == -1 ) {
    exit("There was no selection.");
} else if( s != 10 ) {
    exit("The selection wasn't a point selection.");
} else {
    getSelectionCoordinates(xPoints,yPoints);
    x = xPoints[0];
    y = yPoints[0];

makeOval(x-a/2, y-a/2, a, a);
run("Measure");

ISm = getResult('RawIntDen', nResults-1);
ASm = getResult('Area', nResults-1);

makeOval(x-b/2, y-b/2, b, b);
run("Measure");

Ibig = getResult('RawIntDen', nResults-1);
Ab = getResult('Area', nResults-1);

A=Ibig-ISm;
B=(Ab-ASm);
C=ASm/B;
Intensity=ISm-(A*C);
print(d2s(Intensity,0));
}
```

The following macro was used to determine the MT number and length per cell:

```
// May 2021
// ZMBH Imaging Facility, author: Holger Lorenz (h.lorenz@zmbh.uni-heidelberg.de)
// Zentrum fuer Molekulare Biologie der Universitaet Heidelberg (ZMBH), Germany
// This macro enables object-associated (eg centriole) length measurements (eg microtubules).
// It works with many objects measured within the image in consecutive measurements
// Developed for Enrico Atorino (AG Schiebel)


//Close ROI Manager to start fresh
if(isOpen("ROI Manager")){
    selectWindow("ROI Manager");
    run("Close");
}

//Close Results table prior to analysis to start fresh
if(isOpen("Results")){
    selectWindow("Results");
    run("Close");
}


//While loop starts
condition=true;

number =1;

while (condition) {


run("Set Measurements...", "display redirect=None decimal=2");
//run("Set Measurements...", "  redirect=None decimal=2");

//Identify input (unmodified) image stack for analysis
Img = getImageID();
name=getTitle();
    //print(name);
ImgDirectory = File.directory;



//run("Channels Tool...");


//Stack.setDisplayMode("color");
Stack.setDisplayMode("composite");
Stack.setActiveChannels("0011");
Stack.setChannel(4);
//run("Green");
run("Grays");
Stack.setChannel(3);
run("Red");
//run("Green");

wait(4);
Stack.setChannel(4);
run("Enhance Contrast...", "saturated=0.05");


setTool("rectangle");
waitForUser("Action needed 1", "Outline Area of interest.");
run("To Selection");
run("Select None");

setTool("polyline");
run("Brightness/Contrast...");


ROIcountStart=roiManager("count");


waitForUser("Action needed 2", "Draw lines and click [t] to add tho ROI Manager.");
run("View 100%");
run("Remove Overlay");

ROIcount=roiManager("count");

for (i = ROIcountStart; i < ROIcount; i++) {
    selectImage(Img);
    roiManager("Select", i);
    run("Measure");
    Table.set("Centriole No.", i, number);
}


tableSize=Table.size;

selectWindow("Results");
//run("Summarize");


Table.set("Count", ROIcountStart, ROIcount-ROIcountStart);
Table.update;

selectImage(Img);
run("Select None");
resetMinAndMax();

number = number+1;


types = newArray("continue", "NOT continue");
Dialog.create("Continue?");
Dialog.addChoice("Type:", types);
Dialog.show;
//showMessageWithCancel("Continue?", "To continue, click OK.");

types = Dialog.getChoice();
if(types=="NOT continue"){
    condition=false;
}


}
```

```
//Delete zeros in table
for (j = 0; j < ROIcount; j++) {
    check = Table.get("Count", j);
    //print(check);
    if(check==0){
    Table.set("Count", j, "");
}
}


//Image set to original gray display
Stack.setDisplayMode("grayscale");

//display all lines measured
roiManager("Show All");


//To save everything
showMessageWithCancel("Save?", "For saving both Results and ROI Manager list, click OK.");
//waitForUser("Save?", "For saving Results and ROI Manager list, click OK.");

getDateAndTime(year, month, dayOfWeek, dayOfMonth, hour, minute, second, msec);

if(isOpen("ROI Manager")){
    roiManager("Deselect");
    //roiManager("Save", myDir+"RoiSet_complete_"+timestamp+".zip");
    roiManager("Save", ImgDirectory+"RoiSet_LineLengths_"+year+"."+month+1+"."+dayOfMonth+"_"+hour+"."+minute+"."+second+".zip");
}
if(isOpen("Results")){
    selectWindow("Results");
    saveAs("Text", ImgDirectory+"Results_LineLengths_"+year+"."+month+1+"."+dayOfMonth+"_"+hour+"."+minute+"."+second+".txt");
    //run("Close");
}
```

The graphs of the results were plotted using Prism 8/9/10 software (GraphPad). All Statistic tests (t-test and one-way ANOVA) were performed using the Prism software and the following p-values were used: n.s. stands for not significant $p > 0.05$, * $p < 0.05$, ** $p < 0.01$, *** $p < 0.001$, **** $p < 0.0001$. The brightness and contrast of representative images were linearly adjusted using Fiji. Figures were assembled using Adobe Illustrator (Adobe).

The radial scanning analysis was performed using R version 4.0.3. The raw z-stacks were transferred into the created pipeline and the channel for the centrosome marker was filtered out. The background was subtracted from the sum projection (median filter of size 10). To segmentate cells a second image file with cell masks was used and applied to the corresponding image. The high-pass Laplacian filtering was performed to separate masks that were to close together. This technique sharpens the edges of the mask to avoid overlapping pixels. The starting point of the radial scanning with a distance matrix is the pixel with the highest intensity (after applying gaussian blur) in the cell. The line plot was created with R-studio and the average results were blotted in Prism.

Table 17 Software

Software	Provider
SoftWoRx	GE Healthcare
LAS X	Leica
Huygens Professional	Scientific Volume Imaging
SnapGene	SnapGene
SeqBuilder	DNASTAR
Adobe Illustrator	Adobe Systems Incorporated
Fiji	National Institutes of Health
Prism	GraphPad Software

References

Agircan, Fikret G., Elmar Schiebel, and Balca R. Mardin. 2014. 'Separate to Operate: Control of Centrosome Positioning and Separation'. *Philosophical Transactions of the Royal Society B: Biological Sciences* 369(1650).

Alberts, B., R. Heald, A. Johnson, D. Morgan, M. Raff, K. Roberts, and P. Walter. 2022. *Molecular Biology of the Cell: Seventh International Student Edition*. W. W. Norton.

Arquint, Christian, and Erich A. Nigg. 2016. 'The PLK4-STIL-SAS-6 Module at the Core of Centriole Duplication'. *Biochemical Society Transactions* 44(5):1253–63.

Bahe, Susanne, York Dieter Stierhof, Christopher J. Wilkinson, Florian Leiss, and Erich A. Nigg. 2005. 'Rootletin Forms Centriole-Associated Filaments and Functions in Centrosome Cohesion'. *Journal of Cell Biology* 171(1):27–33. doi: 10.1083/jcb.200504107.

Bahmanyar, Shirin, Daniel D. Kaplan, Jennifer G. DeLuca, Thomas H. Giddings, Eileen T. O'Toole, Mark Winey, Edward D. Salmon, Patrick J. Casey, W. James Nelson, and Angela I. M. Barth. 2008. 'β-Catenin Is a Nek2 Substrate Involved in Centrosome Separation'. *Genes and Development* 22(1):91–105. doi: 10.1101/gad.1596308.

Banterle, Niccolò, and Pierre Gönczy. 2017. 'Centriole Biogenesis: From Identifying the Characters to Understanding the Plot'. *Annual Review of Cell and Developmental Biology* 33(1):23–49. doi: 10.1146/annurev-cellbio-100616-060454.

Basto, Renata, Kathrin Brunk, Tatiana Vinadogrova, Nina Peel, Anna Franz, Alexey Khodjakov, and Jordan W. Raff. 2008. 'Centrosome Amplification Can Initiate Tumorigenesis in Flies'. *Cell* 133(6):1032–42. doi: 10.1016/j.cell.2008.05.039.

Basu, Souradeep, Jessica Greenwood, Andrew W. Jones, and Paul Nurse. 2022. 'Core Control Principles of the Eukaryotic Cell Cycle'. *Nature* 607(7918):381–86. doi: 10.1038/s41586-022-04798-8.

Beaudouin, Joël, Daniel Gerlich, Nathalie Daigle, Roland Eils, and Jan Ellenberg. 2002. 'Nuclear Envelope Breakdown Proceeds by Microtubule-Induced Tearing of the Lamina'. *Cell* 108(1):83–96. doi: 10.1016/S0092-8674(01)00627-4.

Bettencourt-Dias, M., A. Rodrigues-Martins, L. Carpenter, M. Riparbelli, L. Lehmann, M. K. Gatt, N. Carmo, F. Balloux, G. Callaini, and D. M. Glover. 2005. 'SAK/PLK4 Is Required for Centriole Duplication and Flagella Development'. *Curr Biol* 15(24):2199–2207. doi: 10.1016/j.cub.2005.11.042.

Bolhy, Stéphanie, Imène Bouhlel, Elisa Dultz, Tania Nayak, Michela Zuccolo, Xavier Gatti, Richard Vallee, Jan Ellenberg, and Valérie Doye. 2011. 'A Nup133-Dependent NPC-Anchored Network Tethers Centrosomes to the Nuclear Envelope in Prophase'. *Journal of Cell Biology* 192(5):855–71. doi: 10.1083/jcb.201007118.

Bornens, Michel. 2002. 'Centrosome Composition and Microtubule Anchoring Mechanisms'. *Current Opinion in Cell Biology* 14(1):25–34. doi: 10.1016/S0955-0674(01)00290-3.

Bouckson-Castaing, V., M. Moudjou, D. J. Ferguson, S. Mucklow, Y. Belkaid, G. Milon, and P. R. Crocker. 1996. 'Molecular Characterisation of Ninein, a New Coiled-Coil Protein of the Centrosome.' *Journal of Cell Science* 109 (Pt 1:179–90.

Bowler, Mathew, Dong Kong, Shufeng Sun, Rashmi Nanjundappa, Lauren Evans, Veronica Farmer, Andrew Holland, Moe R. Mahjoub, Haixin Sui, and Jadranka Loncarek. 2019. 'High-Resolution Characterization of Centriole Distal Appendage Morphology and Dynamics by Correlative STORM and Electron Microscopy'. *Nature Communications* 10(1). doi: 10.1038/s41467-018-08216-4.

Busson, Sylvie, Denis Dujardin, Anne Moreau, Jim Dompierre, and Jan R. De Mey. 1998. 'Dynein and Dynactin Are Localized to Astral Microtubules and at Cortical Sites in Mitotic Epithelial Cells'. *Current Biology* 8(9):541–44. doi: 10.1016/S0960-9822(98)70208-8.

Can Özcan, Selahattin, Batuhan Mert Kalkan, Enes Çiçek, Ata Alpay Canbaz, and Ceyda Açılan Ayhan. 2023. ‘Prolonged Over-Expression of PLK4 Amplifies Centrosomes through Formation of Inter-Connected Centrosome Rosette Clusters’. doi: 10.1101/2023.10.10.561779.

Cervenka, Igor, Jana Valnohova, Ondrej Bernatik, Jakub Harnos, Matej Radsetoulal, Katerina Sedova, Katerina Hanakova, David Potesil, Miroslava Sedlackova, Alena Salasova, Zachary Steinhart, Stephane Angers, Gunnar Schulte, Ales Hampl, Zbynek Zdrahal, and Vitezslav Bryja. 2016. ‘Dishevelled Is a NEK2 Kinase Substrate Controlling Dynamics of Centrosomal Linker Proteins’. *Proceedings of the National Academy of Sciences of the United States of America* 113(33):9304–9. doi: 10.1073/pnas.1608783113.

Chavali, Pavithra L., Gayathri Chandrasekaran, Alexis R. Barr, Péter Tátrai, Chris Taylor, Evaggelia K. Papachristou, C. Geoffrey Woods, Sreenivas Chavali, and Fanni Gergely. 2016. ‘A CEP215–HSET Complex Links Centrosomes with Spindle Poles and Drives Centrosome Clustering in Cancer’. *Nature Communications* 7(1):11005. doi: 10.1038/ncomms11005.

Chen, Canhe, Fang Tian, Lin Lu, Yun Wang, Zhe Xiao, Chengtao Yu, and Xianwen Yu. 2015. ‘Characterization of Cep85 - A New Antagonist of Nek2A That Is Involved in the Regulation of Centrosome Disjunction’. *Journal of Cell Science* 128(17):3290–3303. doi: 10.1242/jcs.171637.

Conduit, Paul T., Alan Wainman, and Jordan W. Raff. 2015. ‘Centrosome Function and Assembly in Animal Cells’. *Nature Reviews Molecular Cell Biology* 16(10):611–24. doi: 10.1038/nrm4062.

Conroy, Pauline C., Chiara Saladino, Tiago J. Dantas, Pierce Lalor, Peter Dockery, and Ciaran G. Morrison. 2012. ‘C-NAP1 and Rootletin Restrain DNA Damage-Induced Centriole Splitting and Facilitate Ciliogenesis’. *Cell Cycle* 11(20):3769–78. doi: 10.4161/cc.21986.

Dammermann, Alexander, and Andreas Merdes. 2002. ‘Assembly of Centrosomal Proteins and Microtubule Organization Depends on PCM-1’. *Journal of Cell Biology* 159(2):255–66. doi: 10.1083/jcb.200204023.

Dang, Hairuo, Ana Martin-Villalba, and Elmar Schiebel. 2022. 'Centrosome Linker Protein C-Nap1 Maintains Stem Cells in Mouse Testes'. *EMBO Reports* 23(7). doi: 10.15252/embr.202153805.

Dang, Hairuo, and Elmar Schiebel. 2022. 'Emerging Roles of Centrosome Cohesion'. *Open Biology* 12(10). doi: 10.1098/rsob.220229.

Delgehyr, Nathalie, James Sillibourne, and Michel Bornens. 2005. 'Microtubule Nucleation and Anchoring at the Centrosome Are Independent Processes Linked by Ninein Function'. *Journal of Cell Science* 118(8):1565–75. doi: 10.1242/jcs.02302.

Doxsey, Stephen. 2001. 'Re-Evaluating Centrosome Function'. *Nature Reviews Molecular Cell Biology* 2(9):688–98. doi: 10.1038/35089575.

Drosopoulos, Konstantinos, Chan Tang, William C. H. Chao, and Spiros Linardopoulos. 2014. 'APC/C Is an Essential Regulator of Centrosome Clustering'. *Nature Communications* 5(1):3686. doi: 10.1038/ncomms4686.

El-Aouar Filho, Rachid A., Aurélie Nicolas, Thiago L. De Paula Castro, Martine Deplanche, Vasco A. De Carvalho Azevedo, Pierre L. Goossens, Frédéric Taieb, Gerard Lina, Yves Le Loir, and Nadia Berkova. 2017. 'Heterogeneous Family of Cyclomodulins: Smart Weapons That Allow Bacteria to Hijack the Eukaryotic Cell Cycle and Promote Infections'. *Frontiers in Cellular and Infection Microbiology* 7(MAY).

Fang, Guoliang, Dachuan Zhang, Huilong Yin, Lu Zheng, Xiaolin Bi, and Li Yuan. 2014. 'Centlein Mediates an Interaction between C-Nap1 and Cep68 to Maintain Centrosome Cohesion'. *Journal of Cell Science* 127(8):1631–39. doi: 10.1242/jcs.139451.

Fava, Luca L., Fabian Schuler, Valentina Sladky, Manuel D. Haschka, Claudia Soratroi, Lisa Eiterer, Egon Demetz, Guenter Weiss, Stephan Geley, Erich A. Nigg, and Andreas Villunger. 2017. 'The PIDDosome Activates P53 in Response to Supernumerary Centrosomes.' *Genes & Development* 31(1):34–45. doi: 10.1101/gad.289728.116.

Flanagan, Anne Marie, Elena Stavenschi, Shivakumar Basavaraju, David Gaboriau, David A. Hoey, and Ciaran G. Morrison. 2017. 'Centriole Splitting Caused by Loss of the Centrosomal Linker Protein C-NAP1 Reduces Centriolar Satellite Density and Impedes Centrosome Amplification'. *Molecular Biology of the Cell* 28(6):736–45. doi: 10.1091/mbc.E16-05-0325.

Floriot, Sandrine, Laura Bellutti, Johan Castille, Pauline Moison, Sébastien Messiaen, Bruno Passet, Laurent Boulanger, Abdelhak Boukadiri, Sophie Tourpin, Christian Beauvallet, Marthe Vilotte, Julie Riviere, Christine Péchoux, Maud Bertaud, Jean-Luc Vilotte, and Gabriel Livera. 2022. 'CEP250 Is Required for Maintaining Centrosome Cohesion in the Germline and Fertility in Male Mice'. *Frontiers in Cell and Developmental Biology* 9. doi: 10.3389/fcell.2021.754054.

Fry, A M, P. Meraldi, and E. A. Nigg. 1998. 'A Centrosomal Function for the Human Nek2 Protein Kinase, a Member of the NIMA Family of Cell Cycle Regulators'. *Embo j* 17(2):470–81. doi: 10.1093/emboj/17.2.470.

Fry, Andrew M, Thibault Mayor, Patrick Meraldi, York-Dieter Stierhof, Kayoko Tanaka, and Erich A. Nigg. 1998. *C-Nap1, a Novel Centrosomal Coiled-Coil Protein and Candidate Substrate of the Cell Cycle-Regulated Protein Kinase Nek2*. Vol. 141.

Fry, Andrew M., Laura O'Regan, Sarah R. Sabir, and Richard Bayliss. 2012. 'Cell Cycle Regulation by the NEK Family of Protein Kinases'. *Journal of Cell Science*. doi: 10.1242/jcs.111195.

Fry, Andrew M., Josephina Sampson, Caroline Shak, and Sue Shackleton. 2017. 'Recent Advances in Pericentriolar Material Organization: Ordered Layers and Scaffolding Gels'. *F1000Research* 6.

Fu, J., Z. Lipinszki, H. Rangone, M. Min, C. Mykura, J. Chao-Chu, S. Schneider, N. S. Dzhindzhev, M. Gottardo, M. G. Riparbelli, G. Callaini, and D. M. Glover. 2016. 'Conserved Molecular Interactions in Centriole-to-Centrosome Conversion'. *Nat Cell Biol* 18(1):87–99. doi: 10.1038/ncb3274.

Fu, Jingyan, Iain M. Hagan, and David M. Glover. 2015. 'The Centrosome and Its Duplication Cycle'. *Cold Spring Harbor Perspectives in Medicine* 5(1). doi: 10.1101/cshperspect.a015800.

Fujita, Hiroki, Yuki Yoshino, and Natsuko Chiba. 2016. 'Regulation of the Centrosome Cycle'. *Molecular and Cellular Oncology* 3(2).

Fuster-García, Carla, Gema García-García, Teresa Jaijo, Neus Fornés, Carmen Ayuso, Miguel Fernández-Burriel, Ana Sánchez-De la Morena, Elena Aller, and José M. Millán. 2018. 'High-Throughput Sequencing for the Molecular Diagnosis of Usher Syndrome Reveals 42 Novel Mutations and Consolidates CEP250 as Usher-like Disease Causative'. *Scientific Reports* 8(1). doi: 10.1038/s41598-018-35085-0.

Ganem, Neil J., Susana A. Godinho, and David Pellman. 2009. 'A Mechanism Linking Extra Centrosomes to Chromosomal Instability'. *Nature* 460(7252):278–82. doi: 10.1038/nature08136.

Gascoigne, Karen E., and Iain M. Cheeseman. 2011. 'Kinetochore Assembly: If You Build It, They Will Come'. *Current Opinion in Cell Biology* 23(1):102–8.

Gergely, Fanni, and Renata Basto. 2008. 'Multiple Centrosomes: Together They Stand, Divided They Fall'. *Genes & Development* 22(17):2291–96. doi: 10.1101/gad.1715208.

Glotzer, Michael, Andrew W. Murray, and Marc W. Kirschner. 1991. 'Cyclin Is Degraded by the Ubiquitin Pathway'. *Nature* 349(6305):132–38. doi: 10.1038/349132a0.

Godinho, S. A., and D. Pellman. 2014. 'Causes and Consequences of Centrosome Abnormalities in Cancer'. *Philosophical Transactions of the Royal Society B: Biological Sciences* 369(1650):20130467. doi: 10.1098/rstb.2013.0467.

Godinho, Susana A., Mijung Kwon, and David Pellman. 2009. 'Centrosomes and Cancer: How Cancer Cells Divide with Too Many Centrosomes'. *Cancer and Metastasis Reviews* 28(1–2):85–98. doi: 10.1007/s10555-008-9163-6.

Gönczy, Pierre, and Georgios N. Hatzopoulos. 2019. 'Centriole Assembly at a Glance'. *Journal of Cell Science* 132(4). doi: 10.1242/JCS.228833.

Gönczy, Pierre, Silke Pichler, Matthew Kirkham, and Anthony A. Hyman. 1999. 'Cytoplasmic Dynein Is Required for Distinct Aspects of Mtoc Positioning, Including Centrosome Separation, in the One Cell Stage Caenorhabditis Elegans Embryo'. *Journal of Cell Biology* 147(1):135–50. doi: 10.1083/jcb.147.1.135.

Goundiam, Oumou, and Renata Basto. 2021. 'Centrosomes in Disease: How the Same Music Can Sound so Different?' *Current Opinion in Structural Biology* 66:74–82. doi: 10.1016/j.sbi.2020.09.011.

Graser, Susanne, York Dieter Stierhof, and Erich A. Nigg. 2007. 'Cep68 and Cep215 (Cdk5rap2) Are Required for Centrosome Cohesion'. *Journal of Cell Science* 120(24):4321–31. doi: 10.1242/jcs.020248.

Guichard, Paul, Virginie Hachet, Norbert Majubu, Aitana Neves, Davide Demurtas, Natacha Olieric, Isabelle Fluckiger, Akinori Yamada, Kumiko Kihara, Yuichiro Nishida, Shigeharu Moriya, Michel O. Steinmetz, Yuichi Hongoh, and Pierre Gönczy. 2013. 'Native Architecture of the Centriole Proximal Region Reveals Features Underlying Its 9-Fold Radial Symmetry'. *Current Biology* 23(17):1620–28. doi: 10.1016/j.cub.2013.06.061.

Habedanck, Robert, York-Dieter Stierhof, Christopher J. Wilkinson, and Erich A. Nigg. 2005. 'The Polo Kinase Plk4 Functions in Centriole Duplication'. *Nature Cell Biology* 7(11):1140–46. doi: 10.1038/ncb1320.

Hardy, Tara, Miseon Lee, Rebecca S. Hames, Suzanna L. Prosser, Donna Marie Cheary, Mugdha D. Samant, Francisca Schultz, Joanne E. Baxter, Kunsoo Rhee, and Andrew M. Fry. 2014. 'Multisite Phosphorylation of C-Nap1 Releases It from Cep135 to Trigger Centrosome Disjunction'. *Journal of Cell Science* 127(11):2493–2506. doi: 10.1242/jcs.142331.

Haren, Laurence, Tim Stearns, and Jens Lüders. 2009. 'Plk1-Dependent Recruitment of γ-Tubulin Complexes to Mitotic Centrosomes Involves Multiple PCM Components'. *PLoS ONE* 4(6):e5976. doi: 10.1371/journal.pone.0005976.

Hartwell, Leland H., and Ted A. Weinert. 1989. ‘Checkpoints: Controls That Ensure the Order of Cell Cycle Events’. *Science* 246(4930):629–34. doi: 10.1126/science.2683079.

Hata, Shoji, Ana Pastor Peidro, Marko Panic, Peng Liu, Enrico Atorino, Charlotta Funaya, Ursula Jäkle, Gislene Pereira, and Elmar Schiebel. 2019. ‘The Balance between KIFC3 and EG5 Tetrameric Kinesins Controls the Onset of Mitotic Spindle Assembly’. *Nature Cell Biology* 21(9):1138–51. doi: 10.1038/s41556-019-0382-6.

He, Runsheng, Ning Huang, Yitian Bao, Haining Zhou, Junlin Teng, and Jianguo Chen. 2013. ‘LRRC45 Is a Centrosome Linker Component Required for Centrosome Cohesion’. *Cell Reports* 4(6):1100–1107. doi: 10.1016/j.celrep.2013.08.005.

Ishikawa-Ankerhold, Hellen, Janina Kroll, Dominic van den Heuvel, Jörg Renkawitz, and Annette Müller-Taubenberger. 2022. ‘Centrosome Positioning in Migrating Dictyostelium Cells’. *Cells* 11(11):1776. doi: 10.3390/cells11111776.

Izquierdo, D., W. J. Wang, K. Uryu, and M. F. Tsou. 2014. ‘Stabilization of Cartwheel-Less Centrioles for Duplication Requires CEP295-Mediated Centriole-to-Centrosome Conversion’. *Cell Rep* 8(4):957–65. doi: 10.1016/j.celrep.2014.07.022.

Jaiswal, Sonal, and Priyanka Singh. 2021. ‘Centrosome Dysfunction in Human Diseases’. *Seminars in Cell and Developmental Biology* 110:113–22.

Kalkan, Batuhan Mert, Selahattin Can Özcan, Enes Çiçek, Mehmet Gönen, and Ceyda Açılan. n.d. ‘Less Is More: Nek2A Unclusters Extra Centrosomes and Induces Cell Death in Cancer Cells via KIF2C Interaction’. doi: 10.1101/2023.11.21.567992.

Karki, Menuka, Neda Keyhaninejad, and Charles B. Shuster. 2017. ‘Precocious Centriole Disengagement and Centrosome Fragmentation Induced by Mitotic Delay’. *Nature Communications* 8(1):15803. doi: 10.1038/ncomms15803.

Kaseda, Kuniyoshi, Andrew D. McAinsh, and Robert A. Cross. 2012. 'Dual Pathway Spindle Assembly Increases Both the Speed and the Fidelity of Mitosis'. *Biology Open* 1(1):12–18. doi: 10.1242/bio.2011012.

Kim, Kyeongmi, Seongju Lee, Jaerak Chang, and Kunsoo Rhee. 2008. 'A Novel Function of CEP135 as a Platform Protein of C-NAP1 for Its Centriolar Localization'. *Experimental Cell Research* 314(20):3692–3700. doi: 10.1016/j.yexcr.2008.09.016.

Kim, Seongjae, and Kunsoo Rhee. 2014. 'Importance of the CEP215-Pericentrin Interaction for Centrosome Maturation during Mitosis'. *PLoS ONE* 9(1):e87016. doi: 10.1371/journal.pone.0087016.

Kleylein-Sohn, J., J. Westendorf, M. Le Clech, R. Habedanck, Y. D. Stierhof, and E. A. Nigg. 2007. 'Plk4-Induced Centriole Biogenesis in Human Cells'. *Dev Cell* 13(2):190–202. doi: 10.1016/j.devcel.2007.07.002.

Kochanski, R. S., and G. G. Borisy. 1990. 'Mode of Centriole Duplication and Distribution.' *Journal of Cell Biology* 110(5):1599–1605. doi: 10.1083/jcb.110.5.1599.

Krämer, Alwin, Bettina Maier, and Jiri Bartek. 2011. 'Centrosome Clustering and Chromosomal (in)Stability: A Matter of Life and Death'. 5:324–35.

Kratz, Anne Sophie, Felix Bärenz, Kai T. Richter, and Ingrid Hoffmann. 2015. 'Plk4-Dependent Phosphorylation of STIL Is Required for Centriole Duplication'. *Biology Open* 4(3):370–77. doi: 10.1242/bio.201411023.

Kroll, Janina, Robert Hauschild, Artur Kuznetcov, Kasia Stefanowski, Monika D. Hermann, Jack Merrin, Lubuna Shafeek, Annette Müller-Taubenberger, and Jörg Renkawitz. 2023. 'Adaptive Pathfinding by Nucleokinesis during Amoeboid Migration'. *The EMBO Journal* 42(24). doi: 10.15252/embj.2023114557.

Kwon, Mijung, Susana A. Godinho, Namrata S. Chandhok, Neil J. Ganem, Ammar Azioune, Manuel Thery, and David Pellman. 2008. 'Mechanisms to Suppress Multipolar Divisions in Cancer Cells with Extra Centrosomes'. *Genes & Development* 22(16):2189–2203. doi: 10.1101/gad.1700908.

Leber, B., B. Maier, F. Fuchs, J. Chi, P. Riffel, S. Anderhub, L. Wagner, A. D. Ho, J. L. Salisbury, M. Boutros, and A. Kramer. 2010. 'Proteins Required for Centrosome Clustering in Cancer Cells'. *Sci Transl Med* 2(33):33ra38. doi: 10.1126/scitranslmed.3000915.

Lee, Kwanwoo, and Kunsoo Rhee. 2012. 'Separase-Dependent Cleavage of Pericentrin B Is Necessary and Sufficient for Centriole Disengagement during Mitosis'. *Cell Cycle* 11(13):2476–85. doi: 10.4161/cc.20878.

Lim, Shuhui, and Philipp Kaldis. 2013. 'Cdks, Cyclins and CKIs: Roles beyond Cell Cycle Regulation'. *Development* 140(15):3079–93. doi: 10.1242/dev.091744.

Loncarek, Jadranka, and Mónica Bettencourt-Dias. 2018. 'Building the Right Centriole for Each Cell Type'. *Journal of Cell Biology* 217(3):823–35. doi: 10.1083/jcb.201704093.

Lüders, Jens, and Tim Stearns. 2007. 'Microtubule-Organizing Centres: A Re-Evaluation'. *Nature Reviews Molecular Cell Biology* 8(2):161–67. doi: 10.1038/nrm2100.

Lukas, Jiri, Claudia Lukas, and Jiri Bartek. 2004. 'Mammalian Cell Cycle Checkpoints: Signalling Pathways and Their Organization in Space and Time'. *DNA Repair* 3(8–9):997–1007.

Mahen, Robert. 2018. 'Stable Centrosomal Roots Disentangle to Allow Interphase Centriole Independence'. *PLOS Biology* 16(4):e2003998. doi: 10.1371/journal.pbio.2003998.

Mahen, Robert. 2022. 'CNap1 Bridges Centriole Contact Sites to Maintain Centrosome Cohesion' edited by R. Basto. *PLOS Biology* 20(10):e3001854. doi: 10.1371/journal.pbio.3001854.

Malumbres, Marcos, and Mariano Barbacid. 2009. 'Cell Cycle, CDKs and Cancer: A Changing Paradigm'. *Nature Reviews Cancer* 9(3):153–66.

Mardin, Balca R., Fikret G. Agircan, Cornelia Lange, and Elmar Schiebel. 2011. 'Plk1 Controls the Nek2A-PP1γ Antagonism in Centrosome Disjunction'. *Current Biology* 21(13):1145–51. doi: 10.1016/j.cub.2011.05.047.

Mardin, Balca R., Cornelia Lange, Joanne E. Baxter, Tara Hardy, Sebastian R. Scholz, Andrew M. Fry, and Elmar Schiebel. 2010. 'Components of the Hippo Pathway Cooperate with Nek2 Kinase to Regulate Centrosome Disjunction'. *Nature Cell Biology* 12(12):1166–76. doi: 10.1038/ncb2120.

Marthiens, Véronique, Matthieu Piel, and Renata Basto. 2012. 'Never Tear Us Apart – the Importance of Centrosome Clustering'. *Journal of Cell Science* 125(14):3281–92. doi: 10.1242/jcs.094797.

Martínez-Alonso, Diego, and Marcos Malumbres. 2020. 'Mammalian Cell Cycle Cyclins'. *Seminars in Cell and Developmental Biology* 107:28–35.

Matthews, Helen K., Cosetta Bertoli, and Robertus A. M. de Bruin. 2022. 'Cell Cycle Control in Cancer'. *Nature Reviews Molecular Cell Biology* 23(1):74–88. doi: 10.1038/s41580-021-00404-3.

Mayor, Thibault, York-Dieter Stierhof, Kayoko Tanaka, Andrew M. Fry, and Erich A. Nigg. 2000. 'The Centrosomal Protein C-Nap1 Is Required for Cell Cycle–Regulated Centrosome Cohesion'. *Journal of Cell Biology* 151(4):837–46. doi: 10.1083/jcb.151.4.837.

Mazo, Gregory, Nadine Soplop, Won Jing Wang, Kunihiro Uryu, and Meng Fu Bryan Tsou. 2016. 'Spatial Control of Primary Ciliogenesis by Subdistal Appendages Alters Sensation-Associated Properties of Cilia'. *Developmental Cell* 39(4):424–37. doi: 10.1016/j.devcel.2016.10.006.

Meraldi, P., and E. A. Nigg. 2002. 'The Centrosome Cycle'. *FEBS Letters* 521(1–3):9–13. doi: 10.1016/S0014-5793(02)02865-X.

Meraldi, Patrick, and Erich A. Nigg. 2001. 'Centrosome Cohesion Is Regulated by a Balance of Kinase and Phosphatase Activities'. *Journal of Cell Science* 114(20):3749–57. doi: 10.1242/jcs.114.20.3749.

Miller, Paul M., Andrew W. Folkmann, Ana R. R. Maia, Nadia Efimova, Andrey Efimov, and Irina Kaverina. 2009. 'Golgi-Derived CLASP-Dependent Microtubules Control Golgi Organization and Polarized Trafficking in Motile Cells'. *Nature Cell Biology* 11(9):1069–80. doi: 10.1038/ncb1920.

Mogensen, M. M., A. Malik, M. Piel, V. Bouckson-Castaing, and M. Bornens. 2000. ‘Microtubule Minus-End Anchorage at Centrosomal and Non-Centrosomal Sites: The Role of Ninein’. *Journal of Cell Science* 113(17):3013–23. doi: 10.1242/jcs.113.17.3013.

Moniz, Larissa, Previn Dutt, Nasir Haider, and Vuk Stambolic. 2011. ‘Nek Family of Kinases in Cell Cycle, Checkpoint Control and Cancer’. *Cell Division* 6(1):18. doi: 10.1186/1747-1028-6-18.

Mönnich, Maren, Louise Borgeskov, Loretta Breslin, Lis Jakobsen, Michaela Rogowski, Canan Doganli, Jacob M. Schrøder, Johanne B. Mogensen, Louise Blinkenkjær, Lea M. Harder, Emma Lundberg, Stefan Geimer, Søren T. Christensen, Jens S. Andersen, Lars A. Larsen, and Lotte B. Pedersen. 2018. ‘CEP128 Localizes to the Subdistal Appendages of the Mother Centriole and Regulates TGF-β/BMP Signaling at the Primary Cilium’. *Cell Reports* 22(10):2584–92. doi: 10.1016/j.celrep.2018.02.043.

Mountain, V., C. Simerly, L. Howard, A. Ando, G. Schatten, and D. A. Compton. 1999. ‘The Kinesin-Related Protein, HSET, Opposes the Activity of Eg5 and Cross-Links Microtubules in the Mammalian Mitotic Spindle’. *J Cell Biol* 147(2):351–66. doi: 10.1083/jcb.147.2.351.

Nakayama, Keiichi I., and Keiko Nakayama. 2006. ‘Ubiquitin Ligases: Cell-Cycle Control and Cancer’. *Nature Reviews Cancer* 6(5):369–81. doi: 10.1038/nrc1881.

Nam, Hyun-Ja, Ryan M. Naylor, and Jan M. van Deursen. 2015. ‘Centrosome Dynamics as a Source of Chromosomal Instability’. *Trends in Cell Biology* 25(2):65–73. doi: 10.1016/j.tcb.2014.10.002.

Nigg, Erich A., and Andrew J. Holland. 2018. ‘Once and Only Once: Mechanisms of Centriole Duplication and Their Deregulation in Diseases’. *Nature Reviews Molecular Cell Biology* 19(5):297–312.

Nigg, Erich A., and Tim Stearns. 2011. ‘The Centrosome Cycle: Centriole Biogenesis, Duplication and Inherent Asymmetries’. *Nature Cell Biology* 13(10):1154–60. doi: 10.1038/ncb2345.

Ohta, Midori, Koki Watanabe, Tomoko Ashikawa, Yuka Nozaki, Satoko Yoshiba, Akatsuki Kimura, and Daiju Kitagawa. 2018. 'Bimodal Binding of STIL to Plk4 Controls Proper Centriole Copy Number'. *Cell Reports* 23(11):3160-3169.e4. doi: 10.1016/j.celrep.2018.05.030.

Panic, Marko, Shoji Hata, Annett Neuner, and Elmar Schiebel. 2015. 'The Centrosomal Linker and Microtubules Provide Dual Levels of Spatial Coordination of Centrosomes'. *PLoS Genetics* 11(5). doi: 10.1371/journal.pgen.1005243.

Pannu, Vaishali, Padmashree C. G. Rida, Angela Ogden, Ravi Chakra Turaga, Shashikiran Donthamsetty, Nathan J. Bowen, Katie Rudd, Meenakshi V. Gupta, Michelle D. Reid, Guilherme Cantuaria, Claire E. Walczak, and Ritu Aneja. 2015. 'HSET Overexpression Fuels Tumor Progression via Centrosome Clustering-Independent Mechanisms in Breast Cancer Patients'. *Oncotarget* 6(8):6076–91. doi: 10.18632/oncotarget.3475.

Potter, Chloe, Wanqiu Zhu, David Razafsky, Philip Ruzycki, Alexander V. Kolesnikov, Teresa Doggett, Vladimir J. Kefalov, Ewelina Betleja, Moe R. Mahjoub, and Didier Hodzic. 2017. 'Multiple Isoforms of Nesprin1 Are Integral Components of Ciliary Rootlets'. *Current Biology* 27(13):2014-2022.e6. doi: 10.1016/j.cub.2017.05.066.

Quintyne, N. J. 2005. 'Spindle Multipolarity Is Prevented by Centrosomal Clustering'. *Science* 307(5706):127–29. doi: 10.1126/science.1104905.

Rale, Michael J., Rachel S. Kadzik, and Sabine Petry. 2018. 'Phase Transitioning the Centrosome into a Microtubule Nucleator'. *Biochemistry* 57(1):30–37.

Ran, F. Ann, Patrick D. Hsu, Jason Wright, Vineeta Agarwala, David A. Scott, and Feng Zhang. 2013. 'Genome Engineering Using the CRISPR-Cas9 System'. *Nature Protocols* 8(11):2281–2308. doi: 10.1038/nprot.2013.143.

Rattner, J. B., and M. W. Berns. 1976. 'Centriole Behavior in Early Mitosis of Rat Kangaroo Cells (PTK2)'. *Chromosoma* 54(4):387–95. doi: 10.1007/BF00292817.

Remo, Andrea, Xue Li, Elmar Schiebel, and Massimo Pancione. 2020. ‘The Centrosome Linker and Its Role in Cancer and Genetic Disorders’. *Trends in Molecular Medicine* 26(4):380–93.

Remo, Andrea, Erminia Manfrin, Pietro Parcesepe, Alberto Ferrarini, Hye Seung Han, Ugnius Mickys, Carmelo Laudanna, Michele Simbolo, Donatella Malanga, Duarte Mendes Oliveira, Elisabetta Baritono, Tommaso Colangelo, Lina Sabatino, Jacopo Giuliani, Enrico Molinari, Marianna Garonzi, Luciano Xumerle, Massimo Delledonne, Guido Giordano, Claudio Ghimenton, Fortunato Lonardo, Fulvio D’angelo, Federica Grillo, Luca Mastracci, Giuseppe Viglietto, Michele Ceccarelli, Vittorio Colantuoni, Aldo Scarpa, and Massimo Pancione. 2018. ‘Centrosome Linker–Induced Tetraploid Segregation Errors Link Rhabdoid Phenotypes and Lethal Colorectal Cancers’. *Molecular Cancer Research* 16(9):1385–95. doi: 10.1158/1541-7786.MCR-18-0062.

Renkawitz, Jörg, Aglaja Kopf, Julian Stopp, Ingrid de Vries, Meghan K. Driscoll, Jack Merrin, Robert Hauschild, Erik S. Welf, Gaudenz Danuser, Reto Fiolka, and Michael Sixt. 2019. ‘Nuclear Positioning Facilitates Amoeboid Migration along the Path of Least Resistance’. *Nature* 568(7753):546–50. doi: 10.1038/s41586-019-1087-5.

Ring, D., R. Hubble, and M. Kirschner. 1982. ‘Mitosis in a Cell with Multiple Centrioles’. *Journal of Cell Biology* 94(3):549–56. doi: 10.1083/jcb.94.3.549.

Robinson, John T., Edward J. Wojcik, Mark A. Sanders, Maura McGrail, and Thomas S. Hays. 1999. ‘Cytoplasmic Dynein Is Required for the Nuclear Attachment and Migration of Centrosomes during Mitosis in Drosophila’. *Journal of Cell Biology* 146(3):597–608. doi: 10.1083/jcb.146.3.597.

Rosenblatt, Jody. 2005. ‘Spindle Assembly: Asters Part Their Separate Ways’. *Nature Cell Biology* 7(3):219–22. doi: 10.1038/ncb0305-219.

Rosenblatt, Jody, Louise P. Cramer, Buzz Baum, and Karen M. McGee. 2004. ‘Myosin II-Dependent Cortical Movement Is Required for Centrosome Separation and Positioning during Mitotic Spindle Assembly’. *Cell* 117(3):361–72. doi: 10.1016/S0092-8674(04)00341-1.

Sawin, Kenneth E., Katherine LeGuellec, Michel Philippe, and Timothy J. Mitchison. 1992. 'Mitotic Spindle Organization by a Plus-End-Directed Microtubule Motor'. *Nature* 359(6395):540–43. doi: 10.1038/359540a0.

Schindelin, Johannes, Ignacio Arganda-Carreras, Erwin Frise, Verena Kaynig, Mark Longair, Tobias Pietzsch, Stephan Preibisch, Curtis Rueden, Stephan Saalfeld, Benjamin Schmid, Jean-Yves Tinevez, Daniel James White, Volker Hartenstein, Kevin Eliceiri, Pavel Tomancak, and Albert Cardona. 2012. 'Fiji: An Open-Source Platform for Biological-Image Analysis'. *Nature Methods* 9(7):676–82. doi: 10.1038/nmeth.2019.

Schmidt, Kerstin N., Stefanie Kuhns, Annett Neuner, Birgit Hub, Hanswalter Zentgraf, and Gislene Pereira. 2012. 'Cep164 Mediates Vesicular Docking to the Mother Centriole during Early Steps of Ciliogenesis.' *The Journal of Cell Biology* 199(7):1083–1101. doi: 10.1083/jcb.201202126.

Schneider, Maria, Wenshu Lu, Sascha Neumann, Andreas Brachner, Josef Gotzmann, Angelika A. Noegel, and Iakowos Karakesisoglou. 2011. 'Molecular Mechanisms of Centrosome and Cytoskeleton Anchorage at the Nuclear Envelope'. *Cellular and Molecular Life Sciences* 68(9):1593–1610. doi: 10.1007/s00018-010-0535-z.

Schweizer, Nina, Laurence Haren, Ilaria Dutto, Ricardo Viais, Cristina Lacasa, Andreas Merdes, and Jens Lüders. 2021. 'Sub-Centrosomal Mapping Identifies Augmin-ΓTuRC as Part of a Centriole-Stabilizing Scaffold'. *Nature Communications* 12(1):6042. doi: 10.1038/s41467-021-26252-5.

Shalem, Ophir, Neville E. Sanjana, Ella Hartenian, Xi Shi, David A. Scott, Tarjei S. Mikkelsen, Dirk Heckl, Benjamin L. Ebert, David E. Root, John G. Doench, and Feng Zhang. 2014. 'Genome-Scale CRISPR-Cas9 Knockout Screening in Human Cells'. *Science* 343(6166):84. doi: 10.1126/science.1247005.

Shinohara, Hiroshi, Nobuyuki Sakayori, Masanori Takahashi, and Noriko Osumi. 2013. 'Ninein Is Essential for the Maintenance of the Cortical Progenitor Character by Anchoring the Centrosome to Microtubules'. *Biology Open* 2(7):739–49. doi: 10.1242/bio.20135231.

Spalluto, Cosma, David I. Wilson, and Tom Hearn. 2012. 'Nek2 Localises to the Distal Portion of the Mother Centriole/Basal Body and Is Required for Timely Cilium Disassembly at the G2/M Transition'. *European Journal of Cell Biology* 91(9):675–86. doi: https://doi.org/10.1016/j.ejcb.2012.03.009.

Splinter, Daniël, Marvin E. Tanenbaum, Arne Lindqvist, Dick Jaarsma, Annette Flotho, Ka Lou Yu, Ilya Grigoriev, Dieuwke Engelsma, Elize D. Haasdijk, Nanda Keijzer, Jeroen Demmers, Maarten Fornerod, Frauke Melchior, Casper C. Hoogenraad, René H. Medema, and Anna Akhmanova. 2010. 'Bicaudal D2, Dynein, and Kinesin-1 Associate with Nuclear Pore Complexes and Regulate Centrosome and Nuclear Positioning during Mitotic Entry'. *PLoS Biology* 8(4):e1000350. doi: 10.1371/journal.pbio.1000350.

Takao, D., S. Yamamoto, D. Kitagawa, and J. Cell Biol. 2019. 'A Theory of Centriole Duplication Based on Self-Organized Spatial Pattern Formation'. *J Cell Biol* 218(11):3537–47. doi: 10.1083/jcb.201904156.

Theile, Laura, Xue Li, Hairuo Dang, Dorothee Mersch, Simon Anders, and Elmar Schiebel. 2023. 'Centrosome Linker Diversity and Its Function in Centrosome Clustering and Mitotic Spindle Formation'. *The EMBO Journal* 42(17). doi: 10.15252/embj.2021109738.

Toso, Alberto, Jennifer R. Winter, Ainslie J. Garrod, Ana C. Amaro, Patrick Meraldi, and Andrew D. McAinsh. 2009. 'Kinetochore-Generated Pushing Forces Separate Centrosomes during Bipolar Spindle Assembly'. *Journal of Cell Biology* 184(3):365–72. doi: 10.1083/jcb.200809055.

Ueda, Masahiro, Ralph Gräf, Harry K. MacWilliams, Manfred Schliwa, and Ursula Euteneuer. 1997. 'Centrosome Positioning and Directionality of Cell Movements'. *Proceedings of the National Academy of Sciences* 94(18):9674–78. doi: 10.1073/pnas.94.18.9674.

Vermeulen, Katrien, Dirk R. Van Bockstaele, and Zwi N. Berneman. 2003. 'The Cell Cycle: A Review of Regulation, Deregulation and Therapeutic Targets in Cancer'. *Cell Proliferation* 36(3):131–49.

Viol, Linda, Shoji Hata, Ana Pastor-Peidro, Annett Neuner, Florian Murke, Patrick Wuchter, Anthony D. Ho, Bernd Giebel, and Gislene Pereira. 2020. 'Nek2 Kinase Displaces Distal Appendages from the Mother Centriole Prior to Mitosis'. *Journal of Cell Biology* 219(3). doi: 10.1083/jcb.201907136.

Vitre, Benjamin, Nicolas Taulet, Audrey Guesdon, Audrey Douanier, Aurelie Dosdane, Melanie Cisneros, Justine Maurin, Sabrina Hettinger, Christelle Anguille, Michael Taschner, Esben Lorentzen, and Benedicte Delaval. 2020. 'IFT Proteins Interact with HSET to Promote Supernumerary Centrosome Clustering in Mitosis'. *EMBO Reports* 21(6). doi: 10.15252/embr.201949234.

Vlijm, Rifka, Xue Li, Marko Panic, Diana Rüthnick, Shoji Hata, Frank Herrmannsdörfer, Thomas Kuner, Mike Heilemann, Johann Engelhardt, Stefan W. Hell, and Elmar Schiebel. 2018. 'STED Nanoscopy of the Centrosome Linker Reveals a CEP68-Organized, Periodic Rootletin Network Anchored to a C-Nap1 Ring at Centrioles'. *Proceedings of the National Academy of Sciences* 115(10):E2246–53. doi: 10.1073/pnas.1716840115.

Wang, Xiaoqun, Jin-Wu Tsai, Janice H. Imai, Wei-Nan Lian, Richard B. Vallee, and Song-Hai Shi. 2009. 'Asymmetric Centrosome Inheritance Maintains Neural Progenitors in the Neocortex'. *Nature* 461(7266):947–55. doi: 10.1038/nature08435.

Waters, JC, RW Cole, and CL Rieder. 1993. 'The Force-Producing Mechanism for Centrosome Separation during Spindle Formation in Vertebrates Is Intrinsic to Each Aster'. *The Journal of Cell Biology* 122(2):361–72. doi: 10.1083/jcb.122.2.361.

Watts, Ciorsdaidh A., Frances M. Richards, Andreas Bender, Peter J. Bond, Oliver Korb, Oliver Kern, Michelle Riddick, Paul Owen, Rebecca M. Myers, Jordan Raff, Fanni Gergely, Duncan I. Jodrell, and Steven V. Ley. 2013. 'Design, Synthesis, and Biological Evaluation of an Allosteric Inhibitor of HSET That Targets Cancer Cells with Supernumerary Centrosomes'. *Chemistry & Biology* 20(11):1399–1410. doi: 10.1016/j.chembiol.2013.09.012.

Wessel, D., and U. I. Flugge. 1984. ‘A Method for the Quantitative Recovery of Protein in Dilute Solution in the Presence of Detergents and Lipids’. *Anal Biochem* 138(1):141–43. doi: 10.1016/0003-2697(84)90782-6.

Winey, Mark, and Eileen O’Toole. 2014. ‘Centriole Structure’. *Philosophical Transactions of the Royal Society B: Biological Sciences* 369(1650).

Würtz, Martin, Erik Zupa, Enrico S. Atorino, Annett Neuner, Anna Böhler, Ariani S. Rahadian, Bram J. A. Vermeulen, Giulia Tonon, Sebastian Eustermann, Elmar Schiebel, and Stefan Pfeffer. 2022. ‘Modular Assembly of the Principal Microtubule Nucleator γ-TuRC’. *Nature Communications* 13(1):473. doi: 10.1038/s41467-022-28079-0.

Xia, Yuqing, Ning Huang, Zhiquan Chen, Fangyuan Li, Guiliang Fan, Dandan Ma, Jianguo Chen, and Junlin Teng. 2018. ‘CCDC102B Functions in Centrosome Linker Assembly and Centrosome Cohesion’. *Journal of Cell Science* 131(23). doi: 10.1242/jcs.222901.

Yamamoto, S., and D. Kitagawa. 2019. ‘Self-Organization of Plk4 Regulates Symmetry Breaking in Centriole Duplication’. *Nat Commun* 10(1):1810. doi: 10.1038/s41467-019-09847-x.

Yang, Jun, Xiaoqing Liu, Guohua Yue, Michael Adamian, Oleg Bulgakov, and Tiansen Li. 2002. ‘Rootletin, a Novel Coiled-Coil Protein, Is a Structural Component of the Ciliary Rootlet’. *The Journal of Cell Biology* 159(3):431–40. doi: 10.1083/jcb.200207153.

Yang, T. Tony, Weng Man Chong, Won Jing Wang, Gregory Mazo, Barbara Tanos, Zhengmin Chen, Thi Minh Nguyet Tran, Yi De Chen, Rueyhung Roc Weng, Chia En Huang, Wann Neng Jane, Meng Fu Bryan Tsou, and Jung Chi Liao. 2018. ‘Super-Resolution Architecture of Mammalian Centriole Distal Appendages Reveals Distinct Blade and Matrix Functional Components’. *Nature Communications* 9(1). doi: 10.1038/s41467-018-04469-1.

Yang, Zhenye, Jadranka Lončarek, Alexey Khodjakov, and Conly L. Rieder. 2008. ‘Extra Centrosomes and/or Chromosomes Prolong Mitosis in Human Cells’. *Nature Cell Biology* 10(6):748–51. doi: 10.1038/ncb1738.

Ye, Xuan, Huiqing Zeng, Gang Ning, Jeremy F. Reiter, and Aimin Liu. 2014. 'C2cd3 Is Critical for Centriolar Distal Appendage Assembly and Ciliary Vesicle Docking in Mammals'. *Proceedings of the National Academy of Sciences* 111(6):2164–69. doi: 10.1073/pnas.1318737111.

Zhang, Xiaochang, Ming Hui Chen, Xuebing Wu, Andrew Kodani, Jean Fan, Ryan Doan, Manabu Ozawa, Jacqueline Ma, Nobuaki Yoshida, Jeremy F. Reiter, Douglas L. Black, Peter V. Kharchenko, Phillip A. Sharp, and Christopher A. Walsh. 2016. 'Cell-Type-Specific Alternative Splicing Governs Cell Fate in the Developing Cerebral Cortex'. *Cell* 166(5):1147-1162.e15. doi: 10.1016/j.cell.2016.07.025.

Zimmerman, Wendy C., James Sillibourne, Jack Rosa, and Stephen J. Doxsey. 2004. 'Mitosis-Specific Anchoring of γ Tubulin Complexes by Pericentrin Controls Spindle Organization and Mitotic Entry'. *Molecular Biology of the Cell* 15(8):3642–57. doi: 10.1091/mbc.e03-11-0796.

Publication during PhD

Research paper:

Theile, L., Li, X., Dang, H., Mersch, D., Anders, S., & Schiebel, E. (2023). Centrosome linker diversity and its function in centrosome clustering and mitotic spindle formation. *The EMBO Journal*, *42*(17). (doi.org/10.15252/embj.2021109738)

Acknowledgements

First of all, I want to thank Prof. Dr. Elmar Schiebel for the great opportunity to conduct my PhD work in his lab and to be part of a great work environment the last years. His strong passion for science is outstanding and catching and is one of the reasons for the success of his research in the field, along with his motivation to achieve consistently high-quality results.

I would also like to express my special thanks to my second supervisor Prof. Dr. Sylvia Erhardt, Dr. Anne Schlaitz and Dr. S. Ralph Grand for being part of my thesis defence committee and for taking the time to evaluate my work. Furthermore, I want to say thank you to Prof. Dr. Gislene Pereira for her support during my TAC meetings over the last 4 years.

Additionally, I would like to thank Dr. Monika Langlotz from the ZMBH FACS Facility for all the cell sortings and Dr. Holger Lorenz from the ZMBH Image Facility for his great support over the years and the great discussions about microscopy and image processing.

The most important and heartfelt thanks go to the current and former members of the Schiebel lab, especially to the centrosome subgroup for the support through our meetings and the lively discussions about science (and other things). The outstanding cohesion of the group and the grateful support is unique. Special thanks also go to Dr. Xue Li for her supervision and training during the first year and her contributions to our publication. Many thanks also to Dr. Hairuo Dang for her scientific assistance and contribution to our paper. Special thanks to Martin for the daily coffee ordering and the organization of Team Patrick. I would also like to thank Aady, for taking on the challenge of continuing the project and giving me the opportunity to pass on all my knowledge and teach her everything I have learnt over last few years.

Nicht zu vergessen, geht ein gigantisches Dankeschön an meine kleine verrückte Conny, die mich nicht nur als Kollegin jeden Tag unterstützt und teilweise vor dem Durchdrehen bewahrt hat, sondern auch als Freundin jederzeit an meiner Seite stand.

Ein großes Dankeschön geht auch an meine Familie, die mich in jeder Phase meiner akademischen Laufbahn unterstützt hat. Insbesondere meine kleine Schwester Lena, die nicht nur immer für mich da ist, sondern auch den besten JGA organisiert hat und dafür gesorgt hat, dass niemand durchdreht an meiner Hochzeit. Weiterhin möchte ich meinem Mann Nico danken, dass er trotz der Höhen und Tiefen in dieser aufregenden und ereignisreichen Zeit immer versucht hat einen kühlen Kopf zu bewahren und mich nach allen Möglichkeiten tatkräftig unterstützt hat.

Ohne euch wäre das alles nicht möglich gewesen, danke für eure Unterstützung, eure Geduld und eure grenzlose Bereitschaft immer wieder zu versuchen zu verstehen, was ich die letzten 4 Jahre getrieben habe.

Und abschließend an alle, die immer wieder behauptet haben, dass man es als dualer Student an der Universität schwer habe und eine Promotion unmöglich sei: Quod erat demonstrandum.

Vielen Dank!